

Optical sensing for tissue differentiation



Daniel James Evers

OPTICAL SENSING FOR TISSUE DIFFERENTIATION

PROEFSCHRIFT

ter verkrijging van
de graad van doctor aan de Universiteit Twente,
op gezag van de rector magnificus,
Prof. Dr. H. Brinksma ,
volgens besluit van het College voor Promoties
in het openbaar te verdedigen
op vrijdag 10 oktober 2014 om 16.45 uur

door

Daniel James Evers
geboren op
18 november 1978
te Christchurch
(Nieuw Zeeland)

Cover: Jornt van Dijk, persoonlijkproefschrift.nl
Layout: Jornt van Dijk, persoonlijkproefschrift.nl
Printed by: Ipskamp Drukkers BV
ISBN: 978-94-6259-308-4
Online: <http://books.ipskampdrukkers.nl/thesis/dannyevers>

The contents of this thesis have been approved by Prof. dr. T.J.M Ruers and Dr. B.H.W. Hendriks.

The publication of this thesis was financially supported by: Twente University - TNW faculty, Philips Medical Systems, Rijnland hospital, Chipsoft

© D.J.Evers. Enschede, The Netherlands, 2014

PROMOTIE COMMISSIE

Promotor:	Prof. dr. T.J.M Ruers
Co-promotor:	Dr. B.H.W. Hendriks
Overige leden:	Prof. dr. L.F. de Geus-Oei
	Prof. dr. M.M.A.E. Claessens
	Prof. dr. H.J.C.M. Sterenborg
	Prof. dr. R.J. Porte
	Prof. dr. E. Marani
	Dr. A.M. Zeillemaker
	Dr. D.J. Grünhagen
Paranimphen:	V. Brehm
	J.F. Tielemans

CONTENTS

Chapter 1	General Introduction	Page 7
Chapter 2	Summary & Samenvatting	Page 17
Part one		
Chapter 3	Optical Spectroscopy; a review on current advances and future applications in cancer diagnostics and therapy.	Page 23
Part two		
Chapter 4	Diffuse Reflectance spectroscopy: a new guidance tool for improvement of biopsy procedures in lung malignancies	Page 43
Chapter 5	Optical sensing for tumor detection in the liver	Page 59
Chapter 6	Diffuse Reflectance spectroscopy; towards clinical application in breast cancer	Page 73
Chapter 7	Improved identification of peripheral lung tumors using diffuse reflectance and fluorescence spectroscopy	Page 91
Part three		
Chapter 8	<i>In vivo</i> tumor detection in the liver with diffuse reflectance and fluorescence spectroscopy	Page 107
Chapter 9	Monitoring of tumor response to cisplatin using optical spectroscopy	Page 121
Chapter 10	Diffuse reflectance spectroscopy: towards real time quantification of steatosis in liver	Page 139
Part four		
Chapter 11	General Discussion	Page 157
	References	Page 167
	PhD Portfolio	Page 189
	Curriculum Vitae	Page 193
	Acknowledgements	Page 197



Chapter **1**

General introduction

Modern imaging technologies play a crucial role in daily clinical care. In cancer treatment for example, imaging techniques are vital tools for state of the art management in all stages of the cancer care cycle. In cancer *screening*; imaging aims for early detection of small (pre) cancerous lesions, preferably before differentiation into invasive or metastatic disease. In cancer *staging*; several imaging modalities are used to characterize the primary lesion, describe the local extent and determine possible metastatic sites. Detailed knowledge of these issues is essential before an optimal therapeutic plan can be decided on. In cancer *treatment*; complete surgical resection of a tumor is necessary for best chances of long-term survival. New methods for intra-operative imaging are currently tested for optimal intra-operative tumor visualisation aiming for complete tumor resection. Furthermore, accurate tumor localisation is vital for optimal treatment with ablation techniques or radiotherapy. Finally, imaging is essential for *therapy response monitoring* and subsequent management of systemic treatment and thorough follow-up examinations ¹.

Imaging techniques, such as x-ray, ultrasound, computed tomography (CT) and magnetic resonance imaging (MRI) are considered as the gold standard for anatomical imaging. Functional imaging techniques, such as single-photon emission computed tomography (SPECT) and photon emission tomography (PET) are also becoming standard of care in most medical facilities. In the last decade, progressive developments have occurred in the field of diagnostic imaging inducing higher resolution imaging, faster imaging protocols and less ionizing radiation. Besides the introduction of these technical developments in diagnostic imaging a clear trend is noticed towards image guided treatments. At this stage, this is mainly limited to radiological intervention procedures such as local tumor ablations. However, new developments in image guided surgical procedures are aiming for better resection planes and negative tumor resection margins. Conventional imaging modalities have limitations restricting their intra-operative employment for these purposes. With these techniques, the threshold of detection of target tissue is dependent on the minimum spatial resolution of the available imaging technique. Despite recent technological advances, such as the use of novel radiotracers for improved spatial resolution and the combination of different imaging modalities into single examinations (e.g. PET-CT), the minimum spatial resolution of various imaging techniques still has a current range in the order of millimetres which may not be accurate enough for surgical guidance ¹⁻⁵. In addition, the application of conventional imaging modalities is limited in the operating room due to the size of the imaging equipment that is needed.

Biomedical optics could prove a solution for improving these resolution limitations of conventional imaging techniques as well as to adhere to the space requirements within the operating room and the restricted surgical working field. Biomedical optical techniques have more accurate tissue sensing properties than conventional imaging techniques with

spatial resolution capabilities in μm . Another advantage is that they can be incorporated into existing medical tools leading to smart devices for interventional procedures.

Two main fields in biomedical optics can be distinguished; Tomography and Spectroscopy.

Tomography

Tomography is a non-invasive technology that can generate high-resolution images of tissue structures. Several techniques can be distinguished in this field.

Optical coherence tomography (OCT) can generate images of tissue surfaces in real-time using a near-infrared light source. OCT imaging is similar to ultrasound imaging except it uses light instead of sound waves. The physical principle of OCT is based on analysis of tissue by measuring the time delay and intensity of backscattered or reflected light. Differences in the reflected light occur due to variations in the index of refraction of the optical scattering. The achieved image resolutions range from 1 to 15 μm ⁶. OCT can provide direct optical feedback of targeted tissue. Clinical application of OCT systems currently focuses on the fields of ophthalmology and dermatology. In cardiology and internal medicine, incorporation of OCT systems into vascular catheters and endoscopes also enable identification and characterisation of atherosclerotic plaques and intestinal mucosal changes^{7,8}.

Photoacoustic tomography (PAT) uses short pulses of laser light to generate ultrasonic waves creating images of tissue several mm below the surface. Laser pulses, mainly in the far-red or NIR wavelength range, are directed at target tissue. Absorption of the photons produces heat and a subsequent thermal expansion of the absorbing tissue components. This process generates acoustic waves that can be detected by ultrasound detectors. The advantage of this technique compared to optical imaging is that it can present an enhanced resolution of tissue in depths more than 1mm due to weaker scattering of the ultrasound waves. Target tissue absorbers for this technique include blood and water. Current PAT research focuses on use in medical oncology, such as breast and skin cancer⁹⁻¹¹.

Diffuse optical tomography (DOT) creates images of tissue based on differences of absorption and scattering properties after interaction with spectra mainly in the near-infrared light range. DOT can quantify relevant tissue components, such as water, lipid and hemoglobin, based on the known absorption properties of these molecules to the selected light. Depending on the concentrations of these molecules throughout the analysed tissue the reflected light spectrum will differ. Reflection of light depends on the refraction index between extra- and intracellular fluids and cellular components such as nucleoli and mitochondria. The fluctuating degree of density in tissue will generate varying scattering coefficients. Taking these qualities into mind, the main advantage of DOT reflects on its ability to display physiological changes in tissue. Primary focus of the application of DOT in commercial medicine is focussed on the imaging potential of brain and breast tissue¹²⁻¹⁴.

Spectroscopy

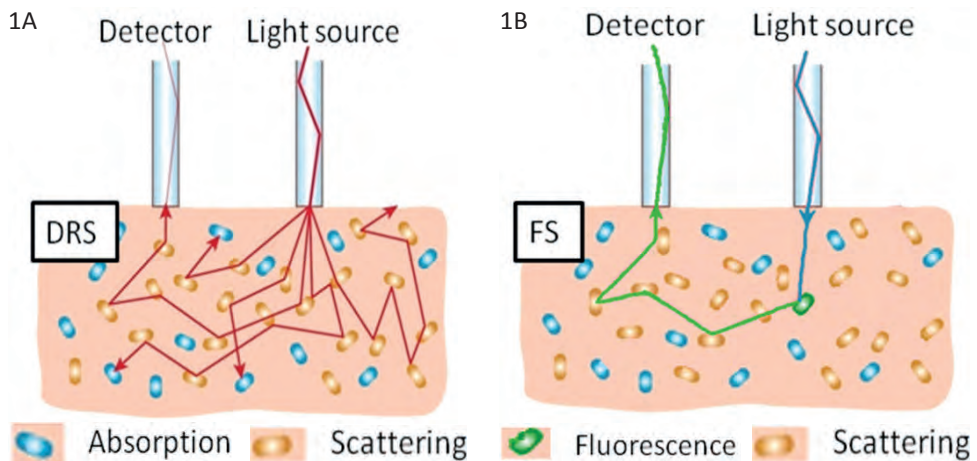
Spectroscopy is the study of the interaction between radiated energy and matter. Optical spectroscopy includes several techniques such as Diffuse Reflectance, Fluorescence and Raman spectroscopy. Using optical spectroscopy techniques, tissue differentiation is possible by analyzing the changes in light spectra after interaction with tissue composition and cellular components. These changes in selected light spectra occur due to processes like absorption, scattering of light or induction of fluorescence. The changed spectral patterns represent specific quantitative biochemical and morphological information from the examined tissues depending on tissue morphology, cellular structure, metabolic rate, vascularity and oxygenation. Depending on the chosen optical spectroscopy technique, specific differentiation between tissues becomes possible based on the differences on a cellular or even a molecular level ¹⁵⁻²².

Diffuse reflectance spectroscopy (DRS) measures the loss in intensity of diffusely reflected light after it has undergone interactions with tissue for each wavelength of light produced by a broadband light source ²². For example, if photons of the same wavelength are emitted in a target tissue sample, not all photons will be recollected due to the absorption and scattering processes (Figure 1A).

The main absorbing molecules or chromophores of the visible light spectrum (400 – 750 nm) in human tissue are oxygenated and deoxygenated haemoglobin and β -carotene.

Figure 1. Schematic overview of two optical spectroscopy techniques.

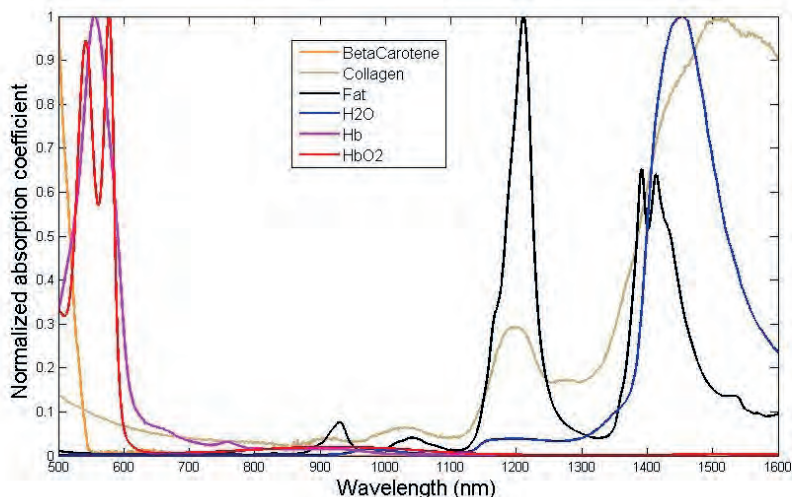
A. Diffuse Reflectance Spectroscopy (DRS); a broadband light spectrum is emitted into tissue and the spectrum of the reflected light is dependent on absorption and scattering interactions within the target tissue. B. Fluorescence Spectroscopy (FS); light of a single wavelength is emitted into tissue. Absorption can result in emission of fluorescent light by the tissue fluorophores.



In the near-infrared light spectrum these are water, adipose tissue and collagen (Figure 2). The absorption coefficient from each chromophore is directly related to its concentration in the tissue specimen. Thus, the higher the concentration of a molecule in a target tissue, the more photons that are absorbed at a specific wavelength and the lower the number of photons that will be recollectd in the reflected light spectrum after tissue interaction. This biological and physiological information can be directly quantified from the reflected light spectrum ²³.

Besides tissue composition, DRS can detect differences in tissue morphology by the analysis of the elastic light scattering. Elastic scattering means that the direction of the wavelength of a photon changes, but the wavelength remains the same before and after the scattering occurrence. The scattering coefficient of a target tissue is unique depending on the underlying cellular structure, the size, the density and the refractive index of each cellular and subcellular component. Tissue structure alterations due to processes like cell death and proliferation of cells can be detected by differences in light scattering ²⁴. Scattering depends on the size of the scatterer. Two types of elastic scattering can be distinguished; 'Rayleigh' scattering occurs if the scattering particle is smaller than wavelength of the photon. Intracellular components like collagen fibrils are examples of Rayleigh scatterers. The 'Mie' theory describes the scattering of photons by particles similar or larger than their wavelength. Cells and main cellular components can cause Mie scattering ²⁵. Analysis of figure 2 shows that little absorption of light between 700 and 1000nm occurs when interacting with biological tissue. Scattering properties of tissue are best analysed between these wavelengths.

Figure 2. Normalized absorption coefficients of deoxygenated-hemoglobin (Hb), oxygenated-hemoglobin (HbO₂), β -carotene, water (H₂O), lipid and collagen.



Fluorescence Spectroscopy (FS) measures the fluorescence signals, which are the result of *inelastic* scattering of absorbed photons by specific tissue molecules also called fluorophores. Fluorescence is caused by re-emission of light with a higher wavelength than the absorbed photon wavelength (Figure 1B). With Fluorescence Spectroscopy biological tissues are examined based on the fluorescent characteristics after illumination with light of one specific wavelength.^{21,22,26} Several known intrinsic fluorophores in human tissue are collagen, elastin, nicotinamide adenine dinucleotide (NADH), flavin adenine dinucleotide (FAD) and porphyrin. Analysis of the fluorescence signal allows tissue discrimination based on differences in cellular structure (collagen en elastin) and cellular metabolism (FAD, NADH and porphyrin)²⁷⁻³⁰. Exogenous fluorophores can also be used for fluorescence tissue analysis^{22,27,31,32}. After wavelength dependent interactions in tissue, the measured spectra not only contain biochemical information due to fluorescence, but they are enriched by morphological information of the tissue due absorption and scattering of the fluorescence light. These two factors can significantly frustrate the specific extraction of quantitative biochemical information from the measured fluorescence spectra²². To be able to identify the specific structural and biochemical information from the fluorescence signal, a combination of FS and DRS is often used in tissue analysis. The ‘intrinsic’ tissue fluorescence can be extracted from the measured fluorescence spectrum by correcting for absorption and scattering from the measured diffuse reflectance spectrum.

The specific optical characteristics of DRS and FS described above render these optical techniques interesting tools for discrimination of different tissue types and studying physiological changes in tissue. Moreover, the characteristics render them interesting for study of transformations that occur in malignancy processes.

Clinical advances with DRS and FS

Many groups have explored clinical applications of optical spectroscopy for various human tissues and organs¹. Several conclusions may be drawn from literature thus far. Until 2010, all research with DRS and FS was mainly performed with visual light (400 - 750nm). Some groups expanded the applied wavelengths up to a maximum of 1000nm. This means that results of the DRS spectra analyses mainly focus on (de-)oxygenated haemoglobin, β -carotene and tissue saturation as well as scattering properties. For the analysis of received data the research groups used several different analysis methods. This renders it difficult to compare results between research groups. In addition, most studies displayed results of only *ex vivo* and animal analyses. In all research involving DRS, sensitivity and specificity reports varied, ranging from 67 to 100% and from 60 to 100% respectively. When DRS is combined with FS, sensitivity and specificity figures displayed are between 70 to 100% and 63 to 100% respectively.

From literature, similarities in various tissue parameters in different organs were apparent when comparing malignant to benign tissue: (1) Malignancies of the breast, lungs, the gastrointestinal tract, the cervix and oral cavity all show increased values of total hemoglobin content, (2) Tissue saturation was decreased in breast-, lung-, gastrointestinal- and oral cavity cancer, aiding to the hypothesis that hypoxia within a tumor could be involved in tumor progression. Other analysed tissue parameters were not uniform in all organs. Collagen levels in breast and kidney cancer are relatively raised, but in cervical, skin, stomach and oral cavity tumors these are relatively decreased compared to normal tissue. Increased scattering has been measured in malignancies of the breast, lung and kidney; meanwhile decreased scattering has been displayed in (pre)-malignant cervical lesions.

Optical spectroscopy system development

The results of previous groups towards clinical applications of spectroscopy techniques were considered very promising. We believed that further progress could be made focussing on improvement of several areas of the spectroscopy technology. First, we considered an extension of the spectral analysis range up to 1600nm. This would include additional tissue chromophores into the analysis algorithm. Towards new hardware, we believe that an extension of the distance between emitting and collecting optical fibers will enable refined analysis of chromophore quantification. We also concentrated on development of miniaturized optical needles to allow less invasive measurements *in vivo*. Finally, we considered modifying the analysis algorithms an important area to improve tissue-sensing accuracy.

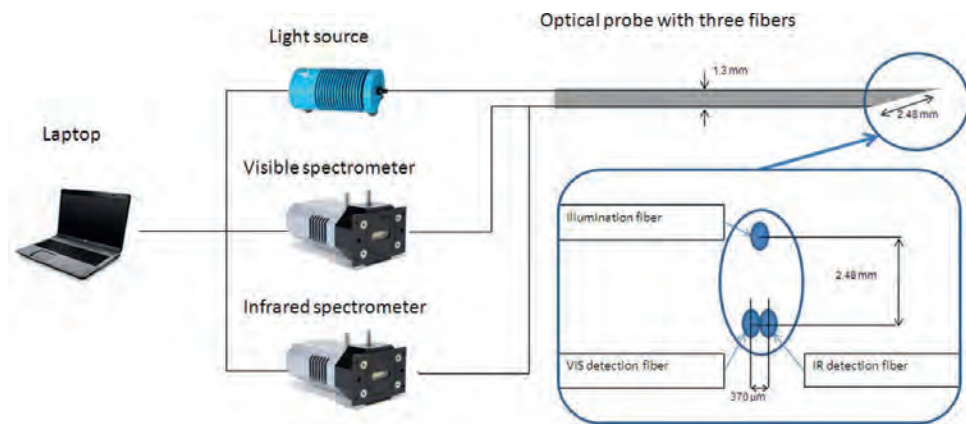
To explore new possibilities for the clinical use of optical spectroscopy, a partnership was formed between Philips Research (Minimal Invasive Healthcare), Twente University (MIRA Institute) and The Netherlands Cancer Institute (NKI-AvL) in 2009 as a basis for this thesis. Development of a spectroscopy console and improvement of data analysis software were the first steps before any clinical experiments could be performed (results were previously published by Nachabé *et al*).

An optical console was developed containing a tungsten halogen broadband light source producing light from 360 to 2500nm, a spectrometer with a silicon detector to resolve light between 400 nm and 1100 nm (Andor Technology, DU420A-BRDD) and a spectrometer with a InGaAs detector to resolve light from 800 up to 1700 nm (Andor Technology, DU492A-1.7). The initially developed optical probe had a diameter of 1.3mm and contained three optical fibers to be connected to the optical setup. One fiber connected to the light source and the two other fibers connected to the spectrometers to

collect diffusely scattered light from the tissue. A close-up of the optical needle tip shows the illumination optical fiber located at a distance of 2.48 mm from the two side-by-side optical fibers that are used to collect the diffused light (Figure 3). Such a setup enables spectral acquisition in the range between 500 to 1600 nm via an optical fiber with its distal end placed against the target tissue sample³³.

An upgraded version of the optical console was later equipped with a semiconductor laser ($\lambda=377$ nm) for combined DRS and FS measurements. Several different new optical needles were developed, some containing 4 optical fibers. The diameter of the available optical needles varied from 0.72 mm tot 1.3 mm.

Figure 3. Schematic display of the optical console. It includes a halogen light source and two spectrometers, which are connected to a needle containing three optical fibres to its tip.



With this new spectroscopy console, the benefits of an extension of the analysis spectrum beyond previously described methods including near-infrared light up to 1600nm were explored. Water and lipid are the dominant absorbers of this near infrared spectrum and are important molecules in biological tissues. Several groups had estimated the concentrations of these chromophores in spectra up to 1000nm. However, quantification is not reliable due to effects of scattering and absorption by other chromophores. These negative effects decrease in spectra above 1000nm. Indeed, Nachabé *et al* showed that water and lipid could be more accurately quantified from near-infrared light spectra^{23,33}.

The analysis of the acquired light spectra formed another challenge. As previously stated, review of the literature displays a variety of different analysis methods utilized by various research groups. The methods can roughly be distinguished into two main groups. The first technique focuses on the shape of the measured spectra, which are statistically analyzed and directly correlated to histological diagnosis. *Partially least square discrimination analysis* is an example, which has the advantage of not requiring

any data processing and disadvantage that no quantitative information of the target tissue is derived³⁴. The second approach is a model-based analysis. An algorithm is used to first translate spectral data into physical properties such as reduced scattering and absorption coefficients for different wavelengths. These are then translated into biologically relevant parameters with subsequent quantitative analysis and correlation to histological results³⁵. Our group mainly focused on a model based approach for our tissue data analysis. This was based on the diffusion theory model developed by Farrell *et al*³⁶. The Levenberg-Marquardt nonlinear inversion algorithm model was used to fit and analyze the measured DRS spectra. The absorption coefficients of each tissue chromophore in pure state are considered prior knowledge and incorporated into the algorithm together with the reduced scattering coefficient²³. The model and calibration procedures were first validated on phantom models and subsequently tested on tissue *ex vivo* and *in vivo*^{23,33}. A *Classification and Regression Tree* (CART) algorithm was then used to classify between different tissue types from the obtained quantified parameters and compare these results to the histological diagnosis³⁷.

In addition, we compared our method for data analysis to the various other methods used by research groups in this field. To this end, the same spectral data we obtained from an *ex vivo* study on human breast tissue was analyzed in 8 different ways³⁸. The performance between the various methods in terms of sensitivity and specificity was diverse. The algorithm we developed was among the best performing analysis methods.

Intrinsic fluorescence was analyzed and calculated via dual analysis of both the diffuse reflectance and fluorescence spectra. By correcting for absorption and scattering the intrinsic fluorescence could be derived. This method was previously described by Müller *et al* and Zhang *et al* and is based on the photon migration theory^{39,40}. This theory describes the circulation of photons in a turbid medium depending on photon-tissue interaction events like absorption, scattering or induction of fluorescence. We used a modified version of this theory that allows real-time fluorescence recovery, aiming at clinical application. It was developed and validated by Müller *et al*²⁶. The corrected spectra were then fitted by using the intrinsic fluorescence spectra (excitation at 377 nm) of collagen, elastin, NADH and FAD which are considered prior knowledge²².

In a pre-clinical phase, we designed and validated an optical console and specialized software for *Diffuse Reflectance Spectroscopy* and *Fluorescence Spectroscopy* analysis of biological tissue. Our optical system comprises several advantages of compared to previous research. In this thesis we describe the initial results of this innovative approach for tissue differentiation in lung, liver and breast cancer and pave the way towards the incorporation of this technology into medical devices and introduction into every day medical procedures.



Chapter **2**

Summary & Samenvatting

This dissertation is divided into four sections. **Part 1** describes a review of the current literature on spectroscopy studies of human tissues at the start of this research project in 2010 (**Chapter 3**).

The **second part** of this thesis highlights the general application of our optical console and analysis approach in an *ex vivo* clinical setting. We focussed on the spectral differences between normal and malignant tissue in lung, liver and breast cancer specimens just after resection. The main study questions we asked ourselves concentrated on the general applicability of the console and the optical needles in a clinical environment; can the hardware be easily used in a clinical environment? Did the specially designed software function as planned; did we receive real-time feed-back of the tissue spectra? What was the performance in biological tissue? Does blood at the tip of the needle have a negative influence on the detection of the scattered spectra for example? Finally, what was the diagnostic accuracy of our system for discrimination between normal and malignant tissue?

We primarily focussed on Diffuse Reflectance Spectroscopy alone. In **chapter 4**, the results are displayed of the performed measurements in lung tissue. **Chapter 5** demonstrates the optical sensing capabilities in liver tissue. **Chapter 6** explains the performance of DRS in human breast tissue, which is technically the most challenging due to the tissue heterogeneity compared to lung and liver tissue. In **chapter 7**, we demonstrate the benefits of adding Fluorescence spectroscopy to DRS in an *ex vivo* analysis of lung tissue compared to the use of DRS alone.

We then developed new optical needles that could be used for *in vivo* analyses as an important next step towards clinical applications with this technology incorporated. **Part 3** describes the performance of our optical spectroscopy system in an *in vivo* environment. We focused on how is the diagnostic accuracy of our spectroscopy system would be compared to the previous *ex vivo* experiments? Is the system functional in an every day clinical situation?

In **chapter 8** the results are presented of an *in vivo* analysis in human liver tissue performed in the operating theater prior to liver resection. **Chapter 9** compares the accuracy for detection and response monitoring of malignant tumors after systemic chemotherapy in a murine model between histology and our spectroscopy system. Finally, we explored the real time quantification and feedback potential of liver steatosis *in vivo* by DRS and FS. This is a clinically relevant question for significant liver surgery like liver transplantation or a major resection (**Chapter 10**).

The dissertation ends in **part 4** with concluding remarks on all presented results and future perspectives towards the development of medical tools equipped with optical spectroscopy technology (**Chapter 11**).

Dit proefschrift is onderverdeeld in vier secties. **Deel 1** beschrijft een overzicht van de huidige literatuur van spectroscopie studies in humaan weefsel ten tijde van de start van dit onderzoeksproject in 2010 (**Hoofdstuk 3**).

Het **tweede gedeelte** beschrijft de resultaten van het toepassen van de optische console in diverse klinische studies *ex vivo*. De nadruk in deze studies lag op de spectrale verschillen tussen normaal en maligne weefsel in resectiepreparaten van de long, lever en borst. We stelden onszelf verschillende onderzoeksvragen: De algemene toepasbaarheid van de console en optische naalden in een klinische setting; hoe was de gebruiksgemak van de hardware? Functioneerde de speciaal ontwikkelde software zoals gepland; kregen we 'real-time' een terugkoppeling van de weefselspectra? Hoe was het functioneren in biologisch weefsel? Heeft bijvoorbeeld bloed op de tip van de naald een negatieve invloed op het detecteren van de weerkaatsende licht spectra? Tenslotte, wat was het onderscheidend vermogen van ons systeem tussen normaal en maligne weefsel?

De eerste studies werden primair met Diffuse Reflectie Spectroscopie verricht. In **hoofdstuk 4** worden de resultaten uiteengezet van metingen in long weefsel. **Hoofdstuk 5** demonstreert het onderscheidend vermogen tussen normaal lever weefsel en lever metastasen. In **hoofdstuk 6** worden de discriminerende prestaties getoond in humaan borstweefsel. Dit was technisch het meest uitdagend gezien de heterogeniteit van borstweefsel in vergelijking met dat van de long of lever. Vervolgens hebben we Fluorescentie Spectroscopie toegevoegd aan DRS en het onderscheidend vermogen van deze gecombineerde technieken ten opzichte van DRS alleen vergeleken in een tweede *ex vivo* analyse van long weefsel (**Hoofdstuk 7**).

Intussen hadden we nieuwe optische naalden ontwikkeld die gebruikt zouden kunnen worden in *in vivo* weefsel analyses. Dit was een belangrijke volgende fase richting het ontwikkelen van optische applicaties voor klinische toepassingen. In **deel 3** zetten we de prestaties van ons optisch spectroscopie systeem in weefsel *in vivo* uiteen. De belangrijkste vraagstellingen waren: Hoe was het discriminerend vermogen *in vivo* ten opzichte van eerdere *ex vivo* experimenten? Verder concentreerden we ons op het functioneren van het systeem in alledaagse klinische situaties.

In **hoofdstuk 8** worden de resultaten getoond van een *in vivo* analyse in lever weefsel peroperatief uitgevoerd net voor een operatieve resectie. **Hoofdstuk 9** vergelijkt de nauwkeurigheid voor detectie en monitoring van response op systemische chemotherapie ten opzichte van de histologie in een muizen model. Tenslotte hebben we de potentie onderzocht van directe kwantificatie en terugkoppeling van lever steatosis door DRS en FS. Dit is een klinisch relevante vraag tijdens uitgebreide lever operaties zoals transplantaties en majeure resecties (**Hoofdstuk 10**).

Dit proefschrift wordt in **deel 4** beëindigd met algemene conclusies van alle resultaten en met een uiteenzetting naar toekomstige stappen richting het ontwikkelen van medische gereedschap met daarin optische spectroscopie technologieën geïncorporeerd (**Hoofdstuk 11**).

Part 1



Chapter **3**

Optical Spectroscopy; current advances and future applications in cancer diagnostics and therapy

D.J. Evers

B.H.W. Hendriks

G.W. Lucassen

T.J.M. Ruers

Future oncology 2012; 8(3): 1-14

INTRODUCTION

Modern tissue imaging technologies are essential tools in state of the art management in all stages of cancer treatment. In cancer *screening*, early detection of a cancer, preferably before differentiation into invasive or metastatic disease, is essential for optimal chance of curative therapy. In cancer *staging*, before an optimal therapeutic plan can be decided on, it is necessary to describe both anatomical extent and histological origin of a suspected malignancy. In cancer *treatment*, complete surgical resection of a tumor is necessary for best chances of long-term survival, optimal intra-operative tumor visualisation improves the accuracy of a complete resection. Moreover, accurate tumor localisation is vital for optimal treatment with ablation techniques or radiotherapy. Finally, imaging is essential for *therapy response monitoring* and subsequent management of systemic treatment.

Various imaging techniques, such as x-ray, ultrasound, computed tomography (CT), single-photon emission computed tomography (SPECT), magnetic resonance imaging (MRI) and photon emission tomography (PET), are used for diagnosis and treatment monitoring in cancer. The threshold of detection of cancer tissue is dependent on the minimum spatial resolution of the available imaging technique. Despite recent technological advances, such as the use of novel radiotracers for improved spatial resolution and the combination of different imaging modalities into single examinations (e.g. PET-CT), the minimum spatial resolution of various imaging techniques still has a current range in the order of millimetres²⁻⁵. This results in a detection threshold for solid tumors at a minimum of 10^8 to 10^9 cells or 0.5 to 1cm^3 of solid tissue¹⁵.

Over the last two decades, one of several new emerging technologies with more accurate tissue sensing properties is that of optical spectroscopy (OS). OS is the study of changes in the spectral distribution of light after interaction with molecules in a tissue. The main notable changes within a light spectrum after interaction with tissue are a result of either absorption or scattering of light or due to the laser induced fluorescence and Raman scattering. Using OS it is possible to obtain an optical fingerprint of the tissue by illuminating tissue with a selected spectral band of light and performing subsequent analysis of the characteristic scattering, absorption, fluorescence and Raman patterns. These spectral patterns present specific quantitative biochemical and morphological information from the examined tissues depending on cellular metabolic rate, vascularity, intra-vascular oxygenation and alterations in tissue morphology. Depending on the chosen OS technique, specific differentiation between tissues becomes possible based on the differences on a cellular or molecular level¹⁵⁻²².

With these differentiation qualities, OS is proving to be more sensitive in determining relevant tissue properties, for example distinguishing normal tissue from malignant tissue, than conventional imaging techniques. Hence, OS is progressively being explored

for sole use as well as combined use with conventional imaging techniques in diagnosis and therapy of cancer^{15,41}. Analysis with OS can be performed on tissue surfaces during endoscopic procedures or on solid organs during minimal invasive or surgical procedures. The wavelengths of emitted light that are generally used in these applications span from the visible (400 - 750nm) to near-infrared (750 - 2500nm) wavelengths. Specific focus of spectroscopic applications has been put towards the early detection and diagnosis of cancer, preferably in the precancerous stages. Furthermore towards the intra-operative analysis of surgical resection margins and finally towards the possibilities of early therapy response monitoring, aiming at decreasing unnecessary overtreatment of ineffective and costly chemotherapy.

With this review we aim to highlight the current advances of the field of optical spectroscopy. We will specifically focus on three of the most practiced optical spectroscopy techniques; Diffuse Reflectance Spectroscopy (DRS), Fluorescence Spectroscopy (FS) and Raman Spectroscopy (RS), and their possible future applications in the detection and treatment of cancer.

Diffuse Reflectance Spectroscopy

DRS measures the intensity of diffusely reflected light after it has undergone absorption and scattering interactions with tissue for each wavelength of light produced by a broadband light source (Figure 1a - chapter 1). The intensity of reflected light after being scattered as a function of the wavelength defines the reflectance spectrum²².

Overall tissue absorption can be analyzed through the known absorption coefficients of physiologically relevant molecules in the tissue in its pure form. The absorption coefficient from each molecule is directly related to the concentration of this absorber in the tissue. The concentration can be directly quantified from the reflected light spectrum. The main absorbers in soft tissues of the visible spectrum of light are oxygenated and deoxygenated haemoglobin and β -carotene. Primary absorbers in the near infrared spectrum of light are water, adipose tissue and collagen²³.

The scattering coefficient contains information of the underlying cellular structure, and is sensitive to size and density of cellular and subcellular structures; thus, it can be altered by changes in tissue such as cell death and proliferation of cells. The onset and progression of cancer is associated with significant changes in tissue structure and composition as well as cellular morphology²⁴. These specific tumor characteristics can be well distinguished by DRS, therefore qualifying this optical technique as a tool in discriminating between benign and malignant tissue.

Fluorescence Spectroscopy

FS focuses on spectral characteristics of specific molecules in tissue after illumination with light of one specific wavelength^{21,22}. These molecules (or fluorophores) will absorb the light energy and be activated from ground state to an excited state. Upon de-excitation the molecules generate fluorescence light with a different wavelength than the excitation wavelength (Figure 1b - chapter 1). The shape and intensity of the fluorescence spectrum depends on the concentrations of the fluorophores in the target tissue²⁷. Discrimination between different tissue types is possible based on the molecular specific fluorescence characteristics. After wavelength dependent interactions in tissue, the measured spectra not only contain biochemical information due to fluorescence, but they are enriched by morphological information of the tissue due absorption and scattering of the fluorescence light. These two factors can significantly frustrate the extraction of quantitative biochemical information from the measured fluorescence spectra²². To be able to identify the specific structural and biochemical information from the fluorescence signal, a combination of FS and DRS is often used in tissue analysis. The 'intrinsic' tissue fluorescence can be extracted from the measured fluorescence spectrum by correcting for absorption and scattering from the measured diffuse reflectance spectrum.

The targeted molecules can be either intrinsic (endogenous fluorophores) or extrinsic (exogenous fluorophores)^{22,27,31,32}. Several endogenous fluorophores are often involved in transformations that occur in the neoplastic process and are therefore interesting for quantitative research. These include: Collagen, Elastin, Nicotinamide adenine dinucleotide (NADH), Flavin adenine dinucleotide (FAD), Tryptophan and Tyrosine.

Raman spectroscopy

RS is based on principles of an inelastic scattering process in which absorption of an incident photon causes a change in the vibrational mode of a molecule. With RS, tissue is illuminated with laser light of one specific wavelength. Absorption of a photon from this laser light has the ability to change the vibration mode of a molecule. A subsequent transition of the molecule from one vibrational level to another results in emitted photons that have a wavelength different from the wavelength of the light used to excite the molecule. This wavelength shift is also called the *Raman shift*. The energy shift of the emitted photon as a result of this phenomenon is unique for this molecule. In a RS spectrum, individual bands are characteristic for specific molecular motions and can therefore be used to identify and quantify specific tissue molecules and thus be used to distinguish different tissue types⁴². For optimal Raman spectra, excitation wavelengths between 700 and 1100 nm are often selected. At these wavelengths absorption by tissues and body fluids are minimal, excited autofluorescence is minimal and the penetration of exciting and scattered radiation is maximal⁴³.

CLINICAL APPLICATION OF OPTICAL SPECTROSCOPY

In recent years several reviews have been published focussed on tissue differentiation using optical spectroscopy. In the following section we will review the results of these studies for the different organ and tissue sites with focus on the three mentioned main fields of OS: DRS, FS and RS.

Skin

Human skin is the most accessible human tissue. With the incidence of skin cancer increasing worldwide, progressive focus is put towards early diagnosis of malignant skin lesions. Moreover, accurate mapping of the extension of the skin lesion is crucial for surgical planning. Many studies with OS techniques have focussed on these clinical questions for (pre) malignant skin lesions.

Brancaleon *et al* investigated BCC lesions *in vivo* with FS. In 18 patients they discovered decreased collagen levels and increased Tryptophan levels in BCC lesions compared to normal human skin ⁴⁴. Rajaram *et al* recently published the design and validation of a spectroscopy system for *in vivo* analysis based on DRS and FS ⁴⁵. This paper displays an *in vivo* analysis of emission spectra within visual light spectra. Clinical studies for early detection and model-based analysis of both melanoma and non-melanoma skin lesions with this system are currently being performed by this group.

The main focus of current research of skin cancer with optical spectroscopy has been with Raman spectroscopy. Gniadecka *et al* developed a Raman spectroscopy system for discrimination of several malignant skin lesions from normal skin tissue ⁴⁶. Discrimination between melanoma and normal skin tissue *ex vivo* was possible with a sensitivity of 84% and specificity of 97%.

Choi and co-workers and Nijssen *et al* investigated Raman techniques for *ex vivo* analysis of basal cell carcinoma (BCC) and normal skin tissue. The former group promotes confocal Raman microscopy as a new method for dermatological diagnosis of BCC ⁴⁷. Yet, their conclusions are based on analysis of only 10 patients in which they focus on changes in the structures of protein and lipid molecules. The Nijssen group draws similar conclusions after measurements using high wave number (2800-3125 cm^{-1}) RS ⁴⁸. Over 500 Raman spectra from 28 tissue samples of BCC and normal skin tissue were compared and a discriminative accuracy of 100% sensitivity and 99% specificity was achieved.

Recently, Lieber *et al* included normal skin samples, BCC lesions, squamous cell carcinomas (SCC) and inflamed scar tissue of 19 patients in a *in vivo* study with a RS system ⁴⁹. They demonstrated 95% overall classification accuracy with a spectrum classification model. Subsequent clinical studies for further validation of their spectroscopy system in a larger patient population are currently in progress.

Oral cavity

Several groups have studied the application of OS for the early detection of (pre) malignant lesions in the oral cavity. Early detection and biopsy of oral lesions in the premalignant phase by technologies more accurate than normal visual examination would be of great clinical importance in the management of these oral anomalies.

Both DRS and FS have been utilised for assessing the oral mucosa. Amelink *et al* compared oral mucosa to oral SCC lesions *in vivo* in 31 patients with a non-invasive differential path-length spectroscopy (DPLS) system, a specific type of DRS. Quantitative information can be obtained from tissue chromophores in the superficial oral mucosa layers with this technique. They described an increased total blood content and a decreased tissue saturation in SCC lesions compared to normal mucosa. Yet, specific differences in the level of tissue saturation were noticed and the authors hypothesize that level of tissue saturation could be related to the aggressiveness of the tumor⁵⁰.

Mallia *et al* published 2 papers with comparable research. Optical spectra were analysed by comparing spectral intensity differences at 545 and 575 nanometer. Authors analyzed spectra from normal oral mucosa to those of dysplastic epithelia, hyperplasia or SCC lesions. Depending on which tissue classes were compared a wide range in classification accuracy was demonstrated. Sensitivity ranged from 70 to 100% and specificity varied between 63 and 100%^{51,52}.

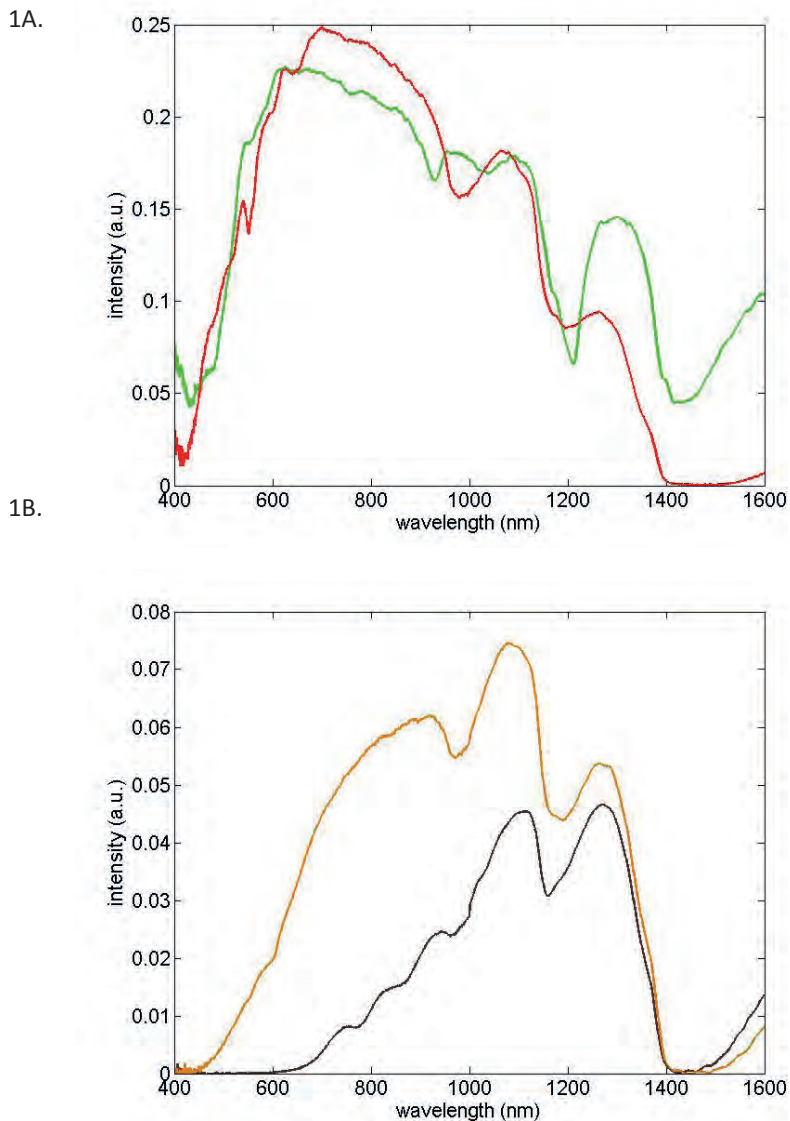
Several groups used a combination of DRS and FS to investigate normal and (pre) malignant oral mucosa with a non-invasive system *in vivo*. De Veld *et al* described results from the spectrum classification of 115 oral mucosa measurements⁵³. With DRS, normal and (pre)malignant were successfully classified with a sensitivity of 82% and specificity of 88%. With FS these figures were 89% and 71%, respectively. Schwarz *et al* reported a sensitivity of 82% and specificity of 87% for the analysis of normal vs. (pre)malignant mucosa⁵⁴. McGee *et al* compared normal oral mucosa to dysplasia and malignant oral lesions of 71 patients⁵⁵. In agreement with the previous mentioned paper from the Amelink group, they demonstrated increased total blood content and decreased tissue saturation in dysplasia and malignant lesions compared to normal mucosa. Moreover, they displayed decreased levels of collagen and β -carotene in malignant lesions.

Breast

Breast tissue can arguably be considered one of the most challenging human tissue types due to the general inhomogeneity of the morphology of both benign and malignant tissue. Important current challenges within breast cancer diagnosis and treatment are the improvement of biopsy accuracy and margin assessment during or shortly after surgical resection. Most research on human breast tissue involving optical spectroscopy

technology has focussed on applications towards improvement in these areas of breast cancer management. An example of typical differences in reflected spectra between adipose tissue of the breast and invasive carcinoma is depicted in Figure 1a.

Figure 1. An example of typical differences in reflected visual and near infra-red light spectra. A. A comparison of spectral differences between adipose tissue (green line) of the breast and invasive carcinoma (red line). B. An example of typical differences in reflected spectra between liver cancer *before* (orange line) and *after* (black line) radiofrequency ablation (RFA) of the liver. These spectra are results of our own data.



All current research with DRS has concentrated on the diversity of tissue absorption and scattering using visible light and near infrared spectra to a maximum of 1000nm emission. Several studies have been performed with diffuse optical spectroscopy (DOS), which is a non-invasive variant of DRS. Cerussi *et al* analysed spectral differences between normal and malignant breast tissue with DOS⁵⁶. They measured increased levels of both total hemoglobin and water content and decreased levels of lipid in malignant tissue. A positive correlation was demonstrated between water content in tumors and the histological grading of the tumor. The clinical feasibility of a DOS system was emphasized in a comparable study by Kukreti *et al*⁵⁷. Malignant breast tumors and benign lesions (fibroadenoma) could be successfully discriminated with a sensitivity of 91% and specificity of 94%.

Five studies with an invasive DRS system have recently been published. Empirical-based analysis of benign versus malignant tissue displayed by Bigio *et al*⁵⁸ and Zhu *et al*⁵⁹ reached a sensitivity of 69% and 83% and a specificity of 85% and 76%, respectively. Two other studies by Brown *et al*⁶⁰ and van Veen *et al*⁶¹ displayed an increase of deoxyhemoglobin as well as reduced saturation levels in malignant tissue. Veen *et al* observed increased collagen levels and scattering in malignant tissue. Interesting results from the Brown study were significant differences in total hemoglobin content and tissue saturation between tumors with and without *Her2Neu* amplification. In a recent study Nachabé *et al* performed an *ex vivo* human analysis discriminating between five tissue classes in the breast³⁸. The overall diagnostic performance was 94%. The results of these studies are difficult to compare due to differences in method and analysis specifics. However, Nachabé *et al* were the first to perform a comparative analysis of the various classification techniques used in literature based on their spectral data. They demonstrated that the discriminative performance between normal and malignant breast tissue was highly dependent on the utilised classification algorithm.

Several groups have published results of FS within the visual light spectrum. Gupta *et al* analysed nearly 1000 spectra from normal breast tissue, fibroadenoma and malignant tissue⁶². The authors found elevated levels of collagen, elastin, NADH and FAD in malignant tissue. Palmer *et al* performed an in-vitro analysis of normal human breast cells and malignant cells lines⁶³. Their results illustrate decreased levels of Tryptophan, yet NADH and FAD levels between the cell types did not differ with statistical significance. Chowdary *et al* compared fluorescence spectra of normal breast tissue, fibroadenoma and malignant disease after 325 nm excitation⁶⁴. Results revealed high concentrations of NADH in malignant compared to benign tissue. In addition, collagen levels were significantly highest in fibroadenoma tissue, followed by malignant tissue compared to normal breast tissue. With these tissue parameters, authors claim accurate classification and discrimination between benign and malignant tissue types to be near 100%.

The Feld group has published several studies of breast tissue using Raman spectroscopy⁶⁵⁻⁶⁷. In a study of this group by Haka *et al*, normal breast tissue was distinguished from fibrocystic change, fibroadenoma and malignant tissue in specimen from 58 patients⁶⁷. They used an algorithm with fat and water as key parameters and achieved 94% sensitivity and 96% specificity for the classification between malignant and normal or benign tissue. Haka *et al* subsequently presented the first *in vivo* analysis of breast tissue with Raman spectroscopy⁶⁵. Breast tissue from 31 patients was examined during partial mastectomy. Authors revealed 93% accuracy distinguishing between normal breast tissue, fibrocystic change and malignant tissue. Yet, only one specimen of malignant tissue was included in this analysis. The same authors also presented the first prospective Raman analysis of *ex vivo* breast tissue from 21 patients⁶⁶. Four breast tissue types were distinguished: normal breast tissue, fibroadenoma, fibrocystic change and malignant tissue. The prospective application of the algorithm resulted in a sensitivity of 83% and specificity of 92%. A main distinguishing factor was the difference in nuclear-to-cytoplasm ratio between the tissue types.

Several papers have been published in which spectroscopy modalities, mainly DRS and FS, have been combined⁶⁸⁻⁷². All display comparable results of spectral analysis of *ex vivo* breast tissue after illumination with visual light. By combined analysis of DRS and FS sensitivity figures ranging from 70% to 100% and specificity figures ranging from 74% and 96% were obtained. Majumder *et al* combined and compared all three spectroscopy modalities⁷³. Successful discrimination of four breast tissue types with DRS alone was described with 72% accuracy and with FS alone with 71% accuracy. A combination of these two yielded an improved accuracy of 84%. Raman spectroscopy was superior with an overall discrimination accuracy of 99%. These promising results remain to be succeeded by prospective and *in vivo* analysis.

Cervix

Apart from breast tissue, another main focus area of optical spectroscopy studies has been on cervical tissue. Two reviews have summarized most of the progress made in this field of human oncology research. Cardenas-Turanzas *et al* summarized results of 26 studies after analysis with DRS or FS. Overall results with DRS revealed sensitivities ranging from 72% to 100% and specificities ranging from 80% to 90%. With FS these figures ranged respectively from 71% to 99% and from 70% to 95%. These data suggest that optical spectroscopy may be able to enhance *in vivo* localisation of cervical abnormalities before advance to an invasive stage⁷⁴. Murali Krishna *et al* concluded main discriminative cervical tissue parameters in FS analysis to be collagen and NADH, which are respectively decreased and increased in (pre) malignant cervical tissue⁷⁵.

More recently, Mourant *et al* compared the spectra of high grade squamous

inter-epithelial lesions (HSIL) to non-HSIL lesions and normal cervical tissue of 36 patients after illumination with visual light ⁷⁶. The main discriminative tissue component of the HSIL lesions from non-HSIL lesions and normal tissue was raised tissue oxygenation. Discrimination between the two groups yielded a 100% sensitivity and 80% specificity. Chang *et al* compared Cervical Intraepithelial Neoplasia 2 (CIN2) lesions from normal cervical tissue and CIN1 lesions with a DRS system in 38 patients ⁷⁷. The authors displayed an increased total hemoglobin content in the CIN2 lesions. In this study, tissue oxygenation was not significantly different between compared tissues. Furthermore, they found a reduced scattering coefficient in these lesions.

Keller *et al* studied the effects of different epithelial (pre)malignancies with Raman spectroscopy including the cervix. In 102 included patients, main discriminative tissue parameters of CIN3 lesions compared to normal cervical tissue were reduced collagen levels and increased DNA content ⁷⁸.

Lung

Studies of human lung tissue have all concentrated on a combination of spectroscopy with endoscopic procedures and the discrimination of normal bronchial surface from (pre) malignant lesions.

Bard *et al* published two papers on optical spectroscopy techniques during endoscopic procedures of the lung. In the first paper, differential path-length spectroscopy (DPLS) was used to differentiate normal bronchus mucosa from dysplastic and malignant lesions ⁷⁹. Main distinguishing parameters of malignant tissue were an increased blood content and scattering and decreased tissue saturation. In the second paper, DPLS results were compared to results of DRS and FS for their discriminative accuracy between malignant and non-malignant lesions during bronchoscopy ⁸⁰. No significant differences were demonstrated in the discriminative accuracy between malignant and non-malignant bronchial lesions for DRS, FS and DPLS. The sensitivities and specificities for the three modalities were respectively 81% and 88%, 86% and 81% and 73% and 82%. For all three modalities combined an improved accuracy towards 90% was determined.

Fawzy *et al* analysed endobronchial cancerous lesions with both DRS ⁸¹ and FS ⁸². They demonstrated a DRS system that could classify between normal and malignant lesions in the superficial bronchial mucosa layers with a sensitivity and specificity of 83% and 81%. As in the Bard papers, the main discriminative parameters were increased blood content and decreased tissue saturation. In a comparable study using a FS system Fawzy *et al* could not match the accuracy described with their DRS system. In an analysis of bronchial mucosa in 40 patients a maximum sensitivity and specificity of 71% and 74% was reached by FS.

Raman spectroscopy was applied in an *ex vivo* lung tissue analysis by Yamazaki *et al*⁸³. Over 200 cancerous and non-cancerous lung tissue samples were analyzed after formalin fixation. Discrimination was possible with a sensitivity of 91% and a specificity of 97%.

Gastrointestinal tract

Improvement of endoscopic procedures has also been the focus for optical spectroscopy studies of the gastrointestinal tract. Georgakoudi *et al* combined DRS and FS in a study in 16 patients for improved recognition of high-grade Barrett's oesophagus⁸⁴. With this spectroscopy analysis using visible light illumination, normal oesophagus mucosa could be distinguished from low- and high-grade dysplasia with a sensitivity of 79% and specificity of 88%. Lovat *et al* focussed on the discrimination of normal mucosa and low-grade dysplasia from high-grade dysplasia and oesophagus cancer with a DRS system in a study of 81 patients⁸⁵. They reached an impressive sensitivity of 92%, yet the specificity was only 60%. Despite the need for a prospective test of the algorithm, the authors conclude that DRS is a reliable tool for targeted biopsy of the oesophagus.

Teh *et al* recently published two studies of *ex vivo* stomach tissue samples with Raman spectroscopy^{86,87}. In the first study, they evaluated the ability of their Raman system to distinguish between normal gastric mucosa and dysplastic gastric tissues. With principle component analysis a maximum sensitivity of 95% and specificity of 91% was yielded. In a subsequent study authors compared Raman spectra from normal gastric tissue to both intestinal-type and diffuse-type gastric adenocarcinomas in 62 patients during gastroscopy. Discrimination between these two specific cancer types could be made due to differences in collagen content, and specific differences in lipid and protein content at 1450 cm⁻¹. Predictive accuracies of the different tissues were between 88 and 94%.

Dhar *et al* and Wang *et al* introduced a DRS system to colonoscopy procedures. The Dhar group focused on differentiation of normal colon mucosa from various (pre) malignant lesions. Authors obtained sensitivities and specificities between 75% and 85% in the differentiating the various colonic tissues⁸⁸. Wang *et al* found increased levels of total hemoglobin and decreased levels of oxygen saturation in (pre) malignant lesions, which corresponds to DRS results in malignant tissue from other organs⁸⁹.

Finally, Chowdary *et al* performed *ex vivo* analysis of colonic tissue with Raman spectroscopy⁹⁰. Revealing discriminative accuracy between normal and malignant tissue of 95%, the authors stressed Raman spectroscopy to be feasible for future *in vivo* study in combination with endoscopical procedures.

Liver

Within liver tissue research has mainly concentrated on the spectral changes during and after ablation therapy. Radiofrequency ablation (RFA) is an increasingly practiced treatment option for patients with liver a malignancy not suitable for surgery. There are two important steps for optimal treatment of liver malignancy with RFA; localization of the ablative needle within the malignant lesions and adequate monitoring of the ablation process. A typical example of differences in optical spectra of a human liver tumor before and after RFA from our own data is depicted in Figure 1b.

Three studies have investigated the optical spectra of porcine or canine liver tissue in combination with spectroscopy towards possible human application. Buttemere *et al* demonstrated a significant increase in scattering and decrease of absorption as a result of thermal ablation *in vivo* in a canine study⁹¹. Moreover, they demonstrated a red shift in fluorescence peak and decrease in overall fluorescence of ablated compared to normal liver tissue. Anderson *et al* performed studies during ablation of both canine and porcine liver focussing on real-time spectral changes in the different zones of ablation⁹². With a combination of DRS and FS, the authors discovered remarkable increases in DRS intensity, with a peak at 720 nm and decreases in FS intensity, with a peak at about 480 nm. In addition, they could correlate specific intensity changes to distinct phases of thermal ablation, while spectral changes remained stable after termination of ablation and when tissue had returned to normal temperature. In subsequent real-time study of porcine liver with FS, the authors were able to accurately detect irreversible cell damage from thermal injury⁹³. They discovered irreversible hepatocellular injury to correlate to an abrupt decrease of 87% fluorescence emission intensity at 470 nm.

Hsu *et al* analysed changes of diffuse reflectance spectra during insertion of an optical needle through metastases of colorectal origin of two human patients⁹⁴. They demonstrated significant decrease of absorbance in the malignant lesions compared to normal liver tissue. Finally, Nachabé *et al* recently demonstrated bile to be an important new tissue absorber in an *ex vivo* analysis of human tissue⁹⁵. Bile was illustrated to be an important discriminative tissue component between normal and malignant liver tissue.

Kidney

Laparoscopy as well as percutaneous local ablation of renal tumor masses has resulted in an increasing need for rapid discrimination of normal from malignant renal tissue. Such need is an important incentive for spectroscopy studies of this organ.

Parekh *et al* compared results from *ex vivo* DRS and FS analysis of both normal kidney tissue and renal tumors⁹⁶. Main discriminative parameters were increased total hemoglobin content, collagen and scattering property in the malignant tissue.

Bensalah *et al* demonstrated significant differences between benign and malignant renal tissue samples *ex vivo* by analysing differences in spectral measurement slopes acquired during DRS ⁹⁷. The same group displayed results of similar analysis with Raman spectroscopy in a subsequent paper ⁹⁸. Authors analysed 27 clear cell and 6 papillary renal tumors in comparison to normal tissue. Classification accuracy between benign and malignant renal tissue spectra was 84%, moreover discrimination between malignant subtypes was possible with 93% accuracy. Improved figures were displayed by Wills *et al* who used Raman spectroscopy for *ex vivo* classification of normal renal tissue from nephroblastoma tissue specimen ⁹⁹. They proved a sensitivity of 94% and specificity of 91%. Lieber *et al* recently performed an analysis of the same renal tumor using both FS and Raman ¹⁰⁰. Authors obtained 81% sensitivity and 100% specificity with FS. In the analysis with Raman spectroscopy these figures were improved to 93% sensitivity and 100% specificity.

Table 1. Comparison of the optically measured physiological tissue parameters in different organs. Symbols indicate whether the parameter is higher (↑), lower (↓) or similar (≈) in tumor compared to normal tissue. Blank areas indicate that the tissue parameter was not reported in the study. DRS – Diffuse Reflectance Spectroscopy, FS – Fluorescence Spectroscopy

Organ	Reference	DRS					FS		
		Blood content	Tissue saturation	β-Carotene	Mean Scatter coefficient	Collagen	NADH	Tryptophan	
Skin	Brancaleon <i>et al</i> [44]					↓		↑	
Oral cavity	Amelink <i>et al</i> [50]	↑	↓						
	McGee <i>et al</i> [55]	↑	↓	↓		↓			
Breast	Zhu <i>et al</i> [59]		↓	↓	↑				
	Brown <i>et al</i> [60]	↑	↓						
	Nachabé <i>et al</i> [38]		~	↓	↑				
	Volynskaya <i>et al</i> [69]	↑		↓			~		
	Zhu <i>et al</i> [71]		↓	↓		↑	↑		
	Palmer <i>et al</i> [63]							↓	
	Keller <i>et al</i> [72]					↑			
Cervix	Mourant <i>et al</i> [76]	~	↑						
	Chang <i>et al</i> [77]	↑	~		↓				
	Keller <i>et al</i> [78]					↓			
Lung	Bard <i>et al</i> [79]	↑	↓		↑				
	Fawzy <i>et al</i> [81]	↑	↓						
Gastro-intestinal tract	Wang <i>et al</i> [89]	↑	↓						
Kidney	Parekh <i>et al</i> [96]	↑			↑	↑			

CONCLUSIONS

Multiple human organs have been included in previous studies towards incorporation of OS in various clinical applications. When comparing discrimination accuracy between the published studies and spectroscopy subtypes the wide range in these figures becomes apparent. In all studies involving DRS, sensitivity and specificity ranged from 67 to 100% and from 60 to 100%, respectively. For FS these figures are respectively between 70 to 100% and 63 to 100%. For RS figures for sensitivity and specificity are given ranging from 82 to 100% and from 87 to 100%. Although, RS may generally show the highest discriminative accuracy, results from the different optical spectroscopy techniques cannot directly be compared. Major disadvantages of RS are that the spectra are more difficult to detect and analyse compared to FS and DRS. Moreover, instrumentation requirements are more rigorous than those for FS and DRS making the clinical application increasingly challenging. These are arguably the main reasons for OS research to focus on clinical applications with DRS and FS.

Despite variations in discrimination accuracy between recent studies, similarities in various tissue parameters in different organs are apparent when comparing malignant to benign tissue (Table 1). Increased values of total hemoglobin content, collagen, NADH and FAD have been measured in breast cancer. In comparison, increased total hemoglobin content has also been displayed in malignancies of the lungs, the gastrointestinal tract, the cervix and oral cavity. Hypoxia within a tumor has been documented to be a crucial factor with progression of the cellular malignancy^{101,102}. Tissue saturation was decreased in breast-, lung-, gastrointestinal- and oral cavity cancer. The group of Sterenborg discovered variations in tissue oxygen saturation of cancer tissue between different organs^{50,61,79,80}. They hypothesized that the tissue saturation measured with spectroscopy could be inversely correlated to the aggressiveness of the tumor.

The measured contents of several other malignant tissue parameters are not uniform in all organs. Collagen levels in breast and kidney cancer are relatively raised, but in cervical, skin, stomach and oral cavity tumors these are relatively decreased compared to the surrounding normal tissue. Increased levels of collagen in breast and kidney malignancies are thought to be due to increased vascularity of the tumors. Collagen type 1 is an important component of artery walls. Another explanation could be the desmoplastic response, or growth of fibrous of connective tissue in and around malignancies of these organs^{96,103}. It must be stated that highest collagen contents in the breast have been measured in benign fibroadenoma^{64,73}. Decreased levels of collagen measured in cancerous tissue could be a result of collagenase or matrix metalloproteinase activity. Collagenases are involved in the transformation process between squamous epithelium and columnar epithelium¹⁰⁴. Up-regulation of matrix metalloproteinases has been demonstrated in skin and oral cavity tumors^{46,55}. Decreased intensities of collagen spectra of the stomach are thought to be a

result of thickening of gastric mucosa layer due to malignant cells proliferation. Spectra intensities of collagen type 4 located in the basal membrane of the stomach are therefore decreased⁸⁷.

The differences of collagen content will have an effect on the differences in the scattering coefficient measured in various malignant tissues. Increased scattering has been measured in malignancies of the breast, lung and kidney; meanwhile decreased scattering has been displayed in (pre)-malignant cervical lesions. These results are conform changes in collagen content in these organs.

Finally, variations in the level of the amino acid Tryptophan have been detected. Levels are generally raised in skin cancer. This has been addressed to hyperproliferation of epidermis of these lesions⁴⁴. However, in breast cancer levels of Tryptophan are decreased, which could be a result of decreased protein content in malignant cells⁶³. Another explanation could be a result of the tissue to which the breast cancer is compared with spectroscopy. Tryptophan levels are higher in adipose tissue compared to glandular tissue. Thus, significant differences in spectroscopy measurements will depend to which *normal* breast tissue and the malignant tissue is compared¹⁰⁵.

Future prospective

OS is an exciting optical technology that could change the workflow of cancer management in the near future. Extensive research across the frontier of human cancers has demonstrated the feasibility of optical spectroscopy for the discrimination of malignant tissue from normal tissue. In the next decade a translation of this technology into clinical practice is expected. Prospective analysis of spectroscopy systems as well as clinical *in vivo* trials in human have recently been initiated. Several areas within the care circle of cancer where OS could cause important improvement are surgical margin analysis, optical biopsy, and therapy response monitoring.

With regard to surgical margin analysis, Wilke *et al* published preliminary results of a prospective study with a novel multi-channel optical spectral device for surgical margin analysis in the operating theatre directly after breast conserving surgery¹⁰⁶. They achieved a sensitivity of 79% and specificity of 67% for immediate post-operative surgical margin analysis compared to histopathology. Future studies towards intra-operative tumor margin analysis will be performed with this optical system. Keller *et al* performed a similar tumor margin analysis of breast tissue directly after excision⁷². With a single-channel optical device DRS and FS analysis was performed at random locations of the excised breast tissue surface. Correct optical classification was achieved with a sensitivity of 85% and specificity of 96%. Many systems, however, still rely on point measurements that significantly limit screening of larger surface areas. For the near future, the main challenge will be the design of optical systems that allow rapid analysis of larger tissue surface areas.

Within clinical practice of interventional radiology, OS techniques are expected to emerge within several years. Several groups are currently concentrating on developing and validating optical biopsy needles for *in vivo* use. Zhu *et al*¹⁰⁵ and Alchab *et al*¹⁰⁷ recently published *in vivo* analysis of a FS device incorporated into a biopsy needle. Zhu *et al* performed FS analysis in various breast tissue location and subsequent biopsy and histopathology analysis were compared. They demonstrated sensitivity and specificity figures of 81% and 87%, respectively. Alchab *et al* published results of a feasibility study with FS-biopsy needle prototype. Results of a prospective study with this biopsy system are to be expected soon.

The introduction of optical spectroscopy techniques into therapy response monitoring of cancer lesions could in theory have an enormous impact on cancer treatment. Current response monitoring is generally only performed after multiple regimens of systemic therapy. The prospect of a novel techniques capable of accurate monitoring of therapy response after only a *first* regimen of systemic chemotherapy would be revolutionary. Several groups have recently focussed on the use of OS for therapy response monitoring. Ostrander *et al* demonstrated differences in redox-ratio in estrogen-receptor positive breast cancer cell-lines in-vitro measured with FS. Decrease of redox-ratio correlated with response to therapy with tamoxifen¹⁰⁸. If these results could be confirmed *in vivo* redox-ratio could be an important monitor or predictor for therapy-response. Palmer *et al* displayed a combined DRS and FS system for the monitoring of tumor physiology *in vivo*, primarily based on tumor oxygenation in murine models. They demonstrated successful results of tissue oxygenation monitoring during fluctuation oxygen supply¹⁸. These results are yet to be validated in humans *in vivo*. For therapy response monitoring in superficial tissues such as breast tissue a non-invasive spectroscopy techniques are already utilised in *in vivo* clinical studies. The Tromberg group^{109,110} and Soliman *et al*¹¹¹ have recently demonstrated promising results of significant differences between treated and non-treated patients within weeks after systemic treatment was started.

In summary, after many years of basic research, optical spectroscopy has reached the point for translation into clinical practice. The technique shows great potential to contribute to clinical decision-making in the field of clinical oncology. Clinical trials are just starting to appear and various clinical applications are currently been investigated.

Part 2



Chapter 4

Diffuse Reflectance spectroscopy: a new guidance tool for improvement of biopsy procedures in lung malignancies

D.J. Evers

R. Nachabé

H.M. Klomp

J.W. van Sandick

M.W. Wouters

G.W. Lucassen

B.H.W. Hendriks

J. Wesseling

T.J.M. Ruers

INTRODUCTION

Essential first steps in the diagnostic work-up after detection of a suspected lung mass include describing the anatomical extent as well as the cellular origin of the tumor. Biopsy or fine needle aspiration of the lesion for further analysis is a crucial step in this process. For intra-thoracic lesions, this is often performed percutaneously. Correct localization of the biopsy needle within the target lesion is essential for success of this procedure and is frequently performed under image-guidance using computed tomography (CT).

Recent studies have reported varying figures of overall accuracy for thoracic biopsies, which respectively range between 67% and 96%¹¹²⁻¹¹⁶. Main factors influencing the biopsy accuracy are location and size of the intra-thoracic lesions as well as respiratory motion during the biopsy procedure. Moreover, even correct localization of the biopsy needle within the target lesion can still result in indefinite pathology diagnosis when the biopsy only consists of necrotic cell debris. Hence, a considerable number of patients undergoing percutaneous biopsies will subsequently require a repeated biopsy or even surgical intervention to obtain tissue material for diagnosis before an individualized treatment plan can be initiated.

In recent years, promising achievements in specific tissue discrimination have been made in the field of diffuse reflectance spectroscopy (DRS), which may allow improved accuracy in cancer diagnostics^{15,17,117}. With this optical technique changes in the spectral distribution of light, as a result of either absorption or scattering of light, are recorded after the light has interacted with molecules in tissue. Subsequently, the collected spectral information is translated into morphological and physiological information. Changes in human tissue associated with malignant transformation include alterations in cellular composition, metabolic rate, vascularity, intra-vascular oxygenation and tissue morphology. DRS is sensitive to such changes in tissue, enabling discrimination between normal tissue and tumor. Ultimately, incorporation of this technology into biopsy needles may improve tip localization of the biopsy needle within the tissue compared to image-guided localization.

Many human tissue types have been subjected to optical spectroscopy with promising results for clinical application of this technique. Only a few studies involving optical spectroscopy have focused on the characterization of human lung tissue. Those published mainly involved the incorporation of DRS or Fluorescence spectroscopy (FS) into bronchoscopy tools^{79-82,118}. Detection of superficial abnormalities during bronchoscopy procedures has proven to be enhanced with use of spectroscopy techniques within this setting. Sensitivity of DRS and FS ranged between 70 and 86%, specificity ranged between 68 and 82%.

Recently, we have developed and validated a novel DRS system combining detection of visual (VIS) and near-infrared (NIR) light spectrum ^{23,33,38,95}. In contrast to most previous studies with DRS that focus on the VIS part of the spectrum, we included the NIR (1000-1600 nm) spectrum, which enables to determine accurately water and lipid content in tissue as these two biological substances mainly absorb light of wavelengths above 900 nm ²³.

The aim of this report is to assess the discrimination accuracy of our DRS system between normal lung tissue and tumor in an *ex vivo* analysis.

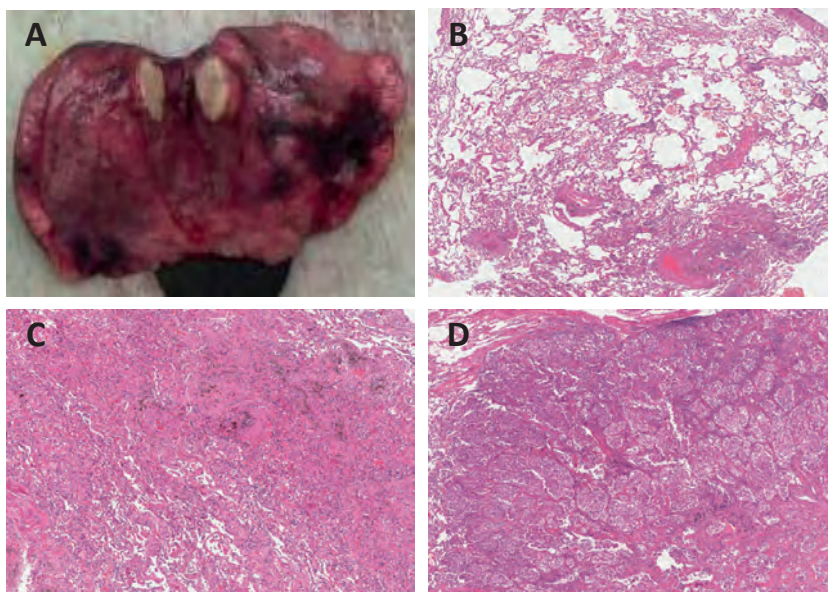
MATERIALS AND METHODS

Clinical study design

This study was conducted at The Netherlands Cancer Institute (NKI-AVL) under approval of the internal review board committee. Lung tissue was obtained from 10 patients who had undergone a pulmonary resection (lobectomy or segmental resection) for primary non-small cell lung cancer or pulmonary metastases.

Directly after resection, tissue was transported to the pathology department for optical spectroscopy analysis. After gross inspection by the pathologist, the optical spectra were collected from macroscopic normal tissue and tumor samples. Spectroscopy measurements were performed on freshly excised tissue within two hours after the resection. Each specific measurement location was digitally photographed during the procedure. Figure 1A depicts a photograph of a resected lung sample with a cut through the tumor. A total of 330 optical measurements were performed on 67 tissue locations of both normal lung tissue and tumor. Resection specimens were then fixed in formalin. The measurement locations were subsequently selected and excised according to the measurement locations on the photos. These tissue samples were paraffin-embedded, cut in 2- to 3- μm -thick sections and stained with standard hematoxylin/eosin staining. An experienced pathologist, who was blinded for the outcome of the spectroscopy analysis, examined the histological slides.

Figure 1. (A) Photograph of a resected lung sample with the tumor visualized. Examples of H&E stained pathology slides of normal lung tissue with (B) pink appearance and (C) dark appearance as well as (D) lung tumor tissue.



Instrumentation

The instrumentation and calibration procedure of our optical spectroscopy model have been described recently by Nachabé *et al*^{23,33,38,95}. In short, *ex vivo* diffuse reflectance spectra were measured with a portable spectroscopic system as described earlier³⁸. The system consists of a console comprising a Tungsten/Halogen broadband light source and two spectrometers. The spectrometers resolve light either between 400 nm and 1100 nm (Andor Technology, DU420A-BRDD, Belfast, Northern Ireland) or from 800 up to 1700 nm (Andor Technology, DU492A-1.7). An optical probe containing three optical fibers was connected to the optical setup. As depicted in Figure 3 in Chapter 1, one fiber is connected to the light source and the two other fibers are connected to the spectrometers to collect diffusely scattered light from the tissue. The optical probe has a diameter of 1.3 mm. The illumination optical fiber is located at a distance of 2.48 mm from the two side-by-side optical fibers that are used to collect the diffused light. Such a setup enables spectral acquisition in the range between 500 to 1600 nm via an optical fiber with its distal end placed against the samples.

Light-tissue interaction and optical spectroscopy

The light delivered by the illumination optical fiber is subject to optical absorption and scattering. Each biological substance in the probed tissue has its intrinsic optical absorption property as a function of wavelength. The most common biological substances that absorb light are blood-derived chromophores such as oxygenated and deoxygenated hemoglobin, but also chromophores water and lipid²³. Oxygenated and deoxygenated hemoglobin have the most dominant absorption coefficients in the wavelength range below 900 nm, whereas water and lipid have the most dominant absorption coefficient above 900 nm²³. Each of these chromophores has a well determined optical absorption spectrum available in literature²³. The total absorption coefficient corresponds to the sum of each of these chromophore-specific absorption coefficient weighted by the respective volume fraction that it occupies within the total probed volume. In addition to absorption, light is also subject to optical scattering in tissue due to its morphological irregularities at a structural level yielding deflection of the light rays after interaction with the different substances present in tissue. The optical scattering is defined by a reduced scattering amplitude at an arbitrarily given wavelength (e.g. at 800 nm) and a slope. The diffused light that is collected at the detection optical fibers corresponds to a non-linear mathematical relation of the wavelength-dependent absorption and scattering properties³⁶. The volume of the probed diffused light in tissue is mainly dependent on the absorption and scattering properties as well as the distance between the illumination and collection fibers. Given the specification of the optical probe that was used in this study and the range of tissue absorption and scattering properties over the wavelength range of interest (i.e. 500 to 1600 nm), the average probed volume is roughly 5 mm³.

Spectral data processing

Two different lung tissue types were classified in the spectral data processing: normal lung tissue and tumor. Furthermore, measured spectra from all included measurement locations were separated into either the *training* data set (N = 171 optical measurements from 35 tissue locations) or the *validation* data set (N = 159 optical measurements from 32 tissue locations). This was accomplished by randomly dividing measurement sets from different tissue locations of both normal lung tissue and tumor from each included patient between the two data sets. The histological breakdown of the optical measurements performed in these patients is displayed in Table 1.

Finally, all acquired spectra were analyzed in two ways: First, an analytical model derived from the diffusion theory was used to estimate the various chromophore volume fractions and scattering coefficients³⁶. Second, a statistical classification of the tissue spectra was performed using partial least squares discriminant analysis (PLS-DA)³⁴.

Model-based analysis.

Validation of the analytical model that was used to recover the chromophore volume fractions and scattering coefficients from the measurements has recently been described^{23,33,38,95}. Diffuse reflectance spectra measured from the tissue were fitted over the wavelength range from 500 to 1600 nm. A non-linear Levenberg-Marquardt inversion algorithm was used to estimate the various unknown chromophores volume fractions from the spectra within the analysis wavelength range. This inversion consists of determining the optimum volume fractions of the chromophores of interest as well as the reduced scattering amplitude (which we arbitrarily defined at 800 nm) and slope, which minimizes best the residual between the model and the measurement²³. A total blood volume fraction is computed as the sum of the estimated oxygenated and deoxygenated hemoglobin volume fraction by considering a total hemoglobin concentration of 150 mg per ml of blood; oxygenation level in tissue computed as the ratio of oxygenated hemoglobin to the total blood volume fraction. The other parameters related to absorption are the water volume fraction and adipose tissue volume fraction. The absorption coefficient of each of these chromophores in its pure state is used as *a priori* knowledge during the fitting procedure. An example of a spectral measurement on a normal lung sample and a tumor sample with the corresponding fitting curve are shown in Figure 2. The spectral characteristics analysis was performed with Matlab software package (MathWorks Inc., Natick, MA). Quantified mean values for tissue parameters were calculated based on all tissue measurements and were displayed in box plots.

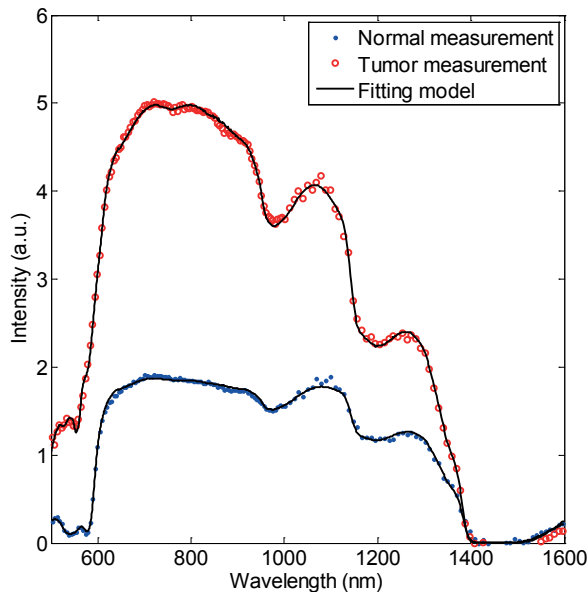
Subsequently, we used the data from the *training* data set to design a decision tree for automated discrimination between normal lung tissue and tumor. This was performed

using the *Gini index maximisation* and has recently been described by Nachabé *et al* ³⁸. By applying this evaluation method, thresholds of the most significantly discriminating tissue parameters are yielded from which all included tissue measurements could be differentiated into either tissue class with the least number of evaluation steps. The calculated thresholds were depicted as a decision tree.

Table 1. Histological breakdown of tissue samples used for data analysis. N = 10 patients.

Measured tissue types	Optical measurement locations (training + validation set) N=67	Optical measurements (training + validation set) N=330	Optical measurement locations (validation set) N=32	Optical measurements (validation set) N=159
Normal Lung tissue	30	145	14	66
Tumor	37	185	18	93

Figure 2. Example of spectral measurements in normal lung tissue with macroscopic pink appearance (see Figure 1B) (blue or point-marked curve) and tumor tissue (red or circle-marked curve) and corresponding fits (black or solid line curves).



PLS-DA analysis.

Partial least squares (PLS) analysis is a regression method to find a linear relationship between a response variable Y (tissue type class) and the independent variables X (spectra). The method is based on finding a number of principal components (PC) that represent as much of the variance in X as possible and are relevant to the response variable Y . The PLS model is generated using part of the data, the *training* data set. A discriminant analysis (DA) method is subsequently performed to obtain thresholds for discriminating the different responses (tissue classes). Prediction of class (tissue type) on the remaining data (the *validation* data set) is obtained by comparing the predicted PLS scores with the DA thresholds. The measured tissue type is assigned to one of the two predefined tissue classes depending on the PLS scores. The PLS-DA algorithm scripts were implemented in MATLAB 7.2 (MathWorks) using PLS Toolbox 5.8 (Eigenvector Research, Inc, Wenatchee, WA).

Statistical analysis

The DRS-estimated quantification of each parameter in the lung tissue cannot be described by a parametric distribution such as the Gaussian distribution. The statistical differences between the two distinguished lung tissues were therefore determined using a non-parametric Kruskal-Wallis test¹¹⁹. P-values smaller than .05 were considered statistically significant.

Discriminative accuracy for both the model-based and PLS-DA analysis were determined by comparing the means of all tissue spectra from each measurement location of the *validation* data set to the yielded thresholds from each analysis method and assigning each collected tissue spectrum to either defined tissue class. These results were then compared to the histology analysis and were subsequently presented in terms of sensitivity, specificity and overall accuracy.

RESULTS

Five of the included patients were men and five were women. All patients were smokers and the average age was 61 years old (range 38 to 74 years). Six of the patients had undergone neo-adjuvant treatment. Eight of the measured tumors were primary lung tumors and the remaining two measured tumors were metastases from the colon and from a melanoma.

Tissue parameter quantification

Tissue parameter quantification was performed as part of the model-based data analysis using all of the 330 collected optical spectra. Quantification was primarily performed on all relevant tissue parameters as well as on the reduced scattering coefficient at three different wavelengths. The tissue parameters with the most discriminative relevance were *total hemoglobin volume fraction*, *water volume fraction*, *adipose tissue volume fraction* and *reduced scattering coefficient at 800 nm* (Figure 3). Significant statistical differences were only demonstrated for *hemoglobin volume fraction* ($P < .001$) and *reduced scattering coefficient at 800 nm* ($P < .01$).

Classification accuracy

Model-based analysis. The computed decision tree based on tissue parameter thresholds is demonstrated in Figure 4. The means of all collected tissue spectra from each measurement location could be assigned to either tissue class based on thresholds yielded from *hemoglobin volume fraction* and *reduced scattering coefficient* in a two-step analysis. Results from the tissue parameter quantification of the validation data set were analysed according to the defined thresholds. Compared to the histology analysis overall discriminative accuracy of the model-based analysis was 84% (Table 2).

PLS-DA analysis. Results from the PLS-DA classification analysis of the spectra are displayed in Figure 5. For several measurements difficulty discriminating between normal lung tissue and tumor was apparent. Overall discriminative accuracy of the PLS-DA analysis was 81% (Table 3).

Figure 3. Boxplots of diagnostically relevant tissue parameters. N = 330 tissue measurements from 67 measurement locations. Hb+HbO₂ = total hemoglobin volume fraction (P = <.001); H₂O = water volume fraction (P = .364); Fat = adipose tissue volume fraction (P = .059); μ_s = reduced scattering coefficient at 800 nm (P = .009).

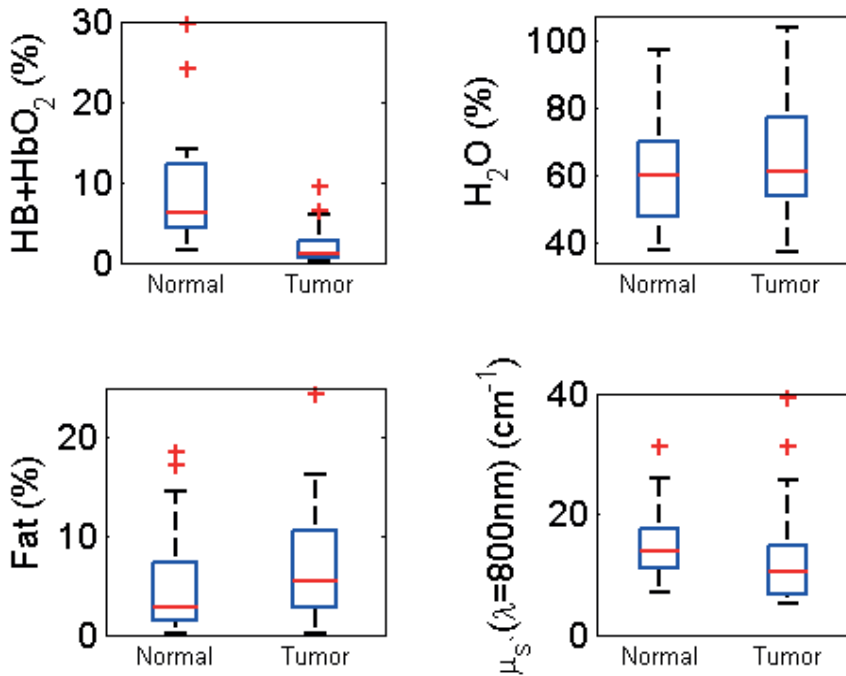


Figure 4. Discriminative thresholds for automated discrimination between normal lung tissue and tumor depicted in a decision tree. Thresholds were calculated based on quantification of tissue spectra from the training data set. N = 37 measurements locations. μ_s = reduced scatter coefficient.

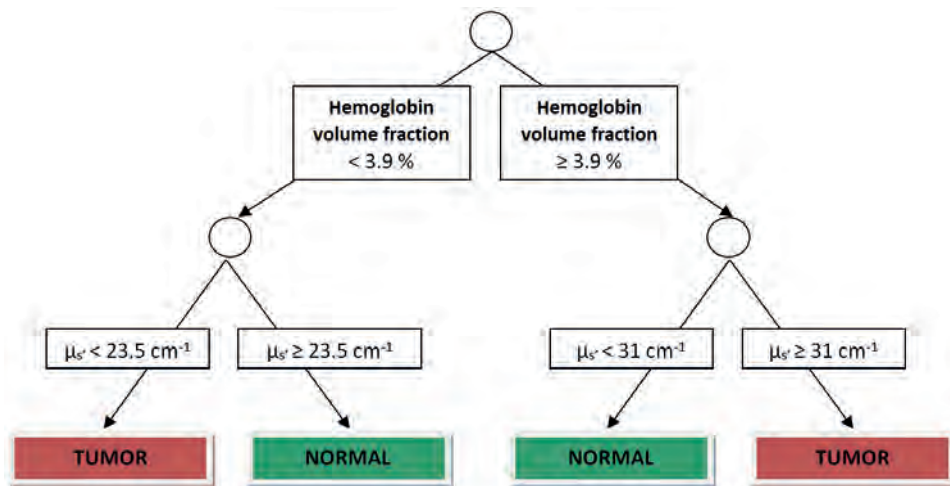


Figure 5. PLS-DA classification of the spectra of DRS measurements comparing normal lung tissue to malignant tissue. Each square represents a tissue measurement from which the spectrum is compared to the spectral thresholds acquired from the training data set analysis. N= 32 measurement locations. Red circles represent the histological diagnosis *tumor* and green squares *normal lung tissue*.

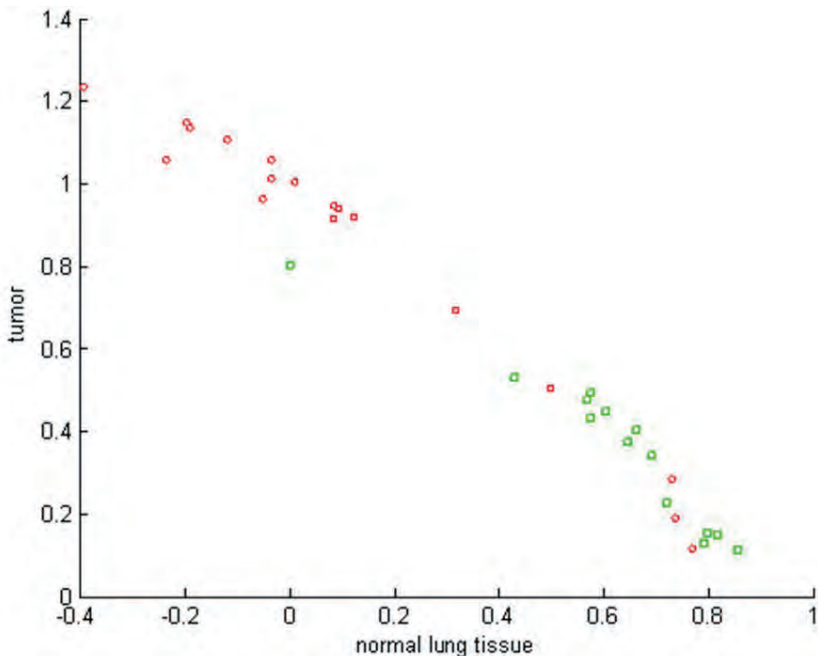


Table 2. Model based classification accuracy of DRS measurements of lung tissue divided into 2 classes compared to the pathology analysis. N= 32 measurement locations. Sensitivity = 89%; Specificity = 79%; Overall accuracy = 84%

Pathology	Model based analysis	
	Tumor	Normal lung tissue
Tumor (N=18)	16	2
Normal lung tissue (N=14)	3	11

Table 3. PLS-DA classification accuracy of DRS measurements of lung tissue divided into 2 classes compared to the pathology analysis. N= 32 measurement locations. Sensitivity = 78%; Specificity =86%; Overall accuracy = 81%. PLS-DA = Partial least squares discriminant analysis.

Pathology	PLS-DA	
	Tumor	Normal lung tissue
Tumor (N=18)	14	4
Normal lung tissue (N=14)	2	12

DISCUSSION

To our knowledge, this report demonstrates first published results of a novel Diffuse Reflectance Spectroscopy system, combining the analysis of spectral results after *ex vivo* lung tissue illumination with both visual and near-infrared light. Research with DRS on other human tissue has proven the potential of this technique for tissue discrimination. As yet, including near-infrared spectra beyond 1000 nm has not been performed^{58-60,77,89}. The advantage of having an additional spectrometer that resolves light above 900 nm is the possibility to measure spectra in a range where water and lipid have high absorption coefficients²³. Therefore accurate volume fractions of these biological substances can be determined and used for classification in addition to the commonly used blood derived chromophores and scattering parameters^{79,80}. Although no significant differences were observed between normal and tumor in water, Figure 3 shows that estimated water distribution is skewed to higher values in tumor than normal lung tissue. We expected that the water volume fraction would be significantly higher in tumor tissue compared to normal because normal tissue consists of air filled alveoli compared to more solid tumor tissue that contains no air. Because of the design of the study, most of the measured normal lung tissue samples resembled a dark appearance. The pathology analysis of these tissue samples showed collapsed alveoli in the normal lung tissue, which caused the darker visual appearance (See Figure 1C). The measurements in normal lung tissue with collapsed alveoli and subsequent decreased fraction of air could hamper the discrimination of normal lung tissue versus tumor based on water content. This phenomenon would not be expected in an *in vivo* setting with mainly air filled alveoli. Therefore DRS measurements including the NIR light spectrum, being able to determine accurately the water volume fraction, could be valuable for the discrimination in an *in vivo* setting. From the box plots, one can further notice that normal lung samples have significantly higher blood volume fraction than seen in tumors. This can be seen in Figure 1A with the malignant white lesion surrounded by normal lung tissue. The scattering of tissue is higher in normal than in tumor samples according to the box plots. This is mainly due to the pockets of trapped air in the alveoli of normal lung tissue (even after excision) that yields to greater light scattering (related to refractive index changes in tissue) as opposed to the solid tumors.

Using two different data analysis methods our DRS system yielded a promising overall discriminative accuracy of 84% for the model-based data analysis and 81% for the PLS-DA analysis compared to the pathology analysis. These results indicate that DRS has the potential to enhance diagnostic accuracy during minimal invasive thoracic procedures in combination with conventional imaging techniques.

In clinical practice, the main objective for correct localization of the needle within the target lesion is accurate identification of the tumor itself. High specificity of an imaging

modality is therefore the most important parameter. Hence, the higher the specificity, the lesser indeterminate results can be expected. In previously published papers specificity for thoracic biopsies, mainly performed with CT guidance, ranges from 83 to 97%. Thus resulting in indeterminate biopsies in 3 to 17% of the patients¹¹²⁻¹¹⁶. An indeterminate biopsy is defined as a biopsy which was thought to be taken from the target lesion, but cannot be characterized as malignant tissue by the pathologist. A combination of biopsy with CT imaging and displayed DRS incorporated in a biopsy needle could in theory improve this biopsy specificity. This hypothesis, however, will have to be proven in future *in vivo* experiments.

Additional arguments can be given about the expected feasibility of DRS in an *in vivo* analysis. First, we would expect tissue scattering to have a more significant discriminative effect in an *in vivo* analysis. Hence, in the *in vivo* setting the alveoli will be filled with air. The expected scattering will therefore be higher compared to the *ex vivo* collapsed alveoli due to the larger refractive index mismatch between air and human tissue. Thus, the expected difference in the scattering coefficient compared to solid tumor will be larger. Second, we expect the water volume fraction to show more difference between the normal and tumor tissue due to the air filled alveoli. Third, we expect a greater number of significant discriminative tissue parameters in *in vivo* measurements. The main discriminative tissue parameters in this study were total hemoglobin volume fraction and the reduced scattering coefficient at 800 nm. Fawzy *et al* and Bard *et al* both demonstrated similar results with these tissue parameters in their *in vivo* analysis of bronchial mucosa^{79,81}. Another important distinguishing parameter in their studies was tissue oxygen saturation. Both studies demonstrated tissue oxygen saturation to be diminished in cancerous lesions in comparison to normal lung tissue. In our DRS analysis, no significant differences in tissue saturation were displayed between normal lung tissue and tumor. Overall fitting results of our optical measurements revealed an average oxygenation in normal lung tissue of 31% (SD $\pm 22\%$) compared to 24% (SD $\pm 22\%$) in measured tumor tissue (data not displayed). This is most likely due to the nature of this analysis and the *ex vivo* optical measurements. Moreover, during the operation the target tissue specimen is progressively impaired from blood circulation before final resection is performed.

For future analysis we plan to combine DRS with Fluorescence spectroscopy. Discriminative accuracy of such a combined spectroscopy system has been proven to be superior to each spectroscopic technique alone in two recent studies of human breast tissue^{69,73}. Thus, an overall improvement of our discriminative accuracy is to be expected in future *in vivo* experiments of lung tissue.

Although our results are promising, a critical assessment must be made. First, although analyses were performed on a significant number of measured spectra, which are comparable to quantities in previously published studies, a restricted number of

patients (n=10) and tissue specimens were utilized. Heterogeneity between patients could have a negative effect on the discriminative accuracy. Second, total hemoglobin volume fraction was demonstrated to be the main discriminative parameter. It is unclear what the discriminative value of a comparable analysis of lung tissue in an *in vivo* setting would be in case of local hemorrhage caused by the optical needle. Hence local hemorrhage during minimal invasive spectroscopy measurement could have a negative effect on optical measurement due to the absorption properties of hemoglobin in the visual spectrum.

In conclusion, a novel Diffuse Reflectance Spectroscopy system was presented for analysis of human lung tissue. Overall discriminative accuracy of the DRS system compared to the pathology analysis was 84% and 81% for model-based and PLS-DA analysis, respectively. Based on the presented results, we conclude that DRS has the potential to enhance diagnostic accuracy in minimal invasive procedures of the lungs. *In vivo* experiments are currently being performed by our group to confirm these results as a next step towards clinical application.



Chapter 5

Optical sensing for tumor detection in the liver

D.J. Evers

R. Nachabé

D. Hompes

F. van Coevorden

G.W. Lucassen

B.H.W. Hendriks

M-L.F. van Velthuisen

J. Wesseling

T.J.M. Ruers

INTRODUCTION

In the last decade, optical sensing by means of diffuse reflectance spectroscopy (DRS) has developed into a promising technique that could make a significant contribution to the diagnosis and treatment monitoring of cancer^{17,117}. DRS is an optical measurement technique that records changes in the spectral distribution of light after its interaction with the molecules of the tissue. Main changes in the reflected spectra are a result of a combination of absorption and scattering of light. By illuminating tissue with a selected spectral band of light and subsequent analysis of the characteristic scattering and absorption patterns, it is possible to obtain an 'optical fingerprint' of the tissue. Such an optical fingerprint represents specific quantitative biochemical and morphological information from the examined tissue and may depend on metabolic rate, vascularity, intra-vascular oxygenation and alterations in tissue morphology. By allowing specific differentiation between tissues, this technique has the potential to be incorporated into optical tools for cancer diagnosis and therapy. As such, DRS is progressively being explored for sole use as well as for combined use with conventional imaging techniques. It has been employed for tissue surface analysis during endoscopic procedures but also for analysis of tissue abnormalities in solid organs^{76,79,81,88,89,97}. Several groups have investigated the improvement of tissue biopsy and surgical margin analysis with DRS for human breast cancer, demonstrating promising results in the discrimination of malignant lesions from normal breast tissue^{60,72,120}.

Also in patients with primary liver malignancy or metastatic disease to the liver, DRS might contribute to daily clinical care. For example, DRS could be incorporated into surgical tools or percutaneous intervention needles enabling direct optical guidance by real time tissue information at the tip of the instrument. Such an approach would result in guided surgery by optical sensing and might improve surgical outcome by predicting resection planes, especially for those lesions that are difficult accessible. In addition, DRS has shown to identify irreversible cell damage during RFA procedures in animal experiments, opening the potential to monitor the efficacy during percutaneous RFA ablations for liver tumors⁹⁴. Finally, DRS could be of additional value by predicting severe steatosis hepatitis and therefore preventing too extensive resections in these high-risk patients¹²¹⁻¹²⁴.

Despite the potential application of DRS in patients with liver malignancies, studies on the use of DRS in human liver tissue are scarce^{91-94,125}. Recently, a cohort analysis in patients with colorectal liver metastases showed that bile concentration, as determined by DRS, was significantly higher in normal liver tissue compared to metastatic tumor tissue⁹⁵. However, in that study a method for tissue characterisation in individual patients was still missing. To proceed to further clinical implementation we now aim to investigate whether DRS is able to discriminate tumor tissue from normal liver tissue in individual

patients. Moreover, we are interested whether the technique could assess the presence of hepatic steatosis, an important limiting factor for extensive liver resections after e.g. prolonged chemotherapy.

MATERIALS AND METHODS

Clinical study design

This study was conducted at The Netherlands Cancer Institute (NKI-AVL) under approval of the internal review board. Liver tissue was obtained from 24 patients undergoing partial liver resection for metastatic colorectal cancer. Shortly after resection, tissue was transported to the pathology department for optical spectroscopy analysis. After gross inspection by the pathologist, the optical spectra were collected from macroscopic normal liver tissue and tumor tissue. From both tissue classes, multiple measurements were performed; in total 393 DRS measurements in normal liver parenchyma and 435 in metastatic liver lesions. After data acquisition, the measurement sites were marked and specimens were fixed in formalin. After fixation, the marked tissue measurement locations were selected for cutting and processed for standard Hematoxylin and Eosin (H&E) staining. An experienced pathologist, who was blinded for the outcome of the spectroscopy analysis, examined the histological slides and visually determined if the measurements location was either tumor or normal liver tissue. In addition, for normal liver tissue the degree of steatosis was determined. The quantitative assessment of steatosis was determined by estimating the percentage of hepatocytes containing lipid droplets (both micro- and macrosteatotic droplets). The pathologic degree of steatosis was estimated with 5% steps.

DRS system and miniaturized optical probe

The instrumentation and calibration procedure of our optical spectroscopy system has recently been described elsewhere by Nachabé *et al*^{23,33,38,95}. The system consists of a console comprising a Tungsten/Halogen broadband light source, two spectrometers and an optical probe with three optical fibers. The two spectrometers resolve light in the visible wavelength range between 400 nm and 1100 nm (Andor Technology, DU420A-BRDD) and in the near infrared wavelength range from 800 up to 1700 nm (Andor Technology, DU492A-1.7), respectively. The developed miniaturized optical probe contains three optical fibers: one fiber is connected to the light source, while the other two fibers are connected to the spectrometers to capture the diffusely scattered light from the tissue³⁸. The average tissue volume that is illuminated is roughly 5 mm³. The acquisition time of each spectrum was on average 0.2 seconds.

Spectral data analysis

The light delivered by the illumination optical fiber is subject to optical absorption and scattering. Each biological substance in the probed tissue has its intrinsic optical absorption

property as a function of wavelength. In the wavelength range between 500 and 900 nm the dominant chromophores are hemoglobin (oxygenated and deoxygenated)³⁷, bile⁹⁵ and β -carotene¹²⁰. In the wavelength range between 900 and 1600 nm, the dominant chromophores are water, fat and collagen³⁸. Each of these chromophores has a well determined optical absorption spectrum available in literature²³. The total absorption coefficient corresponds to the sum of each of these chromophore-specific absorption coefficient weighted by the respective volume fraction that it occupies within the total probed volume. In addition to absorption, light is also subject to optical scattering in tissue due to its morphological irregularity. Optical scattering is defined by a reduced scattering amplitude at an arbitrarily given wavelength (e.g. at 800 nm) and a slope. The scattering characteristics are dependent on the cellular structure of the target tissue and are sensitive to size and density of cellular and subcellular structures. Total scattering is composed of *Mie* scattering (scattering of cellular particles which have a diameter of the same or higher order of magnitude than the wavelength) and *Rayleigh* scattering (scattering of cellular particles which have a diameter smaller than the wavelength).

An analytical model was used to estimate the various chromophore volume fractions and scattering coefficients from all the acquired spectroscopy measurements. This model was first described by Farrell *et al*³⁶. The measurements are fitted with the analytical model by applying a non-linear Levenberg-Marquardt inversion algorithm. Diffuse reflectance spectra acquired from the tissue were fitted and analyzed over the wavelength range from 500 to 1600 nm. Spectral characteristics analysis was performed with a Matlab software package (MathWorks Inc., Natick, MA). Quantified mean values for each tissue parameter were calculated and displayed in boxplots.

Tissue classification analysis

A *Classification And Regression Tree* (CART) algorithm was used to automatically classify each collected tissue into either of the two defined tissue types (normal liver tissue or tumor tissue) based on the parameters (i.e. volume fractions of the various chromophores and the reduced scattering properties) derived from the measurements³⁷. With the CART algorithm, a decision tree is created based on the five most significantly different tissue chromophores and scattering parameters using a leave-one-out (LOO) cross validation scheme. Each spectrum is separately classified as either normal liver tissue or tumor tissue based on the calculated thresholds in the decision tree and was subsequently compared to the histology analysis and presented in terms of sensitivity and specificity. An advantage of the CART method is that the results can easily be interpreted and correlated to clinical details, since the input parameters are thresholds of the calculated values of the main tissue parameters. The CART analysis was performed for all acquired data collectively and also for each included patient individually. For the

individual analysis, all measurements in each defined tissue class were analyzed and compared to the corresponding histological diagnosis. We chose an arbitrary threshold of an 80% agreement between all DRS measurements at a marked tissue site and the histopathological diagnosis of that site to either determine the DRS measurements as correct ($\geq 80\%$) or define the measurements as uncertain ($< 80\%$).

Statistical analysis

The DRS-estimated quantification of each parameter in the liver tissues cannot be described by a parametric distribution such as the Gaussian distribution. The statistical differences between normal liver tissue and tumor tissue were therefore determined using the non-parametric Kruskal-Wallis test ¹¹⁹. P-levels smaller than 0.05 were considered statistically significant. The lipid fraction scored by the pathologist was the area fraction (L_{area}) of the slide containing lipid, while with the DRS method we determine the volume of lipid fraction. Assuming a homogeneous volume distribution this area fraction can be translated in a volume lipid fraction (L_{volume}) according to $L_{\text{volume}} = (L_{\text{area}})^{3/2}$. For the correlation between the DRS and pathologists quantification of steatosis, we used Spearman's rank correlation test. Analysis was performed using SPSS (Statistical Package for the Social Sciences, version 16.0).

RESULTS

A total of 24 patients were included in this study, 14 were male and 10 were female. The origin of the tumor was the colon in 17 cases and the rectum in 7 cases. Figure 1 shows the typical tissue spectra of both normal liver parenchyma and incised liver tumor tissue (colorectal liver metastases) from one of these patients. Notable spectral differences between the two tissue types are apparent. Photos of the corresponding tissue measurements and H&E stained tissue samples of the measurement locations are displayed on the right.

Tissue classification analysis

Figure 2 displays boxplots of the five most significant tissue parameters as determined by spectral analysis. All of these parameters displayed P-values < 0.0001 when distinguishing normal liver tissue from liver tumor tissue. The most significant tissue chromophores were total hemoglobin, fat and bile content. The most significant scattering parameters were the scattering at 800 nm and the ratio between the *Mie* scattering and the total scattering.

Based on these five tissue parameters a decision tree was created using the CART algorithm. Table 1 displays the classification accuracy of this decision tree for all optical DRS measurements when compared to the histology analysis. A total of 780 out of the 828 optical measurements were correctly classified in either normal liver tissue or liver tumor. This resulted in a sensitivity and specificity of both 94%.

The results of the analysis for each patient *individually* are displayed in Table 2. For each patient, the ratio of the number of correctly classified tissue measurements for both normal liver tissue and liver tumor tissue is illustrated. The data show that for each individual patient the defined tissue class on the basis of DRS measurements corresponds to the ultimate histological diagnosis. Therefore, the accuracy of DRS to predict either tissue class (normal tissue or tumor tissue) was 100%.

Hepatic steatosis

Figure 3a represents the correlation of the estimated percentage of steatosis in normal liver tissue as scored by the pathologist to the quantification of fat by the DRS analysis. The Spearman's rank correlation coefficient is 0.86. Figures 3b, c and d display examples of the optical spectra and corresponding histology specimen of three patients with different levels of steatosis in the normal liver parenchyma. The spectrum at the vicinity of 1211 nm is mainly dominated by absorption of light by lipid cells. Alteration of the spectra in this wavelength band is observed with increasing lipid content²³.

Figure 1. Comparison of two typical tissue spectra of normal liver tissue (green) and metastatic liver tumor (red). (A) The optical spectra indicate the intensity of light received by the optical needle as a function of the wavelength for both tissue types. Displayed on the right is an incised resection specimen showing the typical white metastasis in the middle and the different positions of the optical probe in normal liver tissue (B) and tumor tissue (C). Picture (D) and (E) show the corresponding histology micrographs of normal and tumor tissue (H&E staining). * Normal liver parenchyma, ** Liver tumor, † Optical needle.

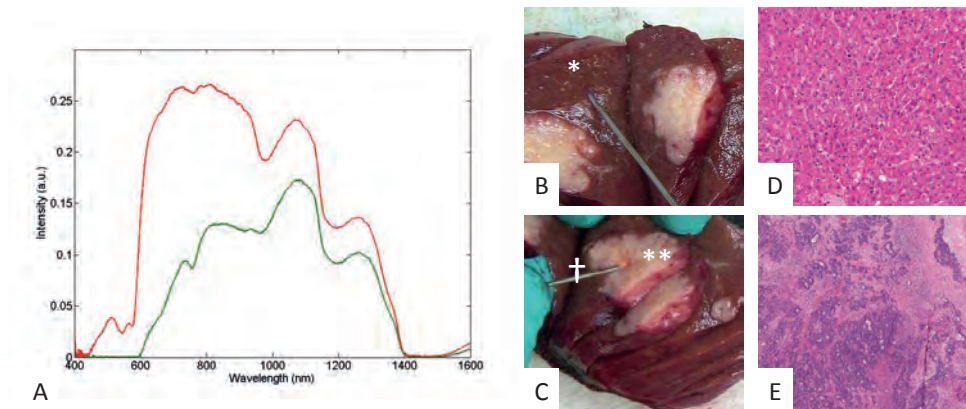


Figure 2. Boxplots of relevant tissue parameters and scattering coefficients calculated by model analysis; N=828 optical measurements. For all boxplots shown the P-values are < 0.0001. The median values for normal liver tissue vs. tumor tissue are respectively: Total haemoglobin concentration 79 μM vs. 27 μM ; Fat 7% vs. 2%; Bile 6% vs. 1%; Scattering amplitude 19 cm^{-1} vs. 11.5 cm^{-1} and Mie to total scattering ratio 0.35 vs. 0.55.

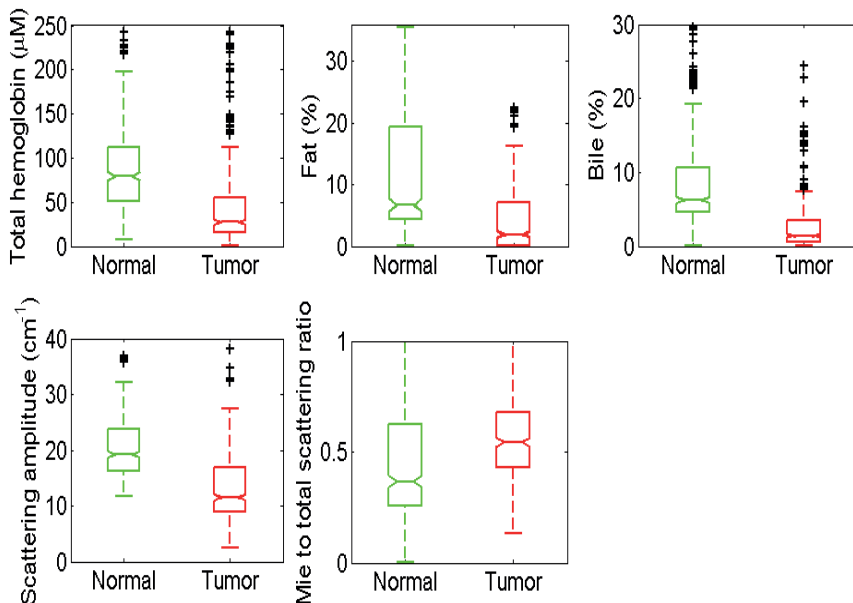


Figure 3. (A) Comparison of the quantification of the total steatosis by DRS compared to the histological analysis by a pathologist. The Spearman's rank correlation is 0.86. Examples of liver biopsies from three patients with different levels of steatosis are displayed below. The optical spectra indicate the intensity of light received by the optical needle as a function of the wavelength. Specific wavelengths from which the fat volume concentration was calculated are indicated with *dashed lines*. For each acquired spectrum, the corresponding histology slide (H&E staining) is displayed on the right. The fat volume % calculated with DRS and determined by pathology analysis for each patient were: (B) 5% and 0%; (C) 18% and 25% and (D) 28% and 45%, respectively.

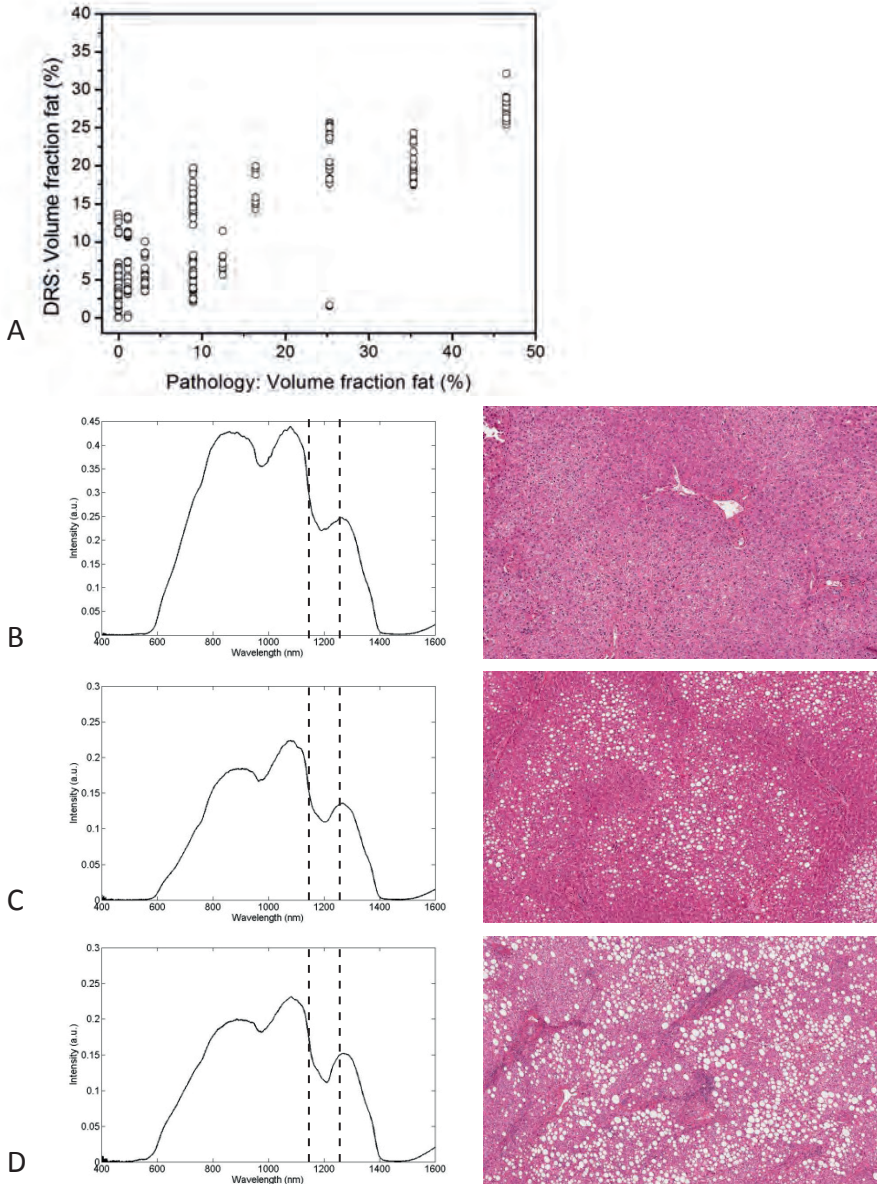


Table 1. Comparison of each optical spectrum classified with CART analysis into normal liver tissue or liver tumor compared to the histological diagnosis for each measurement location. (N = 828 measurements). Sensitivity = 94%; Specificity = 94%

Pathology	DRS	Liver tumor	Normal liver tissue
Liver tumor	(N=435)	410	25
Normal liver tissue	(N=393)	23	370

Table 2. Analysis of all performed optical measurements for each included patient individually. Between brackets, the first number is the amount of measurements the classification model correctly identified, second figure the total number of measurements performed in either normal liver tissue or liver tumor for each individual patient. The clinical diagnosis depends on the accuracy of the DRS measurements; ratio $\geq 80\%$ - the DRS diagnosis is *accepted* or ratio $< 80\%$ - the diagnosis is considered *uncertain*.

	DRS measurements normal liver tissue	Clinical diagnosis	DRS measurements liver tumor	Clinical diagnosis
Patient 1	Normal (5/5)	Normal liver	Tumor (5/5)	Tumor
Patient 2	Normal (23/24)	Normal liver	Tumor (33/35)	Tumor
Patient 3	Normal (19/19)	Normal liver	Tumor (18/18)	Tumor
Patient 4	Normal (20/20)	Normal liver	Tumor (23/24)	Tumor
Patient 5	Normal (10/10)	Normal liver	Tumor (10/10)	Tumor
Patient 6	Normal (10/10)	Normal liver	Tumor (15/15)	Tumor
Patient 7	Normal (10/10)	Normal liver	Tumor (15/15)	Tumor
Patient 8	Normal (10/10)	Normal liver	Tumor (15/15)	Tumor
Patient 9	Normal (9/9)	Normal liver	Tumor (23/23)	Tumor
Patient 10	Normal (16/16)	Normal liver	Tumor (18/18)	Tumor
Patient 11	Normal (20/21)	Normal liver	Tumor (20/20)	Tumor
Patient 12	Normal (15/15)	Normal liver	Tumor (4/4)	Tumor
Patient 13	Normal (16/16)	Normal liver	Tumor (15/15)	Tumor
Patient 14	Normal (27/27)	Normal liver	Tumor (12/13)	Tumor
Patient 15	Normal (15/15)	Normal liver	Tumor (20/20)	Tumor
Patient 16	Normal (15/15)	Normal liver	Tumor (20/20)	Tumor
Patient 17	Normal (15/15)	Normal liver	Tumor (15/15)	Tumor
Patient 18	Normal (15/15)	Normal liver	Tumor (19/19)	Tumor
Patient 19	Normal (14/15)	Normal liver	Tumor (9/10)	Tumor
Patient 20	Normal (19/20)	Normal liver	Tumor (39/40)	Tumor
Patient 21	Normal (15/15)	Normal liver	Tumor (15/15)	Tumor
Patient 22	Normal (25/26)	Normal liver	Tumor (24/25)	Tumor
Patient 23	Normal (20/20)	Normal liver	Tumor (21/21)	Tumor
Patient 24	Normal (25/25)	Normal liver	Tumor (20/20)	Tumor

DISCUSSION

DRS has been demonstrated to be a promising new optical technique for tumor diagnosis by multiple studies for over a decade^{50,51,58,61,68-71,79,81}. For several human tissue types, such as breast and oral cavity, an accuracy of up to 90% and 100% respectively were described for discrimination between normal tissue and tumor tissue. A limited number of studies investigated the application of DRS in human liver tissue, mainly focusing on spectroscopic assessment of thermal ablation^{91-93,124,125}. In a recent paper, however, we demonstrated that the quantification of bile by DRS analysis offers the opportunity for more specific tissue discrimination in liver, such as between normal liver tissue and metastatic tumor tissue⁹⁵. In continuation on these results we hypothesized that also in liver DRS is able to reach a high accuracy for the detection of tumor tissue. In the collective analysis of 828 optical measurements of 24 liver specimens, we indeed observed a sensitivity and specificity of DRS of 94% when compared to the pathology analysis.

The performance of this tissue discrimination was based on the estimated hemoglobin, lipid and bile content as well as the reduced scattering amplitude and the Mie to total scattering ratio. From these derived parameters, it can be seen that normal tissue contains more blood, bile and fat than the tumor tissues. The finding with respect to blood correlates with the macroscopic observations (Figure 1B and 1C) as normal liver is much more abundant in red blood cells compared to metastatic tumor tissue. An interesting observation compared to previous studies in other organs is the decreased total haemoglobin content in liver tumor compared to normal liver parenchyma. Previous studies have all detected higher total haemoglobin content in cancer lesions compared to normal tissue^{50,59,81,89,120}. An explanation for this difference could be due to the fact that normal liver tissue distinguishes itself from most other human organs by a relatively high vascularisation. As notable in figure 1 metastatic lesions often show significant necrotic areas due to poor vascularisation. Bile was less present in tumors as it concerns metastases from colorectal cancer and therefore very little bile is expected at these tumor sites. Another finding is that hardly any fat is present in tumors according to the derived fat content from the optical measurements. In general, hepatic metastases do not contain fat although rare cases with foci of fat in the metastases exist. Furthermore, normal tissue is found to have higher reduced scattering amplitude with a lower Mie scattering contribution as compared to tumor. This suggests that normal tissue has a larger density of small particles than tumors.

It must be noted that the present study was conducted in *ex vivo* liver tissue. It remains to be determined whether all specific tissue parameters will be comparable in human tissue *in vivo*. For example, minor haemorrhages might bear an effect on total haemoglobin content. Oxygenation of tissue might significantly change after resection. For

this reason we excluded this parameter from the analysis. The scattering and fat content parameters are unlikely to change significantly after resection since they are strongly linked to the morphology of the tissue. Also for bile significant differences between *ex vivo* and *in vivo* measurements are unlikely.

The presented results of 94% accuracy for tissue discrimination are promising, but with regards to the diagnostic accuracy of any medical instrument used in clinical practice, the main interest will be the discriminative accuracy within any *individual* patient. An overview of the discriminative accuracy of the DRS measurements for all patients individually is presented in Table 3. DRS measurements predicted the correct diagnosis for both normal and tumor tissue for each patient, indicating the potential of this technology for image guided surgery. The fact that the optical probe we used in this study is already needle sized shows that further development of specific surgical or interventional tools is within technical reach. Such tools could be used for open and laparoscopic surgical procedures as well as for interventional procedures in the radiology department. It should be stressed that the results of DRS measurements, including the analysis, are available almost real time. The present measurement and analysis time at one tissue location is about one second.

In addition, we have demonstrated a high correlation between the estimated fat content of the liver by DRS and the presence of steatosis on histological examination. This is very relevant when major liver surgery is considered, especially in those patients treated extensively with pre-operative chemotherapy. In these patients steatosis is often induced by prolonged chemotherapy and has been related to higher morbidity scores¹²⁶⁻¹²⁹. The presented results suggest that DRS could play a role in intra-operative decision-making concerning the extent of liver resection in these patients.

Although our results are promising as far the use of DRS in the clinical setting is concerned, several steps remain to be taken. First, our conclusions are based on *ex vivo* data. The next step would be to reconfirm these conclusions in an *in vivo* analysis. Furthermore, no primary liver malignancy was included in this study and the feasibility of DRS in primary liver cancer remains to be studied. This is stressed by the fact that bile is demonstrated to be an important discriminative chromophore between normal liver tissue and metastatic liver disease. In contrast to metastatic disease to the liver, primary liver cancer cells can produce bile. Therefore, the discrimination with DRS based on bile concentration might not be as significant for this tumor type as for the colorectal liver metastases presented in this paper. Further studies are needed to investigate these possible differences.

In conclusion, we have demonstrated that DRS discriminates metastatic liver tissue from normal liver tissue with a high accuracy. Moreover, DRS proves to be able to determine the extent of steatosis, identifying those patients at risk for extended resections. These

features illustrate the potential of DRS to be incorporated into image guided surgery tools. A prospective *in vivo* analysis of DRS in liver and tumor tissue is underway to confirm the clinical application of this new technology for real time imaging during surgical procedures as well as for minimally invasive procedures in the radiology department.



Chapter 6

Diffuse Reflectance spectroscopy; towards clinical application in breast cancer

D.J. Evers

R. Nachabé

M.J. Vrancken Peeters

J.A. van der Hage

H.S. Oldenburg

E.J. Rutgers

G.W. Lucassen

B.H.W. Hendriks

J. Wesseling

T.J.M. Ruers

INTRODUCTION

In the last decade, new optical guidance techniques have been implemented for the diagnosis and treatment of cancer ^{130,131}. One of these new optical techniques is *Diffuse Reflectance Spectroscopy* (DRS) ^{17,71,117}. DRS can differentiate tissue characteristics by their intrinsic light absorption and scattering properties at different wavelengths. By illuminating tissue with a selected light spectrum, an 'optical fingerprint' of the tissue is obtained which represents specific quantitative biochemical and morphological information. The characteristics of the DRS spectrum depend on the metabolic rate, vascularity, intra-vascular oxygenation and tissue morphology. Hence, DRS can provide detailed information of the underlying biological composition of tissue and as such has the potential to differentiate tumor tissue from normal tissue. In this way DRS may be able to improve cancer diagnosis and therapy monitoring. For example, DRS could be incorporated into biopsy needles, leading to an optical guided biopsy tool. Such a tool could reduce the number of indeterminate breast biopsies, which presently still range from 5 to 30% ¹³²⁻¹³⁵.

However, breast tissue is arguably been considered one of the most challenging human tissue types for DRS analysis due to inhomogeneity in morphology ¹²⁰. For example, breast tumors show a large diversity in histology, while the composition of normal breast tissue varies according to age and hormonal status. Despite this diversity and inter-patient variation, several groups have focussed on breast tissue discrimination with DRS ^{41,58-60,68,69,71,72}. In these studies the accuracy of DRS to differentiate between normal and malignant breast tissue varies from 65% to 90%. All studies so far have in common that a collective analysis is performed on the DRS data, resulting in an overall discriminative accuracy of DRS for the whole study population.

Although the results reported are promising, discriminative accuracy of DRS may be improved by limiting inter-patient variation. This could be accomplished by an individual patient analysis in which normal tissue is directly compared to tumor tissue for every individual patient. Moreover, such an approach also complies with clinical practice by providing an individual diagnosis to every individual patient.

It is the aim of the present study to determine the diagnostic accuracy of DRS in individual breast cancer patients. When positive, such an approach would be an important step towards the development of intelligent medical tools such as an optical biopsy needle.

MATERIALS AND METHODS

Clinical study design

This study was conducted at The Netherlands Cancer Institute (NKI-AVL) under approval of the internal review board committee. Breast tissue was obtained from 47 female patients who had undergone either a local excision or total mastectomy of the breast due to the presence of a fibroadenoma or (pre)-malignant disease. Shortly after surgical resection, tissue was transported to the pathology department for optical spectroscopy analysis. After gross inspection by the pathologist, the spectroscopy measurements were performed on freshly excised tissue within two hours after resection. The optical spectra were collected from macroscopic normal fat, glandular tissue samples and fibroadenoma lesions as well as from (pre)-malignant tissue samples. On average, five optical measurements were performed at each measurement location. A biopsy was taken from each location for histological comparison. Tissue samples were fixated in formalin, paraffin-embedded, cut in 2- to 3- μm -thick sections and stained with standard hematoxylin & eosin staining. An experienced pathologist, who was blinded for the outcome of the spectroscopy analysis, examined the histological slides. For each measurement location, the percentages of adipose, glandular and fibroadenomatous tissue as well as ductal carcinoma in-situ (DCIS) and invasive carcinoma were scored. The tissue specimen was histologically classified according to the most predominant tissue type within the biopsy specimen.

Instrumentation

The instrumentation and calibration procedure of our optical spectroscopy system has been described in recent papers^{23,33,38}. DRS measurements were performed with a console comprising a Tungsten/Halogen broadband light source, an optical probe with three optical fibers and two spectrometers. The optical probe contains three optical fibers: one fiber is connected to the light source, while the other two fibers are connected to the spectrometers to capture the diffusely scattered light from the tissue (Figure 3 - chapter 1). The two spectrometers resolve light in the visible wavelength range between 400 nm and 1100 nm (Andor Technology, DU420A-BRDD) and in the near infrared wavelength range from 800 up to 1700 nm (Andor Technology, DU492A-1.7), respectively. The average tissue volume that is illuminated is roughly 5 mm³. The acquisition time of each spectrum was on average 0.2 seconds.

Spectral data processing

We distinguished five different breast tissue classes in the spectral data processing: adipose tissue, glandular tissue, fibroadenoma, DCIS and invasive carcinoma. Additionally, we distinguished *normal breast tissue* (all tissue locations of adipose, glandular and fibroadenomatous tissue) from *malignant breast tissue* (DCIS and invasive carcinoma). The light delivered by the illuminating optical fiber is subject to optical absorption and scattering. Each biological substance in the probed tissue has its own intrinsic optical absorption property as a function of wavelength. These specific optical absorption spectra are well determined and available in literature. The total absorption coefficient corresponds to the sum of each of these chromophore-specific absorption coefficients weighted by the respective volume fractions they occupy within the total probed volume. In particular the parameters total haemoglobin concentration (the sum of oxygenated and deoxygenated haemoglobin), water, lipid, collagen volume fractions and β -carotene as well as the scattering amplitude at 800 nm wavelength are determined. Accurate water, lipid and collagen volume fraction could be derived due to the inclusion of the near-infrared part of the spectrum (wavelength range 1000 to 1600 nm)³⁸. In addition, light is also subject to optical scattering in tissue due to its morphological irregularity. Optical scattering is defined by a reduced scattering amplitude at an arbitrarily given wavelength (e.g. at 800 nm) and a slope. The scattering of light was determined because it is dependent on the cellular structure of the target tissue and is sensitive to the size and the density of cellular and subcellular structures. An analytical model was used to extract the chromophore composition and the scattering properties of the tissue samples from the measured spectra over the wavelength range from 500 to 1600 nm^{33,38,69,95,136}. This model was first described by Farrell *et al*³⁶. The measurements were fitted into the analytical model by applying a non-linear Levenberg-Marquardt inversion algorithm. Spectral characteristics analysis was performed with a Matlab software package (MathWorks Inc., Natick, MA). The distribution of the quantified values of each tissue parameter was displayed in boxplots.

Tissue classification analysis

In the spectral data processing, breast tissue was categorized into the five defined tissue classes as well as two groups either as normal breast tissue or malignant breast tissue. A Classification And Regression Tree (CART) algorithm was used to automatically classify each collected tissue into one of the defined breast tissue types based on the chromophore concentrations and scattering parameter values derived from the measurements³⁷. With the CART algorithm, a decision tree is created based absolute thresholds determined from extracted tissue parameters with the most significant

differences between the defined tissue classes. Each spectrum is then separately classified based on the calculated thresholds in the decision tree based on a leave-one-out (LOO) cross validation method and compared to the histology analysis [20]. The CART analysis was performed for all acquired data collectively and also for each included patient individually in which both normal breast tissue and (pre)malignant tissue was measured. It must be noted that the classification between normal breast tissue and malignant breast tissue in the collective analysis was performed by randomly taking an equivalent amount of samples for all tissue classes corresponding to the tissue class with the lowest sample size within both groups. This was done to avoid overestimation of the discrimination accuracy due to the higher representation of one of the tissue classes over the other within either the normal or malignant tissue group. Within the normal breast tissue group, 160 tissue measurements of both adipose and glandular tissue were randomly selected and added to the corresponding number of fibroadenomatous tissue measurements. For the malignant tissue measurements, 120 invasive carcinoma tissue measurements were randomly selected. The CART analysis was performed for all acquired data collectively and also for each included patient individually. For the individual analysis, all measurements in each defined tissue class were analyzed and compared to the corresponding histological diagnosis. We chose an arbitrary threshold of 80% agreement of all DRS measurements at a marked tissue site with its histopathological diagnosis in order to either determine the DRS measurements as correct ($\geq 80\%$) or define the measurements as 'uncertain' ($< 80\%$).

Previously, the CART analysis with LOO cross validation scheme was studied by Nachabé *et al* and compared to other generally used spectral classification algorithms³⁸. The main advantage of the CART method is that the results can easily be interpreted and correlated to clinical details, since the input parameters are thresholds of the calculated values of the main tissue parameters.

Statistical analysis

The DRS-estimated quantification of each parameter in the breast tissue classes cannot be described by a parametric distribution such as the Gaussian distribution. The statistical differences of each parameter in the defined tissue classes were therefore determined using the non-parametric Kruskal-Wallis test¹¹⁹. P-values smaller than 0.05 were considered statistically significant.

RESULTS

Tissue specimens

A total of 47 breast tissue specimen from female patients were included into this study. The mean age at time of operation was 52 years (range 20 – 74 years). Within the 47 resected tissue specimen, 160 measurements were performed in 32 locations of fibroadenomatous lesions, 121 measurements in 24 areas of DCIS and 314 measurements in 35 invasive carcinoma lesions. Five of these lesions were lobular carcinomas and 30 were ductal carcinomas. In addition, 294 measurements were taken in 79 areas of adipose tissue of the breast specimen and 184 measurements in 37 areas of glandular tissue, giving a total of 1073 DRS measurements (Table 1).

Cohort data analysis

Chromophore volume fractions and scattering coefficients were calculated from each tissue measurement using the analytical model. The distributions of each of the six most significantly different tissue parameters for all five distinguished tissue classes are depicted in Figure 1. Adipose tissue is best distinguished from the other tissue classes by fat, water, and β -carotene content, as well as by the scattering coefficient at 800 nm. Also fibroadenomatous tissue can clearly be discriminated from the other five tissue classes based on fat and β -carotene content. For the other tissue classes such as glandular tissue, invasive carcinoma and DCIS there is a notable overlap in the parameters measured and further analysis was performed using the CART algorithm.

Using the results of the most significantly different tissue parameters, each measurement was diagnosed by the CART algorithm and assigned to one of the five defined tissue classes as well as classified as either normal breast tissue or malignant breast tissue. The results of the five-class distribution as indicated by the CART algorithm are displayed in Table 1. A high specificity ($\geq 90\%$) for all tissue classes was noted. The result of discrimination between normal and malignant breast tissue samples is displayed in Table 2. After random selection of the tissue classes within both groups to fit the amount of measurements of the tissue class with the lowest sample size, the comparison of DRS to the pathology diagnosis yielded a sensitivity of 90% and a specificity of 88%. Overall accuracy was 89%.

Tissue heterogeneity

The microscopic heterogeneity of the various tissue samples is illustrated in Figure 2. Three examples of invasive carcinoma are displayed with different percentages of malignant tissue within the specimen based, respectively 20%, 50% and $>90\%$ invasive

carcinoma as determined by pathology analysis. The corresponding measured spectrum for each sample displays notable differences when compared. To further investigate how such differences may affect discriminative accuracy in distinguishing glandular tissue from invasive carcinoma, all of the 314 measurements of invasive carcinoma were divided into <50% or >50% malignant cells within the tissue specimen. Next, the quantification of tissue parameters in both groups was compared to all glandular tissue measurements. The results of the differences in quantification of most notable tissue parameters in the two malignant groups compared to glandular tissue are displayed in table 3. Both malignant groups can be discriminated from glandular tissue based on the parameters total haemoglobin count and fat. No significant differences between malignant and glandular tissue are illustrated for the parameters scattering at 800nm, β -carotene and collagen, when the percentage of invasive carcinoma within the tissue specimen is < 50%. These parameters did illustrate significant discriminative accuracy when ratios of invasive carcinoma are > 50%.

In one of the 47 tissue specimens, all five defined tissue classes were present and could be examined. Results of the tissue and spectral analysis are displayed in Figure 3. For each tissue sample, a marked heterogeneity of the histology is notable. For each tissue class, the acquired optical DRS spectrum is displayed. To discriminate the five tissue classes, the scattering coefficient at 800nm wavelength was plotted versus the fat content. When comparing the five tissue classes for this individual patient based on these two parameters (Figure 3F), the five classes can clearly be discriminated from each other despite tissue heterogeneity.

Individual data analysis

Since, the number of tissue classes was limited per patient, discriminative accuracy was focused on the ability of DRS to differentiate normal breast tissue (adipose, glandular and fibroadenomatous) from malignant breast tissue (invasive carcinoma and DCIS). Results of all performed measurements and the discriminative accuracy between normal and malignant breast tissue on an individual basis are displayed in Table 4. In all patients, except two, the specificity was 100%. In these two patients only 1 out of 10 and 1 out of 17 measurements in benign tissue the DRS diagnosis was false positive for malignancy. In only 3 of the 36 patients the sensitivity for the diagnosis malignancy, as determined from all the measurements, was not 100%. In these 3 patients the percentage of false negative measurements varied from 5 to 37%. When an arbitrary threshold is used of a 80% agreement between all DRS measurements and the pathology analysis for each individual patient to a certain a diagnosis, only in one out of 36 patients (patient 6) the DRS diagnosis was defined 'uncertain'.

Figure 1. Boxplots of most significantly different tissue parameters. DCIS - ductal carcinoma *in-situ*; H₂O - water; μ_s - scattering; μM - micromolar; λ - wavelength; nm - nanometer; cm^{-1} - reciprocal centimeter, '+' indication of 'measurements considered as outliers'

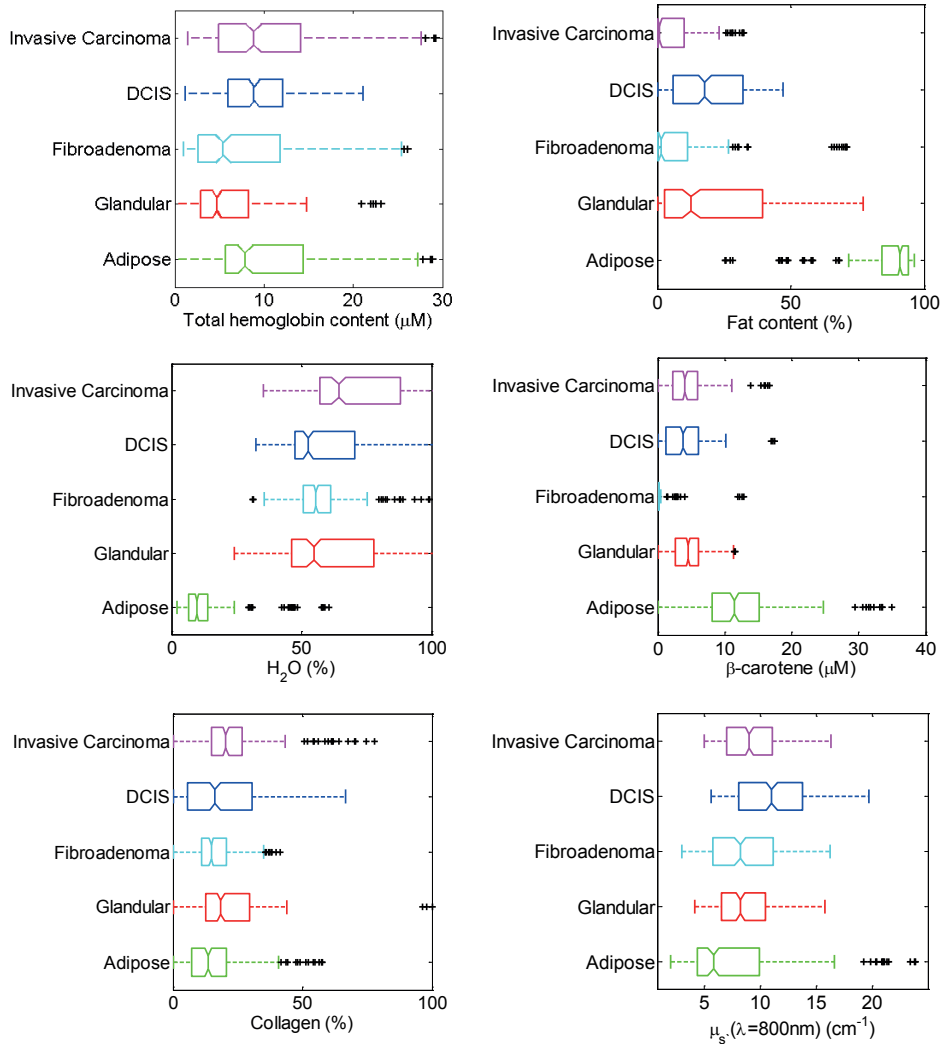


Table 1. Diagnosis for each tissue measurement generated by the DRS analysis compared to the histology diagnosis of the measurement location with the calculated sensitivity and specificity of all the measurements in each tissue class. DRS - diffuse reflectance spectroscopy; DCIS - ductal carcinoma *in-situ*; FA - fibroadenoma ; Sens. - sensitivity; Spec. - specificity

Pathology	DRS	Malignant breast tissue		Normal breast tissue			Sens. (%)	Spec. (%)
		Invasive carcinoma	DCIS	FA	Glandular tissue	Adipose tissue		
Invasive carcinoma (N=314)		268	17	6	23	0	85	90
DCIS (N=121)		22	86	1	12	0	71	95
FA (N=160)		13	5	132	10	0	83	98
Glandular tissue (N=184)		24	12	7	141	0	77	93
Adipose tissue (N=294)		9	6	0	10	269	91	100

Table 2. Classification of tissue measurements defined as normal or as malignant breast tissue. For normal breast tissue 160 measurements of randomly chosen adipose and glandular tissue measurements are included to all fibroadenoma measurements. For malignant tissue 120 measurements of invasive carcinoma were randomly selected and included with all DCIS measurements. A comparison to the pathology analysis yielded a sensitivity of 90%, a specificity of 88% and an accuracy of 89%. DRS - diffuse reflectance spectroscopy

Pathology	DRS	
	Malignant tissue	Normal breast tissue
Malignant tissue (N=241)	217	24
Normal breast tissue (N=480)	58	422

Table 3. Significant differences of the quantification of the most notable tissue parameters of all invasive carcinoma measurements with either <50% or >50% malignant cells within each tissue specimen compared to the glandular tissue measurements. THC - total hemoglobin content; μM - micromolar; nm - nanometer; ~ - Tissue parameter not significantly different for glandular tissue compared to invasive carcinoma; \uparrow / \downarrow - tissue parameter respectively higher of lower in the invasive carcinoma compared to glandular tissue with a P-value < 0.05; $\uparrow\uparrow / \downarrow\downarrow$ - tissue parameter respectively higher of lower in the invasive carcinoma compared to glandular tissue with a P-value < 0.0005.

Parameter	Invasive carcinoma 0-50%	Invasive carcinoma 50-100%
THC (μM)	$\uparrow\uparrow$	$\uparrow\uparrow$
Fat %	$\downarrow\downarrow$	$\downarrow\downarrow$
B-carotene %	~	\downarrow
Collagen %	~	$\uparrow\uparrow$
Scattering (800 nm)	~	$\uparrow\uparrow$

Figure 2. Example of the pathological heterogeneity within several tissue samples defined as invasive carcinoma. a.u. - arbitrary units; nm - nanometer A. Invasive carcinoma \approx 20% B. Invasive carcinoma \approx 50% C. Invasive carcinoma > 90%

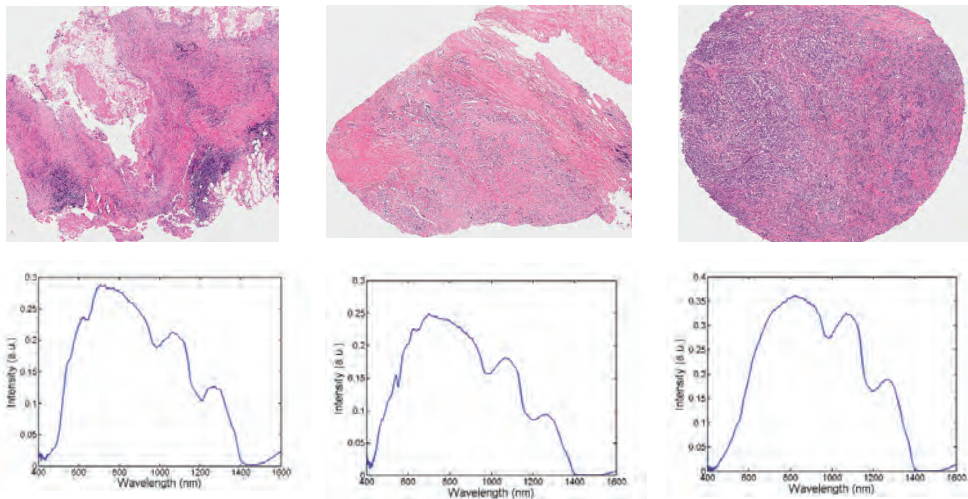


Figure 3. H&E staining of the five different tissue classes within one of the included patient specimen. A. adipose tissue; B. glandular tissue; C. fibroadenomatous tissue; D. DCIS; E. invasive carcinoma. The percentages of the main tissue components as defined by the pathologist. The DRS spectrum for each tissue sample is depicted. In F. the distribution of all the measurements for each defined tissue class based on the quantification of scattering at 800nm and Fat content from each tissue spectrum is illustrated. DCIS - ductal carcinoma in-situ; a.u. - arbitrary units; nm - nanometer; cm⁻¹ - reciprocal centimeter

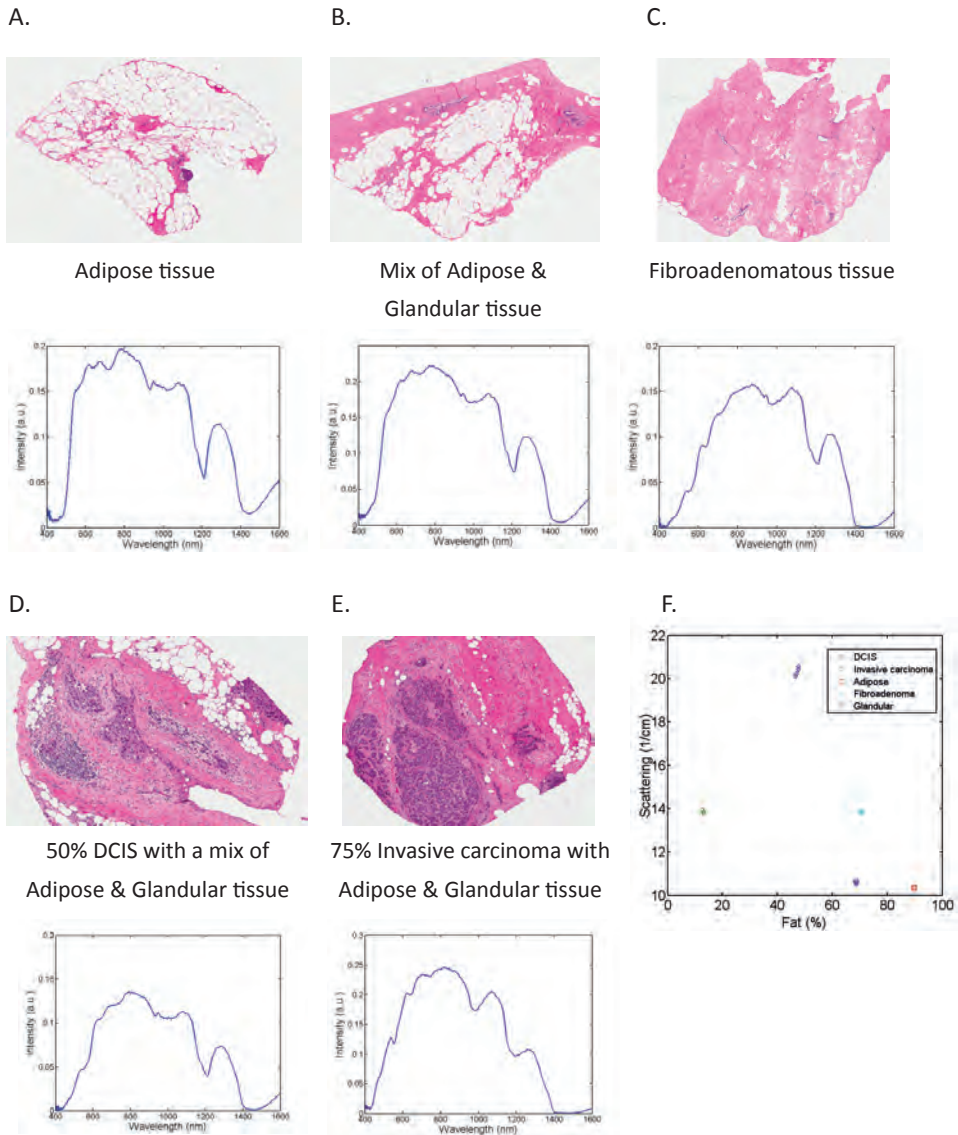


Table 4. Illustration of all measurements for each defined tissue class for each patient individually. The results of the discriminative accuracy between all normal and malignant tissue measurements for each patient in which these both groups were present (N=36). For 11 patients only measurements in normal or benign breast tissue were acquired. FA - fibroadenoma; DCIS - ductal carcinoma *in-situ*; DRS - diffuse reflectance spectroscopy; sens. - sensitivity; spec. - specificity

Patient	Adipose tissue	Glandular tissue	FA	Clinical diagnosis DRS 'normal breast tissue'	Spec. (%)	DCIS	Invasive carcinoma	Clinical diagnosis DRS 'malignant breast tissue'	Sens. (%)
1	10	-	-	10 / 10	100	5	-	5 / 5	100
2	-	-	10	-	-	-	-	-	-
3	5	4	-	9 / 9	100	10	10	20 / 20	100
4	5	-	20	-	-	-	-	-	-
5	5	9	-	14 / 14	100	-	9	9 / 9	100
6	-	10	-	9 / 10	90	8	-	5 / 8	63
7	-	4	-	4 / 4	100	-	20	20 / 20	100
8	-	10	-	10 / 10	100	-	5	5 / 5	100
9	5	4	-	9 / 9	100	-	10	10 / 10	100
10	5	-	-	5 / 5	100	-	10	10 / 10	100
11	-	-	28	-	-	-	-	-	-
12	8	-	25	-	-	-	-	-	-
13	5	-	-	5 / 5	100	21	-	21 / 21	100
14	4	-	-	4 / 4	100	-	20	20 / 20	100
15	5	-	-	5 / 5	100	-	10	10 / 10	100
16	8	5	-	13 / 13	100	-	19	19 / 19	100
17	10	-	-	10 / 10	100	-	7	7 / 7	100
18	5	9	-	14 / 14	100	-	10	10 / 10	100
19	10	-	-	10 / 10	100	-	10	10 / 10	100
20	9	-	10	-	-	-	-	-	-
21	-	-	24	-	-	-	-	-	-
22	10	-	-	10 / 10	100	14	-	14 / 14	100
23	5	-	-	5 / 5	100	-	10	10 / 10	100
24	9	9	-	18 / 18	100	-	19	19 / 19	100

Table 4. Continued

Patient	Adipose tissue	Glandular tissue	FA	Clinical diagnosis DRS 'normal breast tissue'	Spec. (%)	DCIS	Invasive carcinoma	Clinical diagnosis DRS 'malignant breast tissue'	Sens. (%)
25	10	5	-	15 / 15	100	14	-	14 / 14	100
26	10	-	-	10 / 10	100	4	10	14 / 14	100
27	10	10	-	19 / 20	100	20	-	19 / 20	95
28	10	10	-	20 / 20	100	-	10	10 / 10	100
29	10	-	-	10 / 10	100	-	10	10 / 10	100
30	4	-	10	-	-	-	-	-	-
31	5	-	-	5 / 5	100	-	15	15 / 15	100
32	10	10	-	20 / 20	100	-	10	10 / 10	100
33	5	10	-	15 / 15	100	-	5	5 / 5	100
34	6	5	5	16 / 16	100	5	5	10 / 10	100
35	4	10	-	14 / 14	100	-	5	5 / 5	100
36	10	10	-	20 / 20	100	10	10	20 / 20	100
37	5	5	-	-	-	-	-	-	-
38	5	-	-	5 / 5	100	10	10	20 / 20	100
39	5	4	8	-	-	-	-	-	-
40	5	-	5	-	-	-	-	-	-
41	5	5	-	10 / 10	100	-	5	5 / 5	100
42	5	5	-	10 / 10	100	-	5	5 / 5	100
43	10	-	-	10 / 10	100	-	10	10 / 10	100
44	5	5	-	10 / 10	100	-	10	10 / 10	100
45	10	7	-	16 / 17	94	-	10	9 / 10	90
46	8	9	-	17 / 17	100	-	15	15 / 15	100
47	14	10	15	-	-	-	-	-	-
Total	294	184	160	-	-	121	314	-	-

DISCUSSION

Optical technologies, such as DRS, are increasingly being explored to support the diagnostic workflow in breast cancer. Heterogeneity in normal breast tissue and tumor tissue may, however, hamper its diagnostic accuracy. Also in the present study wide heterogeneity in the histology of the breast cancer was observed at the measuring sites. To reduce this inter-patient variability we hypothesized that an individual patient analysis would provide superior discriminative accuracy for DRS measurements compared to the generally performed analysis on patient cohorts.

To challenge this hypothesis we performed a cohort analysis as well as an individual analysis for the different DRS measurements. In addition spectra were acquired in wide wavelength range from 500 to 1600 nm, in contrast to the commonly used 500 to 1000 nm by other research groups^{23,33}.

For the cohort analysis all measurements were grouped as either benign or malignant. Sensitivity and specificity were 90% and 88%, respectively, yielding an overall accuracy of 89%. During individual analysis all measurements per patient were again categorized as either benign or malignant. The discriminative accuracy of this individual analysis was nearly 100%. Only in one patient the diagnosis was uncertain.

Several previous studies have used DRS for analysis on breast tissue^{58,59,68-73,137}. These studies use collective data from all included patients to discriminate normal breast tissue from malignant breast tissue. The resulting sensitivity for distinguishing normal from malignant breast tissue ranged from 67% to 87%, specificity from 76% to 96%. The results from the collective analysis of normal vs. malignant tissue in the present study display comparable results^{58,59,70-73}. Yet, an honest comparison between studies remains difficult due to the many different data analysis techniques used.

In contrast to most other papers, we distinguished five different tissue classes. For this purpose, DRS was performed in a wider wavelength range than previously displayed. Recent findings by Taroni *et al* showed that collagen is an important absorber to include in the model for fitting the measured spectra as it has distinct absorption features above 900 nm¹³⁸⁻¹⁴⁰. Therefore, we measured the absorption coefficient of collagen up to 1600 nm and included it in our model. Moreover, measurements on the wavelengths above 1000 nm allow better quantification of lipid and water fraction of the tissue. The boxplots clearly displayed a notable distribution range of the optical parameters within the different tissue classes. Adipose tissue and fibroadenoma could be well differentiated from the other three tissue classes, yet the discrimination of glandular tissue from DCIS and invasive carcinoma was not straightforward due to overlap in the quantification of the tissue parameters. This has also been reported by Volynskaya *et al*⁶⁹ who did not observe

any significant differences in collagen and β -carotene in these tissue classes as well as by Zhu *et al*⁷¹ with similar concentrations in β -carotene and THC.

To allow further classification several classification algorithms have been described. Volynskaya *et al*⁶⁹ and Zhu *et al*⁷¹ respectively used *logistic* regression analysis and linear support vector machine. In the present study further classification of tissue classes was performed using a Classification and Regression Tree (CART) algorithm. The overall discrimination accuracy of DRS distinguishing 5 tissue classes was 84%. Sensitivity was lowest for glandular tissue (77%) and DCIS (71%). Specificity for all tissue classes was 90% or higher.

The difficulty in discriminating between the three tissue classes glandular tissue, DCIS and invasive carcinoma can be explained when taking into mind that primary malignant degeneration in the breast is generally a gradual evolution of glandular tissue to carcinoma *in-situ* to an invasive carcinoma. Moreover, the large differences in composition between various cancerous lesions, as displayed in Figure 2, cause significant variations in collected spectra. Depending on the proportion of malignant cells within the measured specimen the different tissue parameters will be more or less significantly different from normal glandular tissue as is demonstrated in Table 3.

This difference in tumor composition as well as sampling variation and the resultant effect on the differences in quantification of the tissue parameters in relation to normal glandular tissue prompted us to investigate a more individualised analysis of the DRS measurements. Indeed, overall accuracy of individual analysis was superior to the results of the cohort analysis. Notable improvement in the discrimination accuracy by individual analysis is displayed in the Figure 3. In one of the tissue specimen included in this study, all five distinguished tissue classes could be examined (patient 34 in Table 4). Within the tissue samples of this single patient an inhomogeneous histology is apparent with various percentages of normal and malignant tissue types within each sample. Based on the scattering coefficient at 800nm and fat content each of the five tissue classes could be distinguished.

When we translate these results on individual analysis to the clinical practice of tissue biopsy, it is important to note that the acquisition of data is fast and can be performed real time. This means that accurate positioning of an optical guided biopsy needle within the target lesions becomes possible. The breast tissue analysis for each individual patient resulted in a correct clinical diagnosis of all normal breast tissue measurements and in all but one malignant tissue measurement based on an arbitrary chosen threshold of an 80% agreement between all DRS measurements and the pathology analysis. We therefore argue that, smart biopsy tools that incorporate DRS into the biopsy needle could prevent indeterminate biopsies.

Although demonstrated results in this paper are promising, specific improvements should be noted for future studies. First, the results of this study are based on *ex vivo* analysis, before clinical use of a DRS system can be considered, presented results must be confirmed in an *in vivo* analysis. In addition, the discriminative accuracy for glandular tissue could still be improved. As shown in table 1 the discrimination of glandular tissue is still less reliable than for adipose tissue. This may be due the general histological inhomogeneity in the area of breast tissue.

In conclusion, our results demonstrate that diffuse reflectance spectroscopy could improve the diagnostic workflow in breast cancer. Yet, our results are based on an *ex vivo* analysis and *in vivo* confirmation of these results is the next step towards a possible clinical application. Based on the results presented in this paper, we conclude that the analysis of optical characteristics of different tissue classes within the breast of a single patient is superior to an analysis using the results of a cohort data analysis. We argue that for future application of DRS into clinical practice, such as breast tissue biopsy, emphasis should therefore be put on individual tissue analysis. A prospective *in vivo* analysis of breast tissue is underway to confirm the presented results as a next step towards the clinical application of smart biopsy tools and surgical instruments.



Chapter **7**

Improved identification of peripheral lung tumors by using diffuse reflectance and fluorescence spectroscopy

J.W. Spliethoff

D.J. Evers

H.M. Klomp

J.W. van Sandick

M.W. Wouters

R. Nachabé

G.W. Lucassen

B.H.W. Hendriks

J. Wesseling

T.J.M. Ruers

INTRODUCTION

Although major advances are made in cancer imaging, tissue biopsies are still crucial for accurate diagnosis and treatment planning in lung cancer. Centrally located, easy-accessible lung lesions are generally sampled by bronchoscopy, whereas peripheral lesions are often biopsied by a transthoracic procedure under CT guidance. However, a major drawback of transthoracic needle biopsies is that the area of interest may be either missed or undersampled. Moreover, even when a biopsy needle is correctly localized in the target lesion, it may be non-diagnostic because only necrotic tissue is sampled.

The overall diagnostic accuracy of transthoracic lung biopsies is influenced by tumor size, location, respiratory motion and number of biopsy samples taken from the tumor. Despite the fact that positioning of the biopsy needle can be guided by CT imaging, visualization of relevant structures is often limited due to thresholds in contrast and image resolution¹⁵. Recent studies have reported failure rates for transthoracic biopsies up to 23%¹¹²⁻¹¹⁵.

Optical spectroscopy techniques such as diffuse reflectance spectroscopy (DRS) may address these shortcomings allowing real-time monitoring of tissue characteristics at the tip of a biopsy needle. The spectral response of tissue to broadband light is measured and subsequently analyzed to derive characteristics of light scattering and absorption. These properties enable the discrimination between benign and malignant tissues making DRS a promising technique for lung cancer diagnosis.

In various studies, DRS has been combined with Fluorescence Spectroscopy (FS) to improve identification of cancerous lesions in various organs^{68,69,72,80,81,141-146}. FS adds the possibility to detect intrinsic fluorophores in the measured tissue, such as collagen, elastin, FAD, NADH and porphyrins. Collagen and elastin are structural proteins and associated with cross-links and tissue structure, whereas NADH and FAD levels are indicative for cellular energy metabolism of tumor tissue²⁸. Porphyrins are organic compounds. A specific porphyrin is protoporphyrin IX (PpIX) that combines with ferrous iron to form the heme group. Some cancers such as colorectal tumors and its metastases accumulate diagnostic levels of endogenous PpIX as a result of a tumor-specific metabolic alterations¹⁴⁷. In addition, in a preclinical model a correlation was observed between PpIX and necrotic areas within tumor tissue²⁹. FS might be sensitive to these alterations in fluorophore concentrations.

The potential of combining both reflectance spectroscopy and FS to detect (pre) cancerous lung lesions has already been investigated during endobronchial procedures. Fawzy *et al* found that adding reflectance spectroscopy to FS improves the specificity for endobronchial-cancer detection compared to FS alone⁸². Moreover, Bard *et al* demonstrated that the combined use of DRS, FS and Differential Path length Spectroscopy performed better than each technique separately⁸⁰.

Most studies addressing lung cancer diagnosis with optical spectroscopy are focused on the use of this technique when incorporated in bronchoscopy tools⁷⁹⁻⁸². In previous work, we demonstrated the feasibility of DRS measurements at the tip of a biopsy needle and demonstrated its potential to enhance diagnostic accuracy of *transthoracic* biopsies. When all tissue measurements and patients were analyzed collectively, DRS yielded an overall accuracy for the identification of tumor tissue and lung tissue of 84%¹⁴⁸. The objective of the present study was to evaluate the additional value of FS as well as the potential of the combined system to predict tissue diagnosis in individual patients. To further optimize any biopsy location, the ability of DRS and FS to discriminate necrotic tumor tissue from vital tumor tissue was also investigated.

MATERIALS AND METHODS

Ex vivo lung sample collection

The study was conducted at The Netherlands Cancer Institute-Antoni van Leeuwenhoek hospital (NKI-AVL), under approval of the protocol and ethics review board. Lung tissue was obtained from 13 patients undergoing lobectomy or segmental lung resection for primary non-small cell lung cancer (NSCLC) or lung metastases from colorectal or renal origin.

Instrumentation and spectral calibration

Ex vivo diffuse reflectance spectra were acquired using a portable spectroscopic system that has been described earlier^{23,38,148}. In the present study, the possibility to perform FS was added to the system, which consists of two light sources and two spectrometers (Figure 1). For DRS measurements, a Tungsten halogen broadband light source (360-2500 nm) with an embedded shutter was used. For FS, the system was equipped with a semiconductor laser ($\lambda=377$ nm) to induce autofluorescence. Two spectrometers were included, one which resolves the light from the visible wavelength range, i.e. 400 up to 1100 nm (Andor Technology, DU420A-BRDD) and one which resolves near infrared light from 900 up to 1700 nm (Andor Technology, DU492A-1.7). The calibration procedure has been described elaborately by Nachabé *et al*²³. A 13G optical probe containing four optical fibers was used. Two fibers were connected to the broadband light source and laser and the two other fibers were connected to the spectrometers to capture light from the tissue. For DRS and FS the distance between the exit facets of the emitting and collecting fibers at the distal end was 1.90 mm and 0.32 mm, respectively. The complete optical unit was controlled by custom-made LabView software (National Instruments, Austin, TX) to acquire and save the data.

Figure 1. Schematic overview of the combined DRS and FS optical setup.

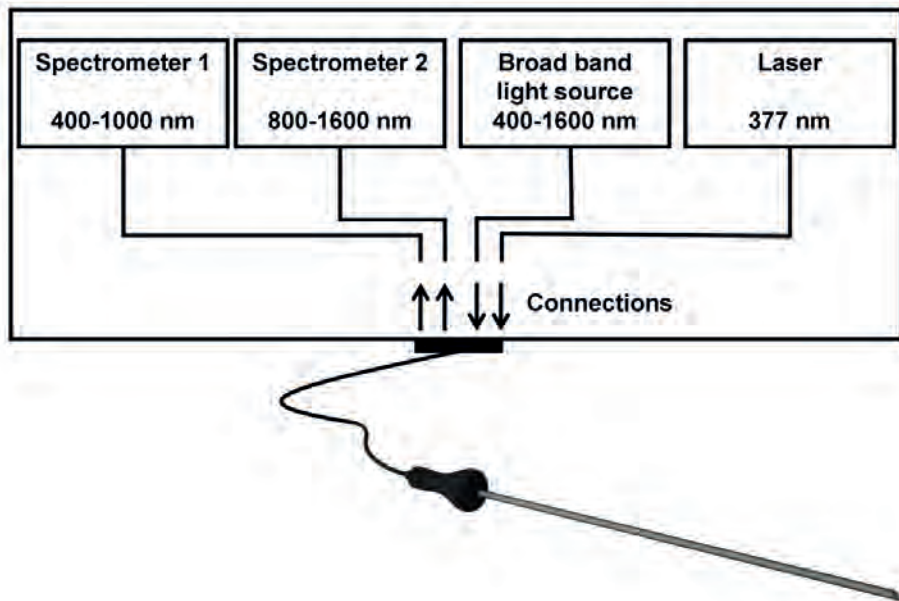
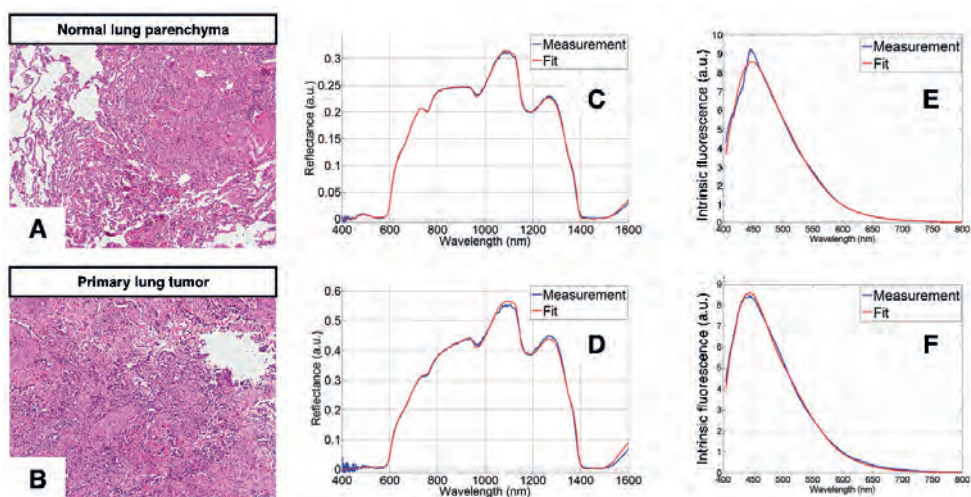


Figure 2. Examples of H&E stained pathology slides of lung parenchyma (A) and primary lung cancer (B) with corresponding spectral measurements. (C) and (D) show typical DRS measurements (blue lines) with corresponding fit (red lines) from lung parenchyma and primary lung cancer, respectively. (E) and (F) show FS measurements (blue lines) with corresponding fitted intrinsic fluorescence (red lines) from the lung parenchyma and primary lung cancer, respectively.



Optical measurements

Within two hours after surgical resection, the freshly excised tissue was grossly inspected by a pathologist and sliced to allow optical measurements of macroscopic tumor tissue and lung parenchyma. In each tissue specimen optical measurements were performed at multiple locations in lung parenchyma and in tumor tissue.

Only areas with a pink appearance were used for the lung parenchyma measurements. This selection was made since earlier experiments by Evers *et al* showed that areas characterized by a darker appearance proved to be collapsed, making any comparison to an *in vivo* setting with air filled alveoli difficult¹⁴⁸. In total 75 DRS and FS measurements were performed in lung parenchyma. A total of 179 DRS and FS measurements were acquired in malignant lung lesions.

Pathological evaluation

After the optical measurements, tissue samples were taken from the measurement locations. These were formalin-fixed and processed according to routine histopathology. Samples were stained with standard hematoxylin/eosin staining and examined by an experienced pathologist who was blinded for the spectroscopic analysis. Apart from tissue differentiation, slides were scored for the percentage of tissue necrosis. Optical measurements were compared to histopathological analysis, as gold standard.

Spectral data analysis

DRS analytical model. In this study a widely accepted analytical model, introduced by Farrell *et al* was used to estimate the various DRS chromophore volume fractions and scattering coefficients³⁶. The main absorbing constituent (chromophores) in normal tissue dominating the absorption in the visible range (400-800 nm) is hemoglobin (oxygenated and deoxygenated), whereas water, fat and collagen are the main absorbers in the wavelength range 900-1600 nm³⁸. The main scattering parameters are the reduced scattering at 800 nm and the Mie-to-total scattering fraction. The total scattering of tissue is assumed to be defined by Mie and Rayleigh scattering. Mie scattering occurs when light meets objects whose size is similar to the wavelength (e.g. biological cells and cellular components), whereas Rayleigh scattering is elastic scattering of light by particles which are much smaller than the wavelength of light (e.g. macromolecular aggregates, collagen fibrils). The validation of the DRS analytic method has been described previously^{23,33}. The input arguments for the model are the absorption coefficient $\mu_a(\lambda)$, the reduced scattering coefficient $\mu'_s(\lambda)$, and the distance between the exit facets of the emitting and collecting fibers at the tip of the probe.

FS analytical model. Intrinsic fluorescence was calculated by correcting the acquired fluorescence spectra for absorption and scattering. For the latter, a modified photon migration method²⁶ was used, based on work by Müller *et al*³⁹ and Zhang *et al*¹⁴⁹. In this theory the light propagation in a turbid medium is described in terms of photons traveling in paths with discrete photon-tissue interaction events where absorption, scattering or induction of fluorescence can occur. The corrected spectra were fitted by using the intrinsic fluorescence spectra (excitation at 377 nm) of collagen, elastin, NADH and FAD as a priori knowledge²². The optical oxidation-reduction (redox) ratio, which is a measure of cellular metabolic state, is defined as the ratio between NADH and FAD^{108,150}. In this work the optical redox ratio is expressed as NADH/ (NADH+FAD). An example of spectral measurements on a lung parenchyma sample and a tumor sample with the corresponding fitting curves are shown in Figure 2.

Porphyrin quantification. As shown by Moesta *et al*¹⁴⁷, cancer tissue may accumulate diagnostic levels of endogenous porphyrins. Quantification of porphyrins using our standard fit procedure, however, was not feasible since the exact wavelength of the fluorescence bands of porphyrins depend on the environment (e.g. pH) in which it is measured¹⁵¹. To still quantify the fluorescence of porphyrins, the area underneath the porphyrin peaks was calculated after removing the background. This was done by connecting the minima on each side of the porphyrin peaks and subtracting the area beneath this line from the total area under the peaks.

Classification and statistics

A Classification and Regression Tree (CART) algorithm was used to evaluate the performance of discriminating the different tissue types on either DRS or FS parameters or both. The CART algorithm is a recursive partitioning method that creates a classification tree from the values derived from a training set of spectral data and subsequently assigns a novel spectrum to a preselected tissue class by using the generated classification tree³⁷. A leave-one-out (LOO) cross validation scheme was used based on the estimated parameters from the fit model. Each spectrum was separately classified as either lung parenchyma or tumor tissue based on the calculated thresholds in the decision tree and was subsequently compared to the histopathological analysis. Outcome was presented in terms of sensitivity and specificity.

For each patient multiple optical measurements were performed at separate locations. These measurements allow individual patient analysis that eliminates bias from inter-patient variation. To investigate the performance of DRS in individual patients, the LOO classification was performed for all measurements on individual patients. Arbitrary, when at least 80% of the measured DRS spectra at a specific measurement site corresponded to histopathological diagnosis of that site, the measurements were considered as being

correctly classified. Otherwise, the measurements were considered uncertain.

The estimated DRS and FS tissue parameters could not be described by a Gaussian distribution. Therefore, a non-parametric Kruskal-Wallis test was applied to evaluate significant differences in optical parameters between lung parenchyma and tumor tissue for a significance level of 1% (i.e., $p < 0.01$)¹¹⁹. Both the quantified DRS and FS parameters were displayed in boxplots.

RESULTS

Patient and tumor characteristics

Thirteen patients were included, median age was 60 years (range 49-70 years). Ten participants were men, all patients were smokers. Six patients had primary lung cancer, six patients had lung metastases from colorectal cancer, and one patient had lung metastasis from renal cell cancer. Optical measurements of one patient were not further used, since the site of measurement showed only mucus at histopathological analysis. The median tumor size was 24 mm (8 - 50 mm).

Optical parameter quantification and classification

In Figure 3, boxplots of relevant DRS and FS parameters are shown. Regarding DRS, lung parenchyma and tumor tissue differed significant with regard to total hemoglobin, hemoglobin oxygenation, water, collagen, reduced scattering at 800 nm and Mie-to-total reduced scattering fraction. No notable amounts of fat were encountered in any of the analyzed tissue samples. For FS measurements, significant differences between lung parenchyma and tumor tissue were observed for: NADH, FAD, and the optical redox ratio.

The DRS and FS parameters were used by the CART algorithm to generate a decision tree and calculate overall diagnostic accuracy. The sensitivity and specificity of the tissue classification between lung tumor tissue and lung parenchyma are displayed in Table 1. With DRS alone, a sensitivity and specificity was achieved of 98% and 86%, respectively. FS alone or a combination of DRS and FS did not improve the results.

Next, the ratio of correctly classified DRS tissue measurements in each individual patient was determined for both lung parenchyma and tumor tissue (table 2). Based on pathology analysis, four patients could not be used for the individual patient analysis. In these patients no lung parenchyma measurements were available. For all patients used, DRS results were identical to histopathology analysis, leading to an accuracy of DRS to characterize lung parenchyma or tumor tissue within one patient of 100%.

To further evaluate whether DRS and FS could differentiate vital tumor tissue from tumor necrosis, measurements were compared to histopathological data on tissue necrosis. Table 1 shows that FS is able to discriminate necrotic and vital tumor areas with

a sensitivity and specificity of both 91%. DRS alone appears to be less specific for tumor necrosis.

The classification tree based on FS measurements showed that the porphyrin peak near 625 nm was the main factor determining the high specificity of FS to distinguish necrotic from vital tumor tissue (figure 4). Therefore the calculated area under the porphyrin peak near 625 nm was compared to the amount of necrosis scored by the pathologist, as shown in Figure 5. The presence of the porphyrin peaks showed a correlation with the amount of necrosis, although considerable variation in porphyrin peak intensity was present. A second observation is that necrosis occurs mainly in secondary tumors rather than in primary tumors.

Figure 3. Boxplots of relevant tissue parameters; N=254 optical measurements. H_2O =water volume fraction, Collagen= collagen volume fraction, μ_s' ($\lambda=800\text{ nm}$) = reduced scattering coefficient at 800 nm.

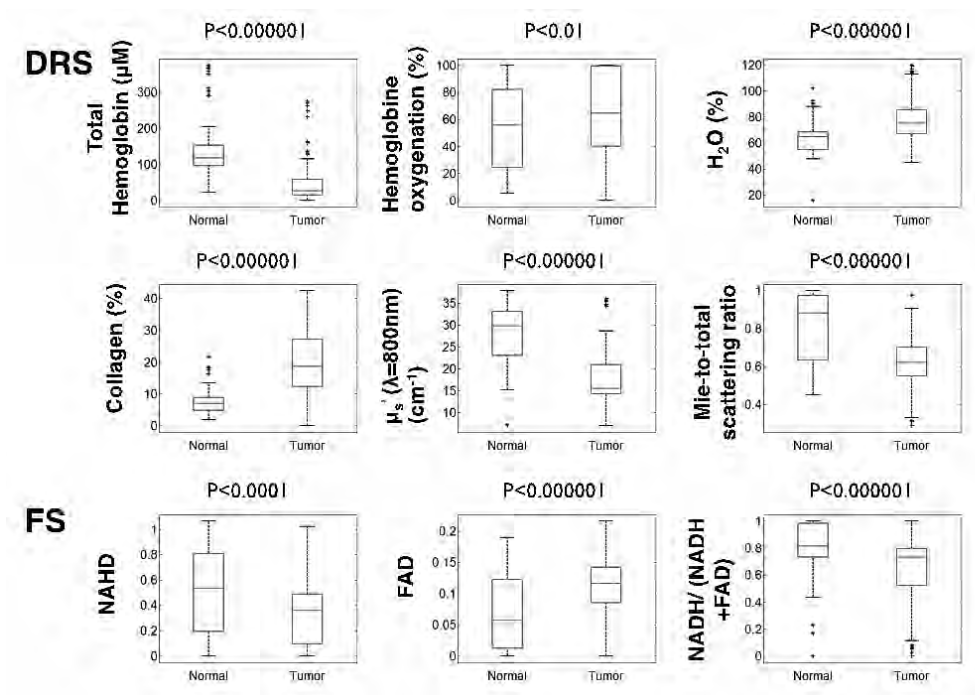


Figure 4. Difference in fluorescence spectra between vital and necrotic tumor tissue. Histology slides of vital (A) and necrotic (B) tissue of two different lung metastases from colorectal cancer with corresponding fluorescence spectra (C) and (D). The blue lines in (C) and (D) are the fluorescence measurements, whereas the red lines are the results of the model-based fitting procedure. (E) illustrates the quantification method of the additional fluorescence peaks at 600-750 nm.

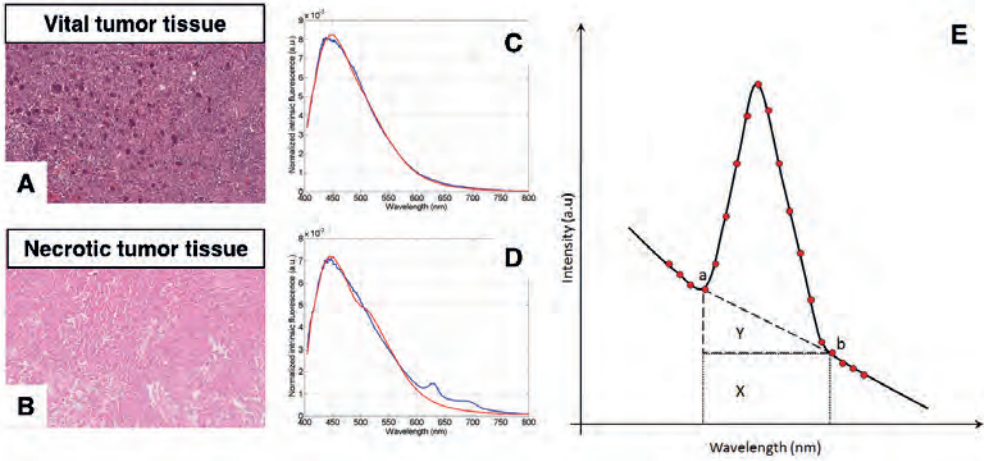


Figure 5. Variation in Porphyrins related to necrosis and tumor type. In patient 13 multiple locations were measured.

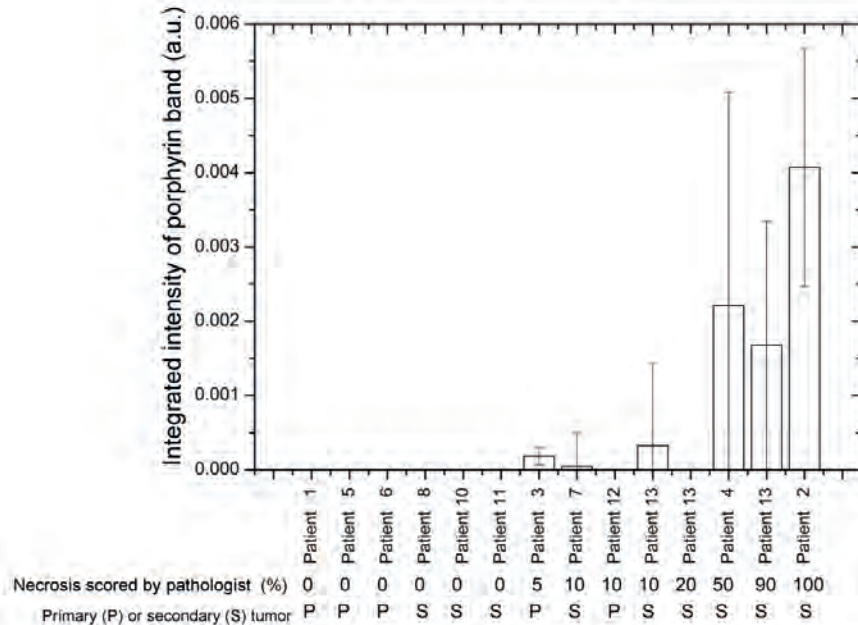


Table 1. Sensitivity and specificity of the tissue classification. Performance of discriminating the different tissue types based on Diffuse Reflectance Spectroscopy (DRS) and Fluorescence Spectroscopy (FS). Upper: discrimination of lung tumor tissue (N=179 measurements) vs. lung parenchyma (N=75 measurements). Lower: discrimination of necrotic (N=123 measurements) vs. vital (N=56 measurements) tumor.

LOO-classification	DRS only (sens/spec)	FS only (sens/spec)	DRS+FS (sens/spec)
Tumor vs. lung parenchyma	98%/ 86%	90%/ 75%	98%/ 86%
Tumor: necrotic vs. vital	88%/ 80%	91%/ 91%	90%/ 95%

Table 2. Diagnostic accuracy by per-patient analysis. Per-patient discrimination for lung parenchyma versus tumor tissue, based on Diffuse Reflectance Spectroscopy (DRS) parameters. Between brackets: the first number indicates the number of correctly classified measurements, the second number represents the total number of measurements taken. The clinical diagnosis was based on histopathological analysis.

	Ratio of correctly classified DRS measurements in lung parenchyma	Clinical diagnosis	Ratio of correctly classified DRS measurements in lung tumor	Clinical diagnosis
Patient 1	Lung parenchyma (9/10)	Lung parenchyma	Tumor (10/10)	Tumor
Patient 2	Lung parenchyma (5/5)	Lung parenchyma	Tumor (10/10)	Tumor
Patient 3	Lung parenchyma (5/5)	Lung parenchyma	Tumor (10/10)	Tumor
Patient 4	Lung parenchyma (5/5)	Lung parenchyma	Tumor (10/10)	Tumor
Patient 7	Lung parenchyma (9/9)	Lung parenchyma	Tumor (5/5)	Tumor
Patient 8	Lung parenchyma (16/16)	Lung parenchyma	Tumor (15/15)	Tumor
Patient 10	Lung parenchyma (10/10)	Lung parenchyma	Tumor (10/10)	Tumor
Patient 12	Lung parenchyma (15/15)	Lung parenchyma	Tumor (10/10)	Tumor
Patient 13	Lung parenchyma (15/15)	Lung parenchyma	Tumor (20/20)	Tumor

DISCUSSION

In this study, both DRS and FS measurements were performed within fresh pulmonary specimens with tumor areas. Several DRS parameters showed significant differences between lung parenchyma and tumor tissue. These discriminating parameters were total hemoglobin, hemoglobin oxygenation, water, collagen, scattering at 800 nm and the Mie-to-total scattering ratio.

In the present study, only optical reference measurements of pink colored lung parenchyma were used, since these were expected to be the most representative for the situation *in vivo*. The overall discriminative accuracy between lung parenchyma and malignant tissue was higher (92%) than observed in a study by Evers *et al* who also included measurements at parenchyma sites with collapsed alveoli¹⁴⁸. The comparison to non-collapsed, pink colored lung parenchyma in this study allowed for optimal identification of tumor lesions in individual patient specimens. This suggests that using optical spectroscopy should be feasible for *in vivo* identification of tumor, for example during transthoracic biopsy.

The differences in optical characteristics, such as in water content, collagen content and scattering parameters can be attributed to the fact that lung parenchyma consists of alveoli which are filled up with air, whereas tumor tissue has a more solid structure. Our setup is able to measure in the near infra-red wavelengths range up to 1600 nm where fat and water absorption bands exist. This enables accurate fraction estimation of these substances²³. Although water content proved to be a good discriminator between lung parenchyma and tumor, no significant amounts of fat were measured in either of the tissues. This is in accordance with the pathology results of the measured samples.

The combined parameters used for analysis contained sufficient information to allow discrimination between lung parenchyma and tumor tissue with a sensitivity and specificity of 98% and 86%, respectively. Individual parameters showed considerable overlap in lung tissue and tumor tissue in the pooled analysis of the patient group (Figure 3). This may partly be due to variations from patient-to-patient. When inter-patient variation was eliminated by using lung parenchyma measurements as internal reference for each individual patient, classification of tumor spectra reached a sensitivity and specificity of 100% for all included patients.

Lung cancers frequently occur in patients with chronic obstructive pulmonary diseases. The relationship between these diseases is instead one based upon mutual risk factors, namely smoking^{152,153}. In chronic obstructive pulmonary diseases like emphysema normal lung tissue architecture is affected, accompanied by the destruction of alveolar walls. Additional research is needed for evaluating effects of obstructive pulmonary diseases on optical parameters.

FS was performed to determine the intrinsic fluorescence of lung parenchyma and tumor. Lower concentrations of NADH and higher concentrations of FAD were observed in tumor tissue compared lung parenchyma, which means a decreased optical redox ratio in tumor. For epithelial cancer it has been found that this ratio increases for tumor cells ^{150,154} as well as for primary human mammary epithelial cell lines ¹⁰⁸. In this *ex vivo* study we found a decrease in optical redox ratio. After resection, the metabolism of tissue may change drastically which could explain the difference in results between our *ex vivo* results and the measurements in cell lines or living tissue.

A particular interesting finding is that additional fluorescence peaks at 625 nm and 690 nm were detected in several tumors, especially when necrotic tissue was present. Although adding FS as additional modality does not improve the potential to detect tumor lesions, it is useful for identification of necrotic tumor parts. This feature could enhance the selection of tumor biopsy sites. For example, this would be important for specific sampling of vital tumor tissue when needed such as for genetic profiling for tailored individual treatment ^{155,156}.

Earlier research has shown that some cancers such as colorectal tumors and its metastases accumulate diagnostic levels of endogenous protoporphyrin IX (PpIX) and other metabolic products of porphyrin as a result of tumor-specific metabolic alterations ¹⁴⁷. Croce *et al* investigated the presence of naturally-occurring porphyrins in a spontaneous-mammary tumour bearing mouse model. In the tumour-bearing mice elevated levels of PpIX were observed in blood plasma, liver, spleen and in tumor mass ²⁹. Remarkably high levels of PpIX were detected in necrotic parts of the tumor compared to the viable tumor areas. They explained that both a failure to complete heme synthesis by the cells still alive and undergoing necrosis and a reversal of the ferrochelatase activity could account for this finding. This study also showed that the presence of porphyrin-peaks correlates with the amount of necrosis. Our findings regarding porphyrins in lung metastasis from colorectal cancer strongly resemble the ones described in primary colorectal tumors and its metastases in liver and lymph nodes ¹⁴⁷. NSCLC can also contain considerable (spontaneous) necrotic parts. Whether porphyrin fluorescence is primarily associated with necrosis or with certain tumor types, is unknown.

In conclusion, DRS allows for accurate real-time identification of lung tumors in individual patients. It has potential to improve transthoracic lung biopsy procedures. The results presented in this work are promising for further development of “smart” biopsy tools incorporating optical technology. Furthermore, FS seems able to detect areas of necrosis. This may either help to identify and biopsy vital tumor during biopsy, or might be used to evaluate response in patients who received chemo-radiation. Clinical studies are necessary to confirm these results and to evaluate indications.

Part 3



Chapter 8

In vivo tumor detection in the liver with diffuse reflectance and fluorescence spectroscopy

D.J. Evers & E. Tanis *

J.W. Spliethoff

V. V. Pully

K. Kuhlmann

F. van Coevorden

B.H.W. Hendriks

M-L. F. van Velthuisen

W. Prevoo

T. J. M. Ruers

* Joint 1st authors for this manuscript

Submitted

INTRODUCTION

Over the last decade, significant effort has been put towards the incorporation of optical guidance techniques into cancer surgery^{157,158}. Among others, the optical spectroscopy (OS) techniques Diffuse Reflectance Spectroscopy (DRS) and Fluorescence Spectroscopy (FS) have been demonstrated to be promising techniques for tumor identification¹. When performing OS, tissue is illuminated by a selected spectral band of light. When reflected after interacting with the tissue, the light spectrum will be changed due to the specific absorption and scattering characteristics of the tissue. This obtained 'optical fingerprint' represents specific quantitative biochemical and morphological information from the examined tissue. For several human tissue types, such as breast, lung and oral cavity, accuracies over 80% have been described for discrimination between normal tissue and tumor tissue in mainly *ex vivo* analyses^{50,51,58,61,68-71,79,81,148,159-161}. Recently, we have demonstrated that also in surgical resection specimens of colorectal liver metastases (CRLM), DRS is able to accurately identify tumor lesions from normal liver^{95,162,163}.

Colorectal cancer (CRC) ranks third on the list of cancer related death. During their lifetime up to half of the CRC patients will develop liver metastases. To date, an increasing number of these patients are operated by laparoscopic or even robotic liver resection. Tactile feedback on tumor position is missing and finding the optimal resection plane is challenging. In addition, many patients receive neo-adjuvant chemotherapy before surgery, resulting in tumor shrinkage and less well defined tumor borders during resection. Under such conditions, where tactile feedback on tumor location is missing or less accurate, smart surgical devices that are able to delineate safe resection planes could be of significant help to the surgeon.

To date, there are no direct *in vivo* methods available to discriminate hepatic colorectal liver metastases from normal liver tissue. During *ex vivo* testing, optical spectroscopy has shown promising results. The aim of the present study is to investigate whether also *in vivo* optical spectroscopy is able to accurately discriminate colorectal liver metastases from normal liver tissue and whether this is influenced by neo-adjuvant chemotherapy.

MATERIALS AND METHODS

Patients

This study was conducted at The Netherlands Cancer Institute under approval of the protocol and ethics review board (protocol number: NL32233.031.10; Netherlands Trial Register: NTR2557). Patients scheduled for an open liver resection for metastatic cancer were eligible for inclusion. Written informed consent was obtained from all patients.

Procedure

Optical measurements were performed during the surgical procedure before transection of the liver parenchyma. The surgeon and radiologist identified the tumor by ultrasound and determined the intended resection plane (Figure 1). A custom-made 14G hollow guidance cannula (INVIVO, Schwerin, Germany) was inserted into the normal liver tissue within the planned resection area and the tip was positioned under ultrasound guidance, first into normal liver tissue and next into tumor tissue. A 15G (1.8mm) optical needle was introduced through the cannula protruding 1cm into the tissue. Theatre lights were dimmed during the optical measurements to prevent contamination of the collected spectra by ambient light. Four sets of five optical measurements were performed; two sets in normal liver tissue and two sets in tumor tissue. Normal liver tissue measurements were performed at least 2 cm from the edge of the metastatic lesion. Directly following the optical measurements an o-twist-marker (OTM3.0SA, Biomed. Instrumente and Produkte GMBH, Türkenfeld, Germany) was inserted through the cannula to mark the measurement locations in normal liver tissue and tumor tissue

Instrumentation

The optical spectroscopy instrumentation and calibration procedure of our system has been described previously^{23,33,38,95}. The system consists of a console comprising a Tungsten/Halogen broadband light source, two spectrometers and a 15G fibre optical needle (INVIVO, Schwerin, Germany) containing four optical fibres. The optical needle tip was slanted and the distance between emitting and collecting fibres was 1.7mm, resulting in a probing depth of ~1-2mm. The diffusely reflected light from the target tissue was collected by the two spectrometers, one which resolves light between 400 nm and 1100 nm (Andor Technology, DU420A-BRDD) and one which resolves light from 800 up to 1700 nm (Andor Technology, DU492A-1.7). The two measured spectra were merged into one single spectrum from 400nm to 1600nm. The acquisition time of each spectrum was on average 0.2 seconds.

Figure 1. Schematic display of the optical measurement setup and photo example of an optical measurement

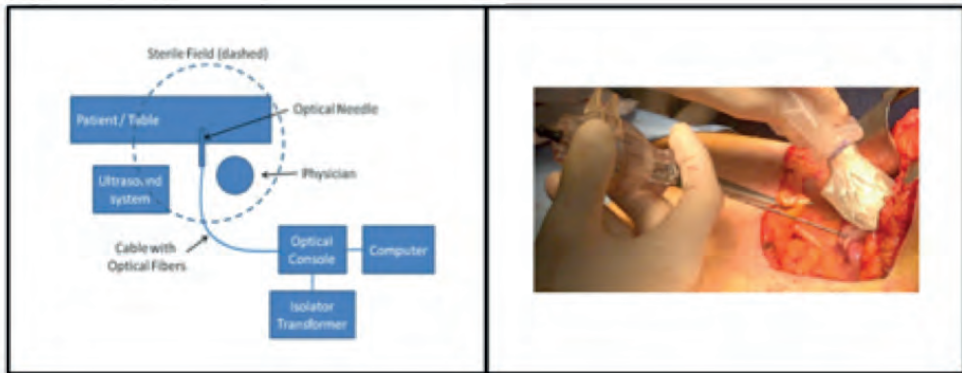
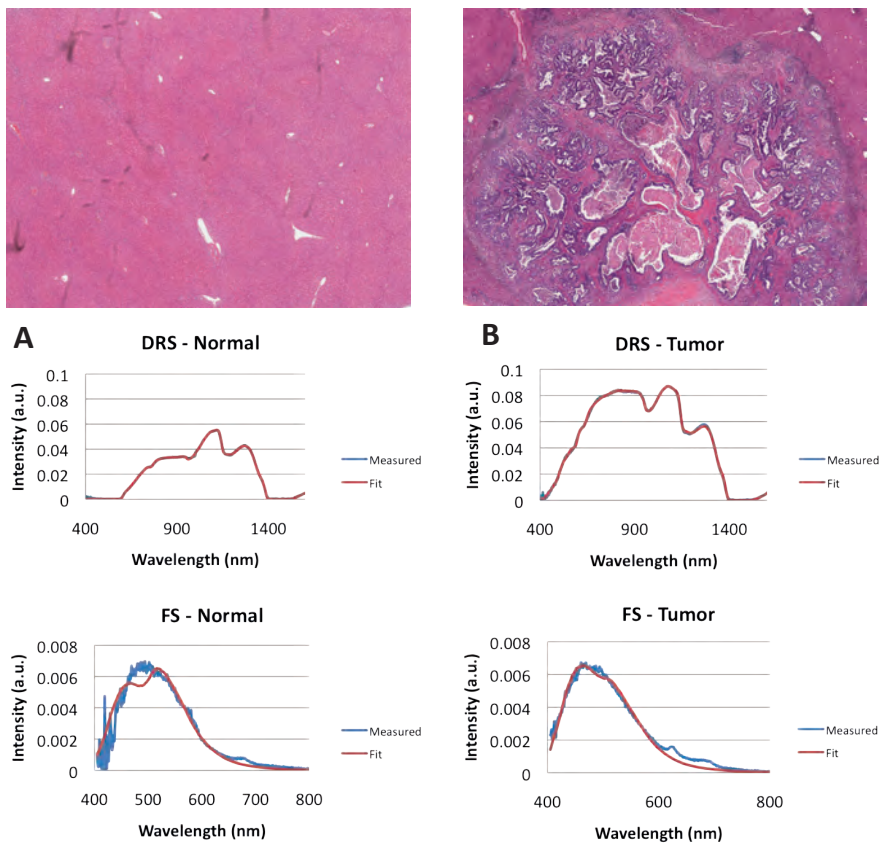


Figure 2. Typical examples of H&E stained pathology slides of the normal liver parenchyma (A) and CRLM (B) with corresponding DRS and FS spectral measurements. Typical results of DRS and FS spectra are displayed with the optical measurement depicted as a blue line and the result of the corresponding fit analysis depicted in a red line.



Diffuse reflectance analysis

Light emitted by the illumination optical fibre is subject to absorption and scattering. Each biological substance in the probed tissue has its intrinsic optical absorption characteristic as a function of wavelength. Hemoglobin (oxygenated and deoxygenated), Methemoglobin, Bile and β -carotene are the dominant chromophores in the wavelength range between 500 and 900nm^{162,164}. Fat, Water and Collagen are the dominant chromophores in the wavelength range between 900 and 1600nm³⁸. These chromophores have a well-determined optical absorption spectrum available in literature^{23,161}. The specific absorption coefficient of these chromophores was calculated from the optical spectrum derived from the probed tissue specimen. The volume fraction of each chromophore within the tissue can then be estimated from the optically obtained absorption coefficients.

The scattering characteristics are dependent on the cellular structure of the target tissue and are sensitive to size and density of cellular and subcellular structures. Optical scattering was defined by a reduced scattering amplitude and slope at an arbitrarily given wavelength of 800nm. The model used to estimate the various chromophore volume fractions and scattering coefficients from all the acquired spectroscopy measurements was first described by Farrell *et al*³⁶. The measurements are fitted with the analytical model by applying a non-linear Levenberg-Marquardt inversion algorithm. Diffuse reflectance spectra acquired from the tissue were fitted and analysed over the wavelength range from 500 to 1600nm. Spectral characteristics analysis was performed with a Matlab software package (MathWorks Inc., Natick, MA).

Intrinsic fluorescence analysis

For FS, the system was equipped with a semiconductor laser (377nm) to induce autofluorescence. Several endogenous tissue molecules are known for dominant emission of fluorescence after excitation at this wavelength, such as are Collagen, Elastin, NADH and FAD. The acquired fluorescence spectra were first corrected for absorption and scattering yielding intrinsic fluorescence spectra. This was performed using a modified photon migration method²⁶ that was based on previous work by Zhang *et al*¹⁴⁹ and Müller *et al*³⁹. Concentrations of each tissue fluorophore could then be calculated. The metabolic state of the tissue, was determined by Optical redox ratio (NADH / (NADH+FAD)).

Pathology

The pathologist located the twist markers and the surrounding liver tissue was excised for tissue analysis. Tissue specimens from all measurement locations were first fixed in formalin, then paraffin embedded and processed according to standard Hematoxylin and Eosin (H&E) staining. Two experienced pathologists, who were blinded for the outcome of the spectroscopy analysis, individually examined all histological slides. Histological analyses were performed at a 400x magnification.

Statistical analysis

Analyses were performed using SPSS (Statistical Package for the Social Sciences, version 16.0). Statistical differences between tumor and normal liver tissue and for type of treatment (chemotherapy vs. non-chemotherapy) were determined using non-parametric Kruskal-Wallis test ¹¹⁹. This test replaces data by rank, adequate when data does not show a Gaussian distribution. *P*- values smaller than 0.05 were considered statistically significant.

A Classification and Regression Tree (CART) algorithm was used to automatically classify tissue measurements into either of the two defined tissue types (normal liver or tumor tissue). CART is a prediction model that can be represented as a decision tree ³⁷. For validation, leave-one-out (LOO) cross validation scheme was used. The main advantage of the CART algorithm is the easy way the data can be interpreted and the clinical relevance. The outcome parameters are sensitivity and specificity.

RESULTS

Seventeen patients were included in the study. The average age was 62 years (range 38 - 74) and the majority of the patients was male (N=13). In total 19 lesions were optically measured and then resected. One patient had 3 lesions resected that were all separately measured. Seven patients (with 9 CRLM lesions) received neo-adjuvant systemic chemotherapy within 3 months before liver resection. The administered chemotherapy regimens consisted of Capecitabine and Oxaliplatin with or without Bevacizumab in a 3-week cycle for 4 to 9 cycles.

A typical example of the DRS and FS spectra in normal liver tissue and colorectal liver metastases, both correlated to histopathology is depicted in figure 2. Clear differences in shape of the spectra can be observed between normal and tumor tissue. Typical for normal tissue is the significant light absorption in the wavelength region 400-600nm due to a rather high Total Hemoglobin Content (THC) in normal liver tissue. The reconstruction of the intrinsic fluorescence (especially the part below 500nm) is hampered by this high THC, as observed in the fluorescence spectrum with considerable 'noise' in this region. Notable observations in the FS spectrum are an additional fluorescence peak only observed in normal tissue at 675nm and a typical shoulder with two additional peaks only observed in tumor tissue at 625 and 680nm.

Tissue parameter quantification

Figure 3 shows boxplots of the various parameters for all of the 19 lesions analysed. All markers showed a significant difference between normal liver tissue and tumor. With regard to DRS, tissue discrimination was best for the tissue chromophores; THC, Bile, and Methemoglobin.

For FS measurements, a significant difference between normal liver tissue and tumor was observed for the Optical redox ratio. In addition, 12 out of 19 tumor measurements showed fluorescence peaks at 625 and 680 nm that were not observed in any of the normal liver tissue measurements. Of these 12 tumor lesions with additional fluorescent peaks, a total of 9 revealed the measured peaks in all tumor locations. The FS spectra of normal liver tissue showed in 11 of the 17 patients a fluorescence peak near 675 nm that was not observed in tumor tissue.

Neo-adjuvant chemotherapy

Seven patients (9 tumor lesions) received neoadjuvant chemotherapy. Figure 4 shows the boxplots for the most discriminative parameters (THC, Methemoglobin, Bile and Optical redox ratio) in patients treated with or without chemotherapy. All parameters showed a consistent trend in both groups (chemo vs. non-chemo). In accordance to the overall analysis (presented in Figure 3) THC, Methemoglobin and Bile are lower in tumor tissue compared to normal liver tissue, while the Optical redox ratio is higher in tumor tissue compared to normal liver tissue.

Tissue classification

The CART algorithm used DRS and FS parameters (THC, StO₂, Water, Scattering at 800nm, Bile, Methemoglobin, Optical redox ratio) to generate a decision tree and to calculate sensitivity and specificity. Table 1 shows the results for discrimination of tumor tissue from normal liver tissue when all data are analysed collectively as well as when the non chemotherapy treated lesions and chemotherapy treated lesions were analysed separately. Adding FS to the DRS parameters does not improve the sensitivity or specificity. Overall accuracy for the whole group using the DRS parameters only was 94%, for the non-chemotherapy group and the chemotherapy group this was 88% and 96%, respectively.

Table 1. Sensitivity and specificity for the discrimination of CRLM from normal liver tissue for DRS, FS and DRS+FS. Results are specified for all lesions, lesions treated by chemotherapy ('chemo') or lesions without pre-treatment by chemotherapy ('non-chemo').

Tumor vs. normal liver parenchyma	Sensitivity			Specificity		
	DRS	FS	DRS+FS	DRS	FS	DRS+FS
Overall (N=484)	95%	84%	94%	92%	61%	89%
Chemo (N=226)	92%	89%	92%	100%	62%	100%
Non-chemo (N=258)	94%	87%	96%	82%	60%	80%

Figure 3. Boxplots of relevant tissue parameters in normal liver tissue (Green) and CRLM (Red) for all 19 measured tumor lesions. An ‘*’ indicates a significant difference between both tissue types.

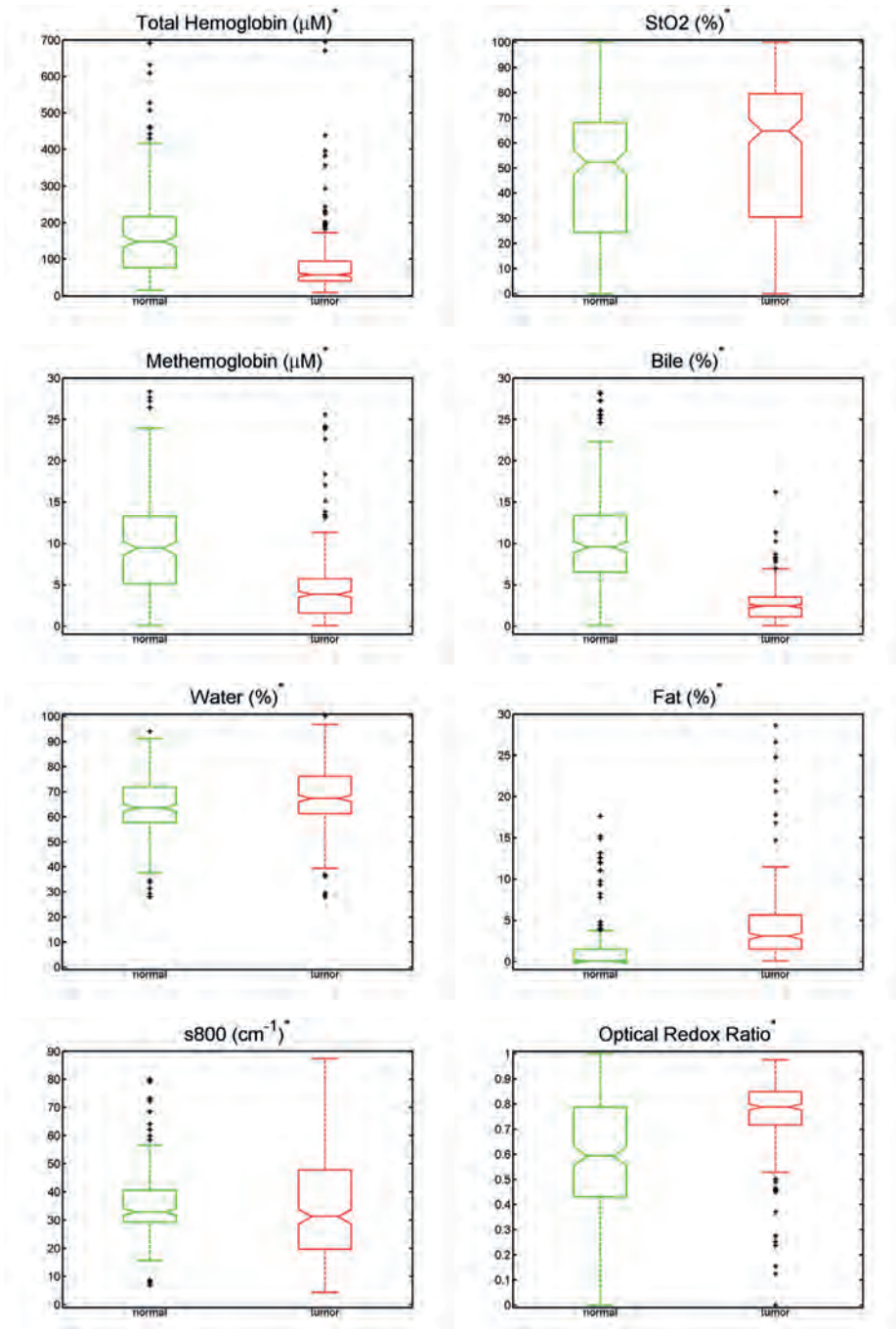
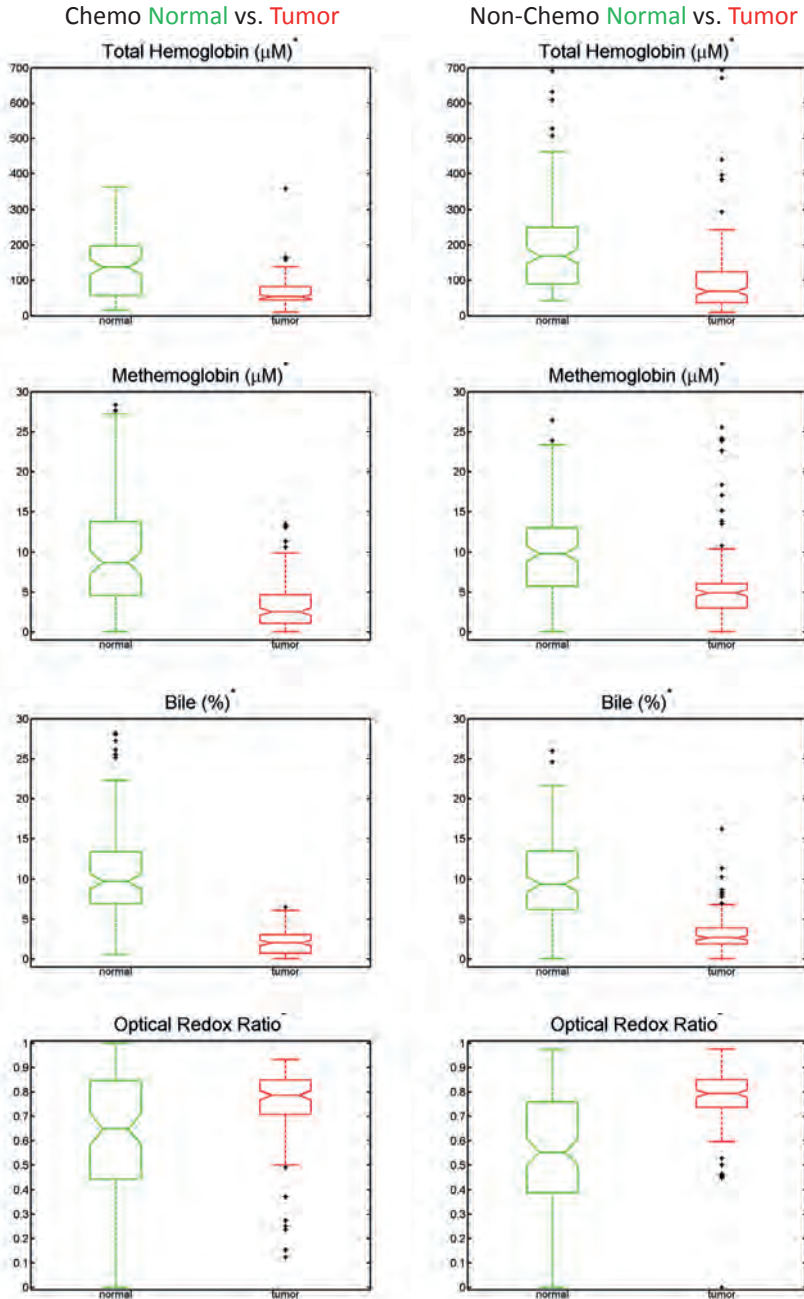


Figure 4: Boxplots of the four most significantly different tissue parameters in normal liver tissue (Green) and CRLM (Red) for chemotherapy (N=7 patients with 9 tumor lesions / left column) and non-chemotherapy treated patients (N=10 patients / right column). An '*' indicates a significant difference between both tissue types.



DISCUSSION

Technical advances in the treatment of liver malignancies, such as laparoscopy as well as the increased use of tumor modulating agents such in neo-adjuvant systemic treatment, call for an increased necessity for new technologies aiding the surgeon to correctly locate and resect the entire tumor volume in the liver. In previous studies, we have shown that DRS and FS can be used to identify various types of tissue in *ex vivo* experiments^{148,165}. In liver tissue, we have also demonstrated that DRS can accurately discriminate normal liver tissue from CRLM in an *ex vivo* model with a sensitivity and specificity of 94%¹⁶³.

In the present study, we aimed to make the next step towards incorporation of optical spectroscopy into surgical tools. We therefore investigated the accuracy of DRS and FS for discriminating between CRLM and normal liver tissue *in vivo* using a 15 Gauge disposable needle. We have shown that DRS can accurately discriminate tumor tissue from normal liver tissue with a sensitivity and specificity of 95% and 92%, respectively. These results confirm the conclusions of our previous *ex vivo* study on liver tissue. The addition of FS did not give added value to the overall accuracy when excluding the additional peaks found in the FS. Finally, earlier systemic chemotherapy treatment had no negative effect on the DRS accuracy; sensitivity was 92% and specificity reached 100% for chemotherapy treated patients. This is important as neo-adjuvant chemotherapy can influence tumor size and borders can be less clear. These results arguably render DRS a possible surgical tool for identification of CRLM during liver surgery.

The most significantly discriminative tissue chromophores observed with DRS were THC, bile and methemoglobin. The lower concentrations of THC and bile in tumor tissue are comparable to our previous *ex vivo* liver analysis. Hence, these two tissue parameters can be considered important parameters for future liver tissue analysis with DRS. Moreover, we previously hypothesized that small bleedings at the tip of the optical needle could hamper our discriminative accuracy *in vivo*. The levels of THC measured in both normal liver and tumor were a factor 2 higher than we previously observed in our *ex vivo* analysis¹⁶³. However, no macroscopic bleeding was observed during the procedures. Yet, based on the notable observed distinguishing accuracy of THC, we can conclude that bleeding is not a negative issue during minimal invasive analysis of liver tissue with DRS. The chromophore methemoglobin was only recently added to our analysis algorithm. Methemoglobin is a state of hemoglobin that cannot bind oxygen¹⁶⁴. It naturally occurs in about 1% of the normal human blood. Methemoglobin is regularly formed in areas with oxidative stress and raised serum levels are linked with the presence of solid tumors¹⁶⁶. Taking these characteristics of methemoglobin into account, we recently included this chromophore into our analysis algorithm. We observed significantly lower

levels of methemoglobin levels within the tumors compared to the surrounding normal liver tissue. This is comparable to the results of detected THC. We believe that this can be linked to the differences in tissue vascularisation; liver parenchyma is notably higher vascularised compared to the tumor lesions, in particular towards the centre of the tumor lesion ¹⁶⁷. It can therefore be regarded as an important discriminative parameter for human liver tissue.

Fat was another significantly discriminating chromophore in our previous *ex vivo* liver analysis ¹⁶³. The levels were lower in the *ex vivo* tumor lesions. We hypothesized that *in vivo* the discriminative importance for this chromophore would also be confirmed. In the present *in vivo* analysis, we found significantly higher levels in the tumor lesions. Closer histological analysis of the normal liver tissue specimens revealed only 3 of the 17 included patients to have steatosis levels of any significance (resp. 8%, 30% and 35% steatosis). The steatosis from the other 14 patients was below 5%, most of which 0% or 1%. Liver steatosis <5% is traditionally considered as 'no steatosis' in the literature ^{159,168}. The low overall levels of steatosis and the low amounts of fat measured within the tissue, makes that this parameter is difficult to judge and may greatly differ between patients, depending on the degree of steatosis in the liver. Based on these data, we believe that the chromophore fat should not be included as an important discriminating parameter in future analyses.

For FS measurements, the only tissue parameters that were significantly different between normal liver tissue and CRLM were NADH and FAD. This may reflect the low specificity for discrimination between normal liver tissue and CRLM realised with FS. Certainly the high absorption of hemoglobin may hamper the calculation of intrinsic fluorophores between 400 and 600nm. NADH and FAD are molecules that are both involved in the energy metabolism of a cell. Cellular energy in the form of ATP can either be generated via oxidative phosphorylation in which FAD is oxidated to FADH₂ or via aerobic glycolysis in which NAD⁺ is transformed into NADH. During carcinogenesis, cellular metabolism often changes from oxidative phosphorylation to aerobic glycolysis ^{104,169,170}. Thus, an increased redox ratio will often be observed in tumor tissue in comparison to normal liver cells *in vivo*. Also our study shows that the liver tumors display a significantly increased optical redox ratio.

Although FS did not add to the overall discriminative accuracy of our analyses, several notable fluorescence peaks were observed between 600 and 700nm. Two peaks (at 625 and 680 nm) were only observed in tumor tissue, but not in all tumors. Peaks at these wavelengths are thought to correspond with porphyrin-like molecules. We have previously seen these fluorescent peaks in analysis of *ex vivo* lung and murine tumors ^{165,171}. Porphyrins are organic compounds and are known to form the haem group when combined with ferrous iron. Colorectal tumors and CRLM have been shown to

accumulate specific porphyrins as a result of a tumor-specific metabolic alteration ¹⁴⁷. Correlation between porphyrins and necrotic areas within tumor tissue has also been observed in a preclinical model ²⁹. The intensity of the signal of both peaks was not constant for the various measured spectra in each tumor. We observed areas with high and low intensity, which could be due to the variation in necrotic areas.

We also observed a significant fluorescent peak at 675nm in normal liver tissue of several patients, which was not present in any of the tumor tissues. Chlorophyll is an exogenous molecule that is known to emit a fluorescent signal at this 675nm. It is present in various vegetables and fruit and is known to accumulate within the liver upon consumption ¹⁷². It could therefore be related to food intake of the patients. The fact that the appearance of these three additional fluorescent peaks seems to be defined to either tumor or normal liver tissue renders that they could be used as additional discriminative factors if present. The value of these results needs to be investigated in future analysis.

Systemic chemotherapy is involved in the current treatment of an increasing number of patients with CRLM. There is no clear literature on the (increased) risk of an involved resection margin after neo-adjuvant chemotherapy, but we know R1/R2 resections are independently associated with early recurrence and decreased disease-free and overall survival ^{173,174}. If optical spectroscopy is to be incorporated in surgical tools for CRLM resection, it is important to determine if the discriminative accuracy of this technology is hampered as a result of neo-adjuvant chemotherapy. The results of our CART analysis show that the discrimination of CRLM from normal liver tissue is not affected when patients were treated by pre-operative chemotherapy.

The results of the first *in vivo* study of liver tissue with DRS and FS towards development of new 'optical surgical tools' can be considered very promising. Yet, they only give proof of principle in a small number of patients. The next step is to confirm and validate our results in a larger patient population. Further study of FS will be needed to investigate if this technique has added value with DRS towards an application in daily liver surgery. Specific interest should be put on the evaluation of the addition fluorescent peaks between 600nm and 700nm for this purpose.

In conclusion, we have demonstrated that DRS can accurately discriminate tumor from normal liver tissue. The discriminative accuracy is not hindered by pre-treatment with systemic chemotherapy. These results confirm previous findings of an *ex vivo* analysis. Addition of FS does not further enhance discriminative accuracy, but does provide additional fluorescent parameters that could prove of added value for distinguishing CRLM from normal liver tissue.



Chapter 9

Monitoring of tumor response to cisplatin using optical spectroscopy

J.W. Spliethoff

D.J. Evers

J.E. Jaspers

B.H.W. Hendriks

S. Rottenberg

T.J.M. Ruers

INTRODUCTION

Monitoring of the individual tumor response is crucial for optimizing systemic treatment in cancer patients, particularly as treatments trend towards individualized patient care¹⁷⁵⁻¹⁷⁸. Therapy response assessment is generally performed by anatomical imaging using the standardized RECIST (response evaluation criteria in solid tumors) criteria based on changes in anatomical tumor size¹⁷⁹. However, standard-of-care anatomical imaging modalities, such as CT, are unable to objectively evaluate treatment response at the early stages of treatment. In addition, shrinkage of tumors can be minimal even when treatment is effective. This phenomenon is most obvious in certain tumor types, like sarcomas or gastrointestinal stromal tumors¹⁸⁰, as well as with new targeted drugs that lack direct intrinsic cytotoxic activity, such as bevacizumab¹⁸¹.

A modality that is based on functional contrast rather than on anatomical features alone, may improve response monitoring. An example of functional imaging is Positron Emission Tomography (PET) using ¹⁸F-FDG. Nowadays, ¹⁸F-FDG PET has been used for early response monitoring and outcome prediction, although the accuracy is still dependent on the tumor type and the treatment used¹⁸²⁻¹⁸⁴.

In the last decade, optical sensing, by means of diffuse reflectance spectroscopy (DRS) and autofluorescence spectroscopy (AFS), has been used to improve the identification of cancerous lesions in various organs^{141-146,185-189}. Both modalities enable tissue characterization by measuring the spectral response after the tissue is illuminated with a selected spectral band of light. Depending on the tissue composition and its structure, a specific “optical fingerprint” is acquired. This optical fingerprint represents specific quantitative morphological, biochemical, and functional information from the probed tissue, making it a promising technique for the detection of chemotherapy-induced alterations.

Tromberg’s group investigated the changes in optically measured biomarkers during chemotherapy in breast cancer using diffuse optical spectroscopy (DOS)¹⁹⁰⁻¹⁹³. DOS imaging using a handheld probe was used to scan the breasts of patients with locally advanced breast cancer before, during and after chemotherapy. The results of these studies showed that optically derived tissue parameters strongly correlate with and, in some cases, predict pathologic response. A study by Falou *et al* also suggested that responders and non-responders could be differentiated with DOS¹⁹⁴. Finally, the biomedical engineering group at Duke University showed that a combination of DRS and AFS can be applied to monitor drug concentrations and tumor physiology *in vivo* in a preclinical mouse model¹⁹⁵.

Studies thus far, have mainly focused on the non-invasive application of optical sensing by hand-held optical transducers used to scan tissue surfaces. This approach has a clear advantage for breast tumors, but may limit the applicability of optical sensing

for deep seeded tumors such as in the lung or kidney. Recently, we described an optical needle probe able to perform optical measurements in tumor tissue^{189,196,197}. Optical measurements conducted through very fine needles (smaller than 27G), open the potential to assess treatment response of (solid) tumors at deep tissue sites¹⁹⁸. The aim of this study was to investigate whether dual-modality DRS-AFS, incorporated in a small needle probe, was able to monitor the dynamics of tumor response after treatment with cisplatin, using a preclinical mouse model for BRCA1-mutated breast cancer.

MATERIALS AND METHODS

Animal study protocol

In this study, Brca1^{-/-}; p53^{-/-} mammary tumors were generated in a mouse model for hereditary breast cancer previously described by Liu *et al*¹⁹⁹. These tumors have been demonstrated to be sensitive to cisplatin at a maximum tolerated dose (MTD) of 6 mg/kg administered intravenously²⁰⁰.

Small fragments of tumor (1-2 mm in diameter) were orthotopically transplanted into the fourth right mammary fat pad of 36 female (FVB/N HanHSD WT) animals (6-8 weeks of age) as described previously²⁰⁰. Starting two weeks after tumor grafting, the onset of tumor growth was checked at least three times per week. Tumor size was determined by caliper measurements (length and width in millimeters) and tumor volume (in mm³) was calculated using the following formula: $0.5 \times \text{length} \times \text{width}^2$.

Once the tumor volume reached 400-800 mm³, the animals were separated into control and treatment groups. Animals in the treatment group (N=18) received cisplatin (1 mg/ml in saline/mannitol) at a dose of 6 mg/kg (MTD) in a single intravenous injection into the tail vein. Animals in the control group (N=18) received an equivalent amount of saline.

DRS and AFS tumor measurements were performed *in vivo* after inserting the spectroscopy needle percutaneously (through the skin) into the tumors. Baseline measurements were performed on day 0, immediately after treatment/placebo administration, and then on days 1, 2, 4 and 7 afterwards. These time points were selected from a previous pilot study. To evaluate whether eventual changes in the optical profile were systemic or tumor-specific, 8 animals from each group were randomly chosen for additional *in vivo* measurements in liver and muscle tissue on days 2, 4 and 7.

After each session of optical measurements, 3-5 animals from each group were sacrificed to obtain tumor tissue for histopathological evaluation. Tumor samples were dissected into three parts: these were snap-frozen in liquid nitrogen, fixed in 4% formalin, or fixed in acetic acid-formalin ethanol-saline.

The tumor model used is known to be very sensitive to the MTD of Cisplatin, whereas non-treated tumors grow rapidly. This could result in control animals being removed from the experiment based on humane endpoints (tumor volume >1500 mm³), or in a minimal amount of measurable tumor tissue in the treated animals before the end of the experiment. Therefore, animals with slightly higher tumor volumes were included in the treatment group. Throughout the course of the experiment, starting three weeks before the tumor grafting, the animals were given a purified diet to eliminate autofluorescence from chlorophyll²⁰¹. During the optical spectroscopy measurements, the animals were

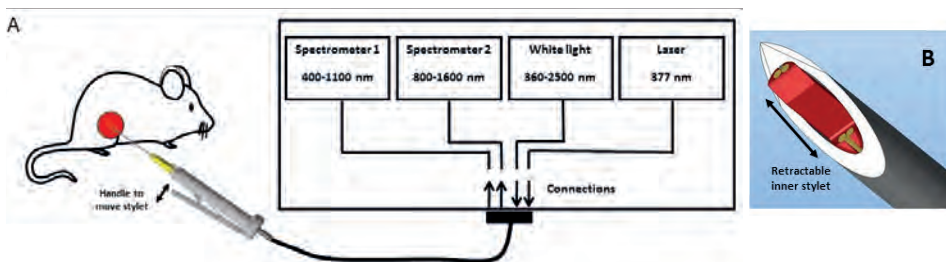
deeply anaesthetized using 1.5% isoflurane mixed with oxygen. All animal procedures were approved by the Animal Ethics Committee of the Netherlands Cancer Institute.

Optical spectroscopy using a miniaturized optical probe

DRS and AFS measurements were performed using a portable spectroscopic system, which consists of two light sources and two spectrometers (Figure 1). For the DRS measurements, a Tungsten halogen broadband light source (360-2500 nm) with an embedded shutter was used. For AFS the system was equipped with a semiconductor laser ($\lambda=377$ nm) to induce autofluorescence. One spectrometer was used to resolve light in the visible wavelength range, i.e. 400 nm till 1100 nm (Andor Technology, DU420A-BRDD), the other to resolve near infrared light from 900 to 1700 nm (Andor Technology, DU492A-1.7). The spectrometers were controlled by a custom-made LabView software user-interface (National Instruments, Austin, TX) to acquire and save the data. The calibration procedure has been described elaborately by Nachabe *et al*²⁰².

A custom fiber-optic needle which can probe tissue at the needle tip was developed. The needle consisted of a 21G (0.82mm) outer cannula and a 22G adjustable stylet (Figure 1B), containing four identical fibers with a core diameter of 100 μ m. To minimize tissue damage, the optical fibers were retracted during needle insertion. The optical fibers were protruded after positioning the needle at the right position to establish optimal tissue contact. Two fibers were connected to the broadband light source and laser, while the two other fibers were connected to the spectrometers to capture diffusely scattered light and fluorescence from the tissue. Two different source-detector separations (SDS) were utilized (1.5mm and 0.15mm). The spectra acquired with the 1.5 mm SDS were used for the DRS data analyses, whereas the DRS spectra measured with the 0.15 mm SDS were used to correct for absorption and scattering in the fluorescence spectra.

Figure 1. Schematic overview of the combined DRS and AFS optical setup. The system measures diffuse reflectance (400-1600 nm) and intrinsic fluorescence (400-800 nm) of tissue through the use of a miniaturized 21G needle with a retractable inner fiber-optic stylet.



Diffuse Reflectance spectral analysis

Three to five DRS spectra were collected from each animal on each measurement day, consecutively. To interpret the acquired DRS spectra, a widely accepted analytical model, introduced by Farrell *et al*²⁰³, was used to estimate the various DRS absorption and scattering coefficients. The absorption coefficients represent the concentration of physiologically relevant absorbers in the tissue, such as hemoglobin, water and fat, as well as functional parameters like tissue oxygenation. The main scattering parameters are the reduced scattering coefficient (at 800 nm), the reduced scattering slope of the Mie scatterer (Mie scattering slope) and the Mie-to-total scattering fraction. The Mie scattering slope is related to the average particle size²⁰⁴. In the Mie-to-total scattering fraction the total scattering of tissue is assumed to be composed of Mie and Rayleigh scattering. In tissue, Mie scattering represents scattering caused by biological cells and cellular components, whereas Rayleigh scattering is elastic scattering of light by particles, which are much smaller than the wavelength of light (e.g. macromolecular aggregates such as collagen fibrils). The validation of the DRS analytic method has been described previously by our group^{202,205}.

Intrinsic fluorescence modeling and quantification

Intrinsic fluorescence from the tissue was calculated by correcting the acquired fluorescence spectra for absorption and scattering using the short SDS DRS spectra. For the latter, a modified photon migration method²⁰⁶ was used based on the work by Müller *et al*²⁰⁷ and Zhang *et al*¹⁴⁹. The corrected spectra were fitted using the fluorescence spectra (excitation at 377 nm) of endogenous tissue fluorophores (collagen, elastin, NADH and FAD) as *a priori* knowledge. The optical oxidation-reduction (redox) ratio, which is linked to the metabolic state of the tissue, was defined as $\text{NADH}/(\text{NADH}+\text{FAD})$ ^{169,208}. Since collagen and elastin have almost identical fluorescence spectra, estimated amounts of collagen and elastin were combined as Collagen + elastin.

In case the tissue contained diagnostic levels of endogenous fluorophores other than the ones included in the standard fit model, the area underneath the fitted curve (known fluorophores) was subtracted from the total area under the original curve (measured fluorescence).

Histopathologic analyses

Samples were stained with both standard hematoxylin & eosin (HE) and Masson's Trichrome dyes. The HE stained sections were used to quantify vital, necrotic and fibrotic tissue fractions. The necrotic and fibrotic fractions were calculated as a percentage of the overall tissue area across each section. For this purpose at least 10 different fields were investigated at a 400x magnification.

Immunohistochemical analysis of tumors was performed using anti- γ H2AX [rabbit polyclonal, Cell Signaling, #2577, 1:50 in 1% bovine serum albumin diluted in phosphate saline buffer], anti-cleaved caspase-3 [rabbit polyclonal, Cell Signaling, #9661, 1:100 in 1% PBSA], and anti-Ki67 probes (Dako; 1:100). For evaluation of the amount of lipids, frozen sections were mounted on glass slides and stained with Oil-red. All histopathology was evaluated by an experienced pathologist in a blinded study setting. The pathology findings were used to cross validate the longitudinal changes in the optical end-points.

Two-photon excitation microscopy

Intrinsic fluorescence in tumor was imaged using a two-photon confocal microscopy setup. These experiments were carried out to relate the differences in fluorescence spectra obtained with AFS to specific structures in the tissue slices. Snap frozen tumor pieces were sliced in 25 μ m thick sections, kept unstained and unfixed, and mounted onto glass microscope slides. The two-photon excitation source was a Ti:Sapphire laser tuned to 790 nm. The excitation light (equivalent to a single-photon excitation wavelength of 395 nm) was delivered to and the emitted light was collected from the sample through a Leica Confocal microscope (with a Leica HCX IRAPO 25x water immersion objective with a numerical aperture of 0.95) coupled to a Leica TCS SP5 tandem scan head operating at 500 lines/sec. A photomultiplier served as the detector. For each tumor sample, fluorescence images were obtained in the wavelength ranges of 400-500 nm, 500-600 nm, and 600-700 nm. This was done to compare the relative intensity of fluorescence at these spectral ranges between treated and control animals.

Statistical analysis

To examine the trends in optical parameters over time, a linear regression model was performed in MATLAB 7.13 (MathWorks Inc, Natick, MA). The fixed-effects terms in the models were treatment (Controls vs. cisplatin), time (day), and their interactions. A slope and intercept were fit for the data of both the treated and control group using maximum likelihood estimation. For the significance of fixed effects a likelihood ratio test was statistically compared to a chi-squared distribution with one degree of freedom (for one coefficient being eliminated). For all tests, statistical significance was set at $P < .05$.

RESULTS

Longitudinal trends in DRS parameters and tumor volume

DRS parameter quantification was performed as part of the model-based data analysis using a total of 712 DRS spectra. The longitudinal changes for the average tumor volume and various DRS parameters over time are shown in Figure 2. In the control animals, the tumor volume increased during the entire follow-up period, whereas the tumors of the cisplatin-treated animals started to shrink two days after treatment. For the DRS parameters, the trends during follow up were significantly different between the treated and the control groups for the Mie scattering slope ($P < .0001$), Mie-to-total scattering fraction ($P < .001$), Tissue oxygenation ($P = .035$) and Fat volume fraction ($P < .0001$).

Longitudinal trends in AFS parameters

The fluorescence spectra and corresponding model fits for two representative animals (one treated and one control animal) on day 0, 2, 4, and 7 are shown in Figure 3. In the tumor of the treated animal an increasing deviation between the measurements and the fitted curves was observed from day 2 onwards, between 500 nm and 800 nm. This indicates that fluorophores other than the ones included in the standard fit model (collagen, elastin, NADH, FAD) were measured. This additional fluorescence activity (from now on called Fluorescence residual) was seen in all the treated tumors at day 4 and 7.

The longitudinal kinetics for each model-fitted AFS parameter and the calculated Fluorescence residual across all treated animals and control animals are shown in Figure 4. The plotted linear trend for the Fluorescence residual in tumor was significantly different between the treated and the control groups ($P = .018$). No significant trends were observed for the Total fluorescence intensity, Collagen + elastin and the Optical redox ratio.

Figure 5 shows the longitudinal changes of the Fluorescence residual in tumor, liver, and muscle across all animals from both groups. The additional fluorescence is not present in muscle and liver tissue, indicating a tumor-specific effect.

Two-photon confocal microscopy

In an attempt to better understand the origin of the additional autofluorescent emission (mainly above 600 nm) seen in the treated animals, two-photon confocal fluorescence microscopy images recorded in a spectral range of 600-700 nm were compared with adjacent tissue sections that were stained with HE (Figure 6). The samples were collected after one week of follow-up, i.e. when the differences seen in AFS signals were maximal. In the treated-tumor samples numerous fluorescent foci were present. These foci correlated with cellular structures rather than with collagen deposits or necrotic areas. It remains to

be determined whether this specific fluorescence originated from stromal or tumor cells. For the two-photon images recorded in the spectral range 400-500 nm and 500-600 nm, no considerable differences were seen when comparing both groups.

Evaluation of histology and histochemical biomarkers

The evaluation of pathological response of tumors to cisplatin using various histological dyes and immunohistochemical biomarkers is illustrated in Figure 7. A strong increase in nuclear DNA damage was seen 24 hours after cisplatin administration using γ -H2AX as a marker. From day 2 onwards, a significant decrease in the proliferation marker Ki-67 and an increase in apoptosis-related cell death (cleaved caspase-3 marker; CC3) were observed. Analysis of Masson's Trichrome (MT) stained slides showed increased amounts of fibrotic tissue 4 to 7 days after treatment which corresponded to the HE images. An increase in lipids (Oil-red) was seen over time.

In Figure 8A and 8B fractions of vital, necrotic and fibrotic tumor tissue for both groups are shown as quantified on the HE stained tissue slides. These data indicate that the pathological response to cisplatin in this tumor model corresponds with the replacement of viable tumor tissue by fibrosis, without a considerable increase in necrosis. The longitudinal changes in these histopathological endpoints were compared against changes in prominent optical parameters as shown in Figure 8C and 8D. In the treated group a major shift in both histology and optical endpoints was seen, whereas minimal changes were observed across all of these parameters in the control group.

Figure 2. Longitudinal changes in tumor volume and DRS parameters measured for both groups across time: Tumor volume (A), Mie scattering slope (B), Mie-to-total scattering fraction (C), Total hemoglobin (D), Tissue oxygenation (E), Reduced scattering (F), Fat volume fraction (G), and Water volume fraction (H). The bars represent the mean for each parameter computed across all available animals, at each particular time point, for both the treated (red) and control (blue) groups. The dashed lines represent the corresponding regression lines. P values are shown at the top of each plot.

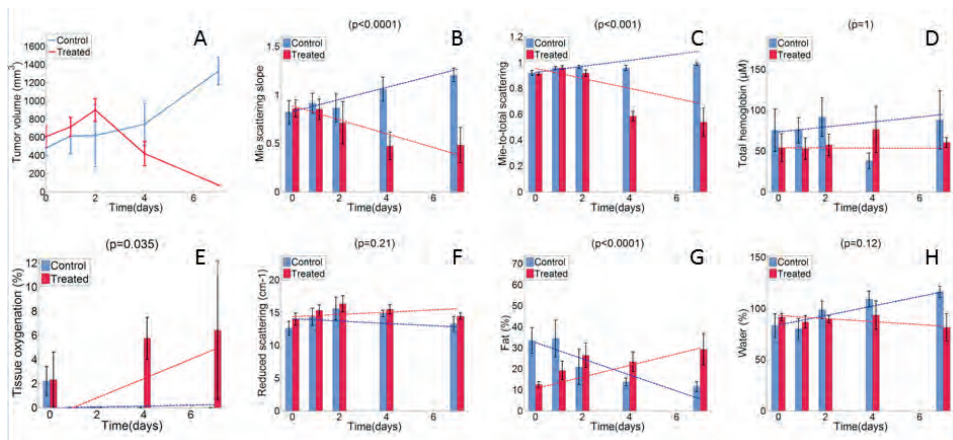


Figure 3. Auto-fluorescence spectra for a representative animal in the control group and the treated group during one week of follow-up. The blue lines are the fluorescence measurements, whereas the red lines are the results of the model-based fitting procedure. The green lines illustrate the residual due to the presence of additional fluorescence, which is specifically seen in the treated animals after two days.

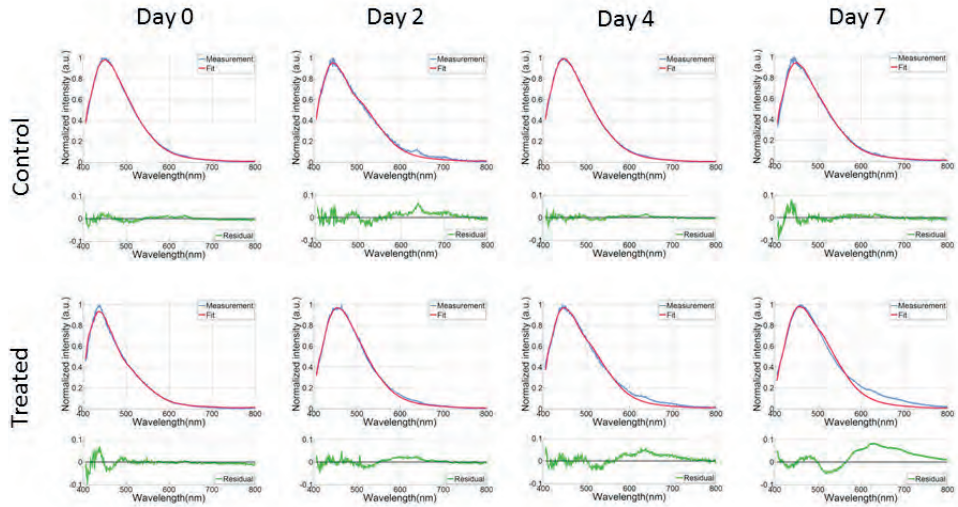


Figure 4. Longitudinal trends in AFS parameters measured for both groups across time: Total fluorescence intensity (A), Collagen + elastin (B), optical redox ratio (C), and Fluorescence residual (D). The bars represent the mean for each parameter computed across all available animals, at each particular time point, for both the treated (red) and control (blue) groups. The error bars are SE's. The dashed lines represent the corresponding regression lines. P values are shown at the top of each.

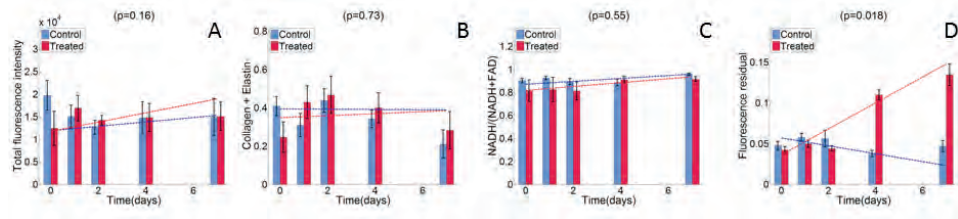


Figure 5. Course of fluorescence residual in tumor (A), liver tissue (B), and muscle tissue (C) over time. The data of muscle and liver tissue shown here were obtained from 16 (8 per group) of the animals that were sacrificed at day 2, 4 or 7, whereas (A) represents the full cohort. The error bars are SE's.

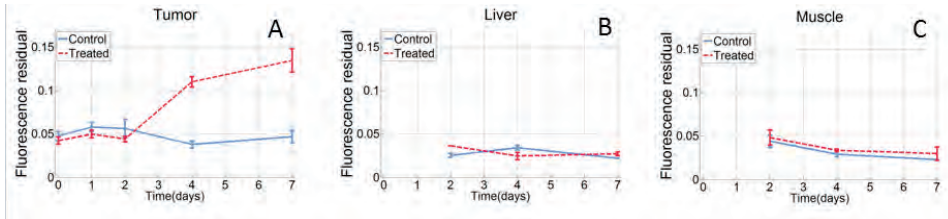
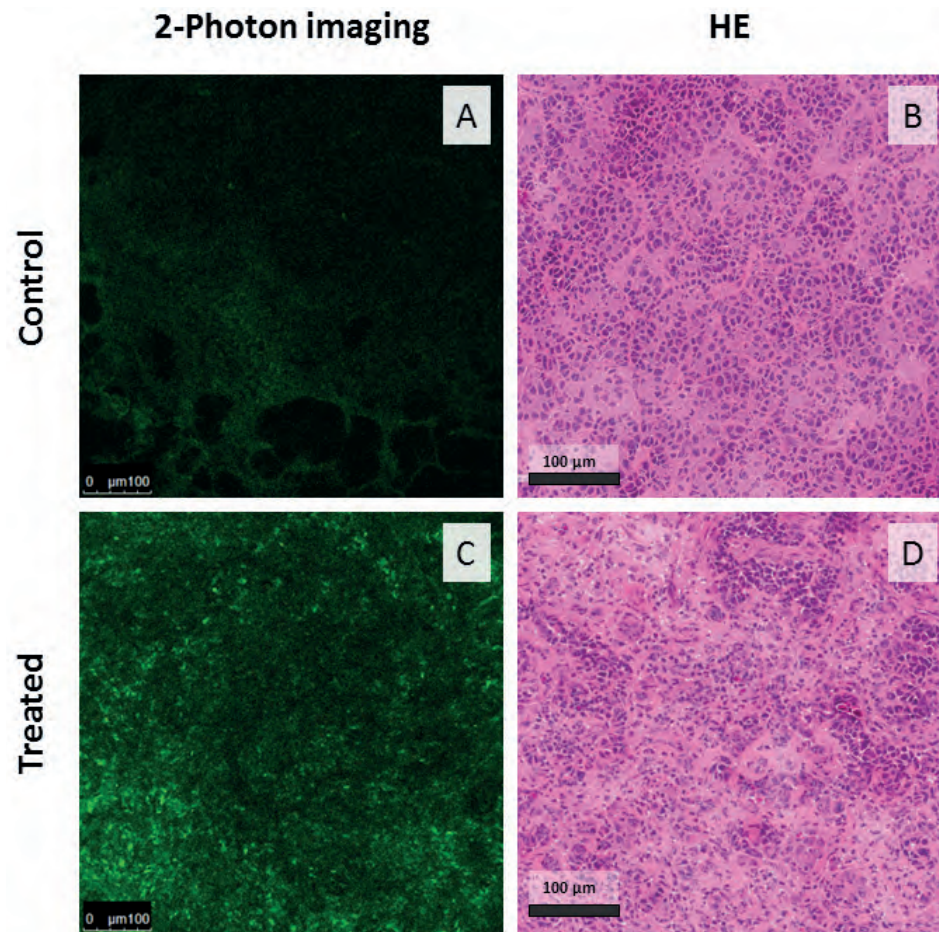


Figure 6. Two-photon confocal microscopy images (600-700 nm) of tumor sections of a representative control (A) and treated animal (C). Effective excitation was at 395 nm and the intensity scale is the same in both of the two-photon images. The samples were collected after one week of follow-up, i.e. when the differences seen in AFS signals were maximal. In the treated tumor samples numerous fluorescent foci were present within the cells. (B) and (D) show corresponding HE images.



9

Figure 7. Tumor pathological response to a MTD Cisplatin. Scale bar = 100 μ m. HE (A) and Masson's Trichrome (MT; B) stained tumor sections showing replacement of viable tumor tissue by fibrosis, especially after day 2 onwards. The γ -H2AX (C), Ki-67 (D), and anti-cleaved caspase 3 (CC3; E) markers showed a strong increase in DNA-damage, a decrease in proliferation and an increase in apoptosis-related cell death, respectively. An increase in the amount of lipids (Oil-red stain) was seen across time.

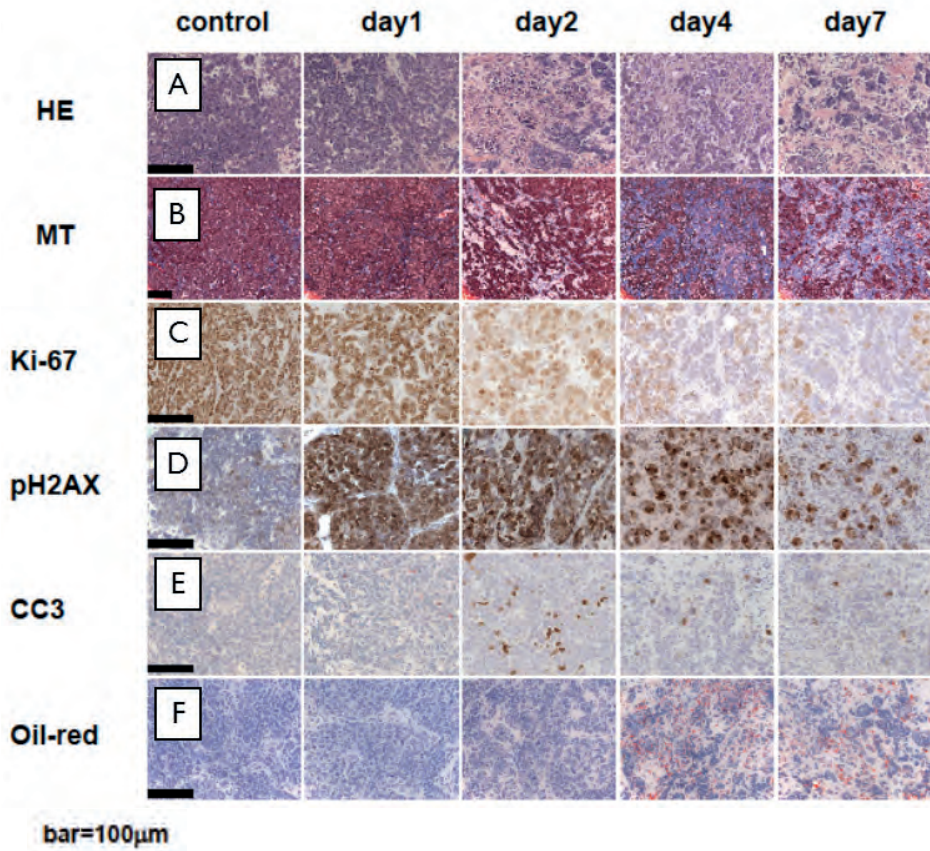
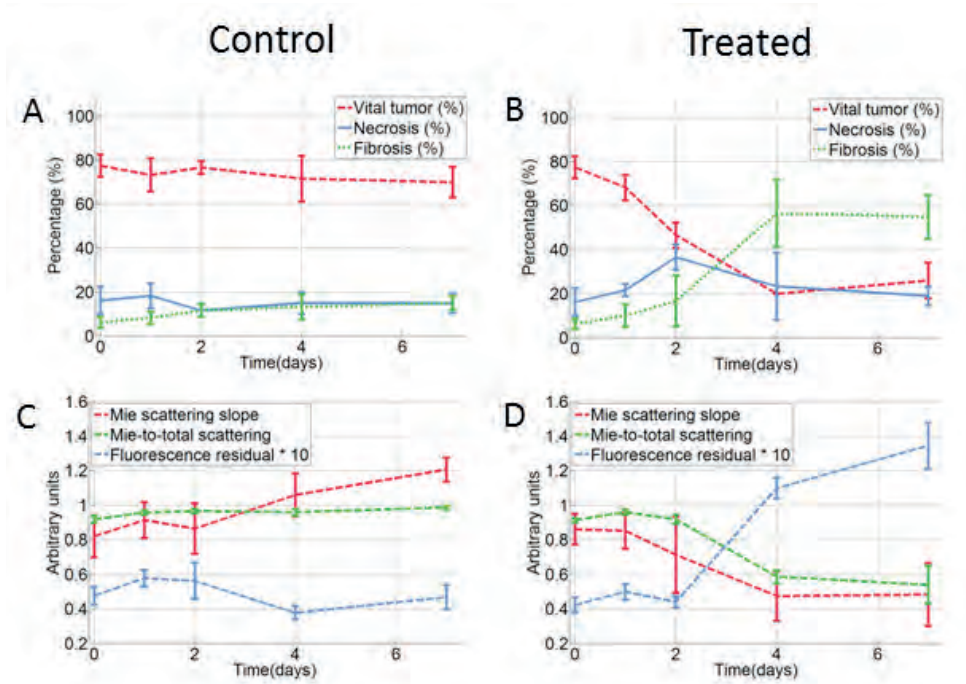


Figure 8. Comparison of histology and optical spectroscopy end points. The upper two figures show the temporal changes in mean fractions of vital tumor tissue, necrosis and fibrosis for the control group (A) and treated groups (B), as assessed by histological staining using HE. The lower two figures (C) and (D) show temporal changes in the Mie scattering slope, the Mie-to-total scattering fraction, and the fluorescence residual for both groups. Error bars indicate SE.



DISCUSSION

In this study, we used a combination of DRS and AFS to investigate cisplatin-induced changes in tumor physiology and morphology across a period of one week in a mouse model for hereditary breast cancer. The changes in optical endpoints were compared against the degree of pathological response. The results showed that various DRS and AFS parameters in the treated animals significantly changed throughout the course of treatment relative to the untreated animals. These parameters were the Mie scattering slope ($P < .0001$), Mie-to-total scattering fraction ($P < .001$), Tissue oxygenation ($P = .035$), Fat volume fraction ($P < .0001$), and Fluorescence residual ($p < .018$). Furthermore, the observed changes appeared to be proportional to the degree of vital tumor tissue and the formation of fibrosis.

Optical scattering characteristics are dependent on the size and density of cell nuclei and organelles as well as on the composition of the extracellular matrix (e.g. macromolecular aggregates, collagen fibers). In the histopathological evaluation, considerable alterations in the extracellular matrix (formation of fibrosis) and in the size and the density of (sub) cellular structures were observed in the tumors of the treated animals. These morphological and structural changes may lead to changes in tissue scattering properties that in turn may translate into changes in the Mie scattering slope and Mie-to-total scattering fraction. Although significant fibrosis and cellular disintegration after treatment with cisplatin may explain these specific changes, further research is needed to provide a better understanding of these relationships.

Tumor tissue oxygenation values of untreated animals remained hypoxic over time, whereas tumors of treated animals became progressively more oxygenated. This is consistent with previously reported results, where improved oxygenation of tumor tissue was observed due to tumor regression and altered metabolism after treatment with doxorubicin^{195,209,210}. For example, Vishwanath *et al* performed DRS using a surface probe and showed that mammary-tumor tissue oxygenation in treated mice increased after doxorubicin administration relative to the untreated controls.

A particularly interesting finding was the additional fluorescence observed in the treated group. Based on two-photon imaging, the extra fluorescence was specifically found in the cellular components of tumor tissue treated with cisplatin. Fluorescence was tumor specific and not observed in liver or muscle tissue of the treated animals. Earlier research has shown that some cancers accumulate diagnostic levels of endogenous protoporphyrin IX and other metabolic products of porphyrin as a result of tumor-specific metabolic alterations^{147,211}. Quantification of porphyrins using standard fit procedures is challenging, since the exact wavelength of the fluorescence bands of porphyrins strongly depend on the environment (e.g. pH) where it is measured^{147,211}. Whether porphyrin fluorescence

is primarily associated with certain tumor types or with response to systemic therapy is unknown. The exact basis of the additional autofluorescence emission observed in this study will be investigated in future studies.

The AFS spectra were fitted using the intrinsic fluorescence spectra of collagen, elastin, NADH and FAD as *a priori* knowledge. No considerable change over time was observed in these parameters. This may be due to the presence of significant amounts of unknown fluorescence which was not taken into account in the AFS curve fitting procedure, and hence may have influenced quantification of minor effects of the other fluorophores such as collagen, elastin, NADH and FAD.

The use of a broad spectral range in combination with a model-based analysis allows proper estimation of most individual DRS parameters. Some caution is advised concerning the Total hemoglobin contents within this study. Although a thin 21G optical needle (0.72mm) was used, minor bleeding at the tip of the needle may have caused high values for average Total hemoglobin content. However, a 14G coaxial cannula combined with a fiber-optic needle was successfully used to measure tissue optical properties in human breast tissue during surgery in a previous clinical study by Brown *et al*²¹². This indicates that small bleedings are not necessarily a problem when optical spectroscopy technology is applied *in vivo*. It also indicates the feasibility, within a clinical setting, of monitoring changes in perfusion and blood content of tumors by using a needle-based fiber-optic tool. Both parameters may be of specific interest for evaluation of tumor responses to anti-angiogenic drugs.

Earlier research suggests that cancer cells show specific alterations in different aspects of lipid metabolism. For example, the high proliferation of cancer cells requires large amounts of lipids as building blocks for biological membranes²¹³, whereas apoptosis related cell-death is associated with an accumulation of cellular lipids²¹⁴. Our setup is able to measure in the near infra-red wavelength range up to 1600 nm where fat and water absorption bands exist. This enables reliable estimation of these substances²⁰². In this study, histopathological analysis using Oil-red showed an increase in the amount of lipids in tumor sections for the treated animals. This is consistent with the increase in apoptosis-related cell death seen in the anti-cleaved caspase-3 images and the clear increase in fat volume fraction ($p < .0001$) measured with DRS for the same animals. Regarding the control group, the high off-set of fat % at day 0 and the decrease in the average fat volume fraction during follow up may be explained by the lower average “starting” tumor volume in the control animals (as compared to the treated animals), as well as the subsequent progressive growth of these tumors and the associated decrease in lipid content.

In the current study we used a tumor model that is known to be very sensitive to the MTD of cisplatin. Further studies in animal models with drug resistant tumors are needed to explore the differences in optical parameters in these settings. Moreover, it is likely that

the changes in tumor tissue vary based on the specific treatment given. To provide a more complete understanding of the relationship between optical spectroscopy parameters and pathological response, the effect of other drugs on spectroscopy parameters needs to be investigated further.

Conventional anatomical imaging alone lacks the sensitivity for early response monitoring or assessing the effect of new targeted therapies, which do not necessarily result in a change in tumor size. For these purposes, functional information, such as that obtained by ^{18}F -FDG PET ¹⁸¹⁻¹⁸³ and contrast-enhanced MRI ²¹⁵ is more suitable. Optical spectroscopy is a relatively new functional imaging technique that may contribute to fast response evaluation and timely shifting of systemic treatment. This could be of great clinical benefit, even when it requires (minimal) invasive optical spectroscopy measurements in the tumor. In a time of personalized medicine, repeated tumor core biopsy is increasingly used during the course of treatment to generate a genetic or epigenetic profile allowing selection of the best possible treatment. Repeated biopsies may, however, be confounded by intra-tumor heterogeneity ²¹⁶. By performing optical spectroscopy along the needle path, an “optical tumor profile” can be recorded covering a relatively large volume of tumor tissue. E.g. Nachabe *et al* ²¹⁷ showed that optical spectroscopy measurements at the tip of a needle allowed real-time tissue characterization during percutaneous interventions. As such, optical spectroscopy offers the potential to measure real time alterations in the optical profile during systemic treatment. In this way, it may help to personalize cancer treatments and may improve cost effectiveness of systemic treatment in cancer.

In conclusion, this study shows that dual-modality diffuse reflectance–autofluorescence spectroscopy provides quantitative functional information that corresponds well with the degree of pathologic response of systemic treatment. This could be of considerable value for the monitoring and prediction of cancer therapy efficacy based on individual patient response. Further studies including resistant tumor models and various therapeutic drugs are needed to verify the initial findings of this work.



Chapter 10

Diffuse reflectance spectroscopy: towards real time quantification of steatosis in liver

D.J. Evers

A.C. Westerkamp

J.W. Splethoff

V. Pully

D. Hompes

B.H.W. Hendriks

W. Prevoo

M-L.F. van Velthuisen

R.J. Porte

T.J.M. Ruers

Submitted

INTRODUCTION

Liver steatosis is one of the most important risk factors for primary non-function or early graft failure after orthotopic liver transplantation (OLT). Liver steatosis ranges from the less severe non-alcoholic fatty liver disease (NAFLD) to severe non-alcoholic steatohepatitis (NASH) ²¹⁸. Steatosis is generally characterized quantitatively and qualitatively. Steatosis is traditionally quantified as *none* (<5%), *mild* (5% to 33%), *moderate* (33% to 66%), or *severe* (>66%) dependent on the percentage of hepatocytes containing fat vacuoles ^{160,168,219-221}. Within the degree of fat accumulation in the hepatocytes, the histological evaluation of steatosis can be qualified in two major patterns; microvesicular and macrovesicular steatosis. Microvesicular steatosis solely, has been shown to have no negative impact on outcome ²²²⁻²²⁴. Yet, several studies have shown that moderate and severe macrovesicular steatosis of liver grafts is associated with impaired graft function after transplantation ²²⁵⁻²²⁸.

Assessment of fatty liver grafts during OLT is still a challenge for the transplant team. Surgical evaluation of fat accumulation by visual inspection and palpation during organ procurement has low predictive values and remains subjective ²²⁹. Conventional imaging technologies also have their limitations in steatosis analysis and quantification. Ultrasound (US) is widely used in clinical practice to detect fatty infiltration by assessing the echogenicity in the liver. Disadvantages of this technique are that it is not quantitative, prone to inter-observer variance and its sensitivity is reduced in morbidly obese patients ¹⁶². Computer tomography, magnetic resonance imaging, and magnetic resonance spectroscopy are able to visualize intrahepatic fat very accurately. The limitations of all three techniques are the inability to differentiate between macro- and microvesicular steatosis and the relatively time consuming and logistic efforts involved in these methods during a donation procedure ^{230,231}. New techniques such as electrical bioimpedance have recently been used to assess hepatic steatosis with high reliability ²¹⁹. Yet, only results in an animal set-up have been displayed.

Invasive histological evaluation still remains the gold standard for assessment of steatosis in liver tissue ²³². However, discrepancy in histological analysis has been described due to variability in interpreting the histological assessment per biopsy and the inter-observer variation among expert pathologists ²³³.

Over the last decade, diffuse reflectance spectroscopy (DRS) has been suggested to be a potential diagnostic tool for objective and quick assessment of tissue lipid concentration ^{95,163,234}. During DRS, tissue is illuminated by a selected light spectrum. By subsequent analysis of absorption and scattering characteristics, an 'optical fingerprint' is obtained which represents specific biochemical and morphological information of the tissue examined. DRS is consequently able to determine the amount of fat in the tissue that is illuminated. The goal of the present study is to investigate whether DRS allows to quantify steatosis in human liver tissue in an *in vivo* as well as in an *ex vivo* clinical setting.

MATERIALS AND METHODS

Clinical study design

The study was conducted at The Netherlands Cancer Institute - Antoni van Leeuwenhoek hospital (NKI-AVL) between October 2009 and December 2012, under approval of the protocol and ethics review board. Optical measurements were performed both *in vivo* and *ex vivo*.

For *in vivo* measurements, 17 patients were included that were scheduled for partial liver resection mainly because of metastatic disease. Written informed consent was obtained from all patients. Before liver resection was performed, a 15 Gauge optical needle (Figure 1a, Invivo, Schwerin, Germany) was inserted into normal liver tissue *within* the planned resection area (Figure 1B and 1C). Ultrasound guidance (Hitachi Aloka, ProSound SSD-4000) was used to confirm the location of the tip of the needle to be in normal liver tissue and at least 2 cm from the liver tumor. A total of 242 optical measurements were performed at 49 different measurement locations. After the optical measurements, a twist coil marker (OTM 3.0SA, BIP GmbH, Türkenfeld, Germany) was inserted to mark the exact measurement location.

Ex vivo optical measurements were performed in normal liver tissue from 41 patients after partial liver resection. These patients included the 17 patients from the previously mentioned *in vivo* analysis combined with 24 additional patients that underwent only *ex vivo* measurements of resected liver tissue. Directly after liver resection DRS measurements were performed within benign liver tissue at least 2cm from the metastatic sites. Several measurement locations were determined within each tissue specimen and on average 5 consecutive DRS measurements were performed at each measurement location. A biopsy was then directly taken from all specific measurement locations for further histopathological analysis. A total of 636 DRS measurements at 127 different measurement locations were collected (Figure 1D).

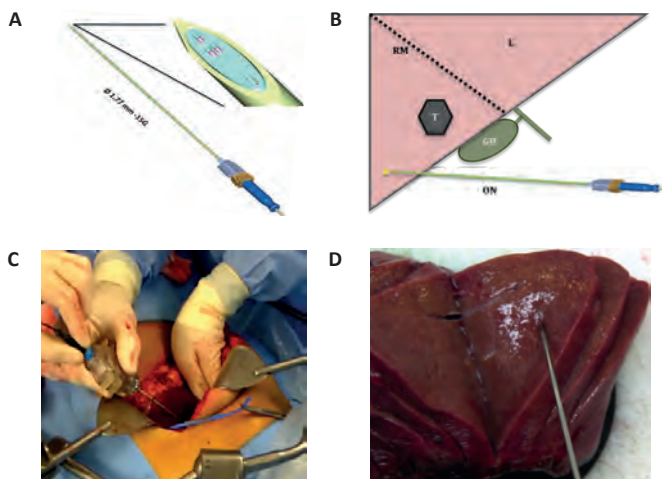
Optical spectroscopy instrumentation

Recently, Nachabé *et al* described the instrumentation and calibration procedure of our DRS system^{23,33,38,95}. The DRS system consists of a console comprising a Tungsten/Halogen broadband light source and two spectrometers. The two spectrometers resolve light in the visible wavelength range between 400 nm and 1100 nm (Andor Technology, DU420A-BRDD) and in the near infrared wavelength range from 800 up to 1700 nm (Andor Technology, DU492A-1.7), respectively. An optical probe containing four optical fibers is attached to the DRS system for optical measurements¹⁶⁵. One fiber was connected to the light source and two fibers were connected to the spectrometers to capture the diffusely scattered light from the tissue in this study. The remaining fiber was not used. The average tissue volume that is illuminated with the probe is roughly 5 mm³. The acquisition time of each spectrum was on average 0.2 seconds.

Histo-pathologic analysis

A pathologist located the twist markers inserted into the resected liver tissue after the *in vivo* measurements and excised the surrounding liver tissue for tissue analysis. These biopsies as well as the biopsies retrieved from the *ex vivo* measurements were first fixed in formalin, then paraffin embedded and processed for standard hematoxylin and eosin (H&E) staining. Three experienced pathologists, who were blinded for the outcome of the DRS results, individually examined the histological slides and visually determined the amount of steatosis within the benign liver tissue. A semi-quantitative assessment of steatosis was determined by estimating the percentage of hepatocytes containing lipid droplets (both microvesicular and macrovesicular steatosis droplets) in 10 consecutive fields (magnification 25x). Macrovesicular steatosis was defined as fat vesicles larger than the cell nucleus, often displacing the nucleus. Microvesicular steatosis was defined as fat vesicles with similar size or smaller than the liver cell nucleus. The pathologic degree of steatosis was estimated with increments of 5% steps. If both steatosis types were evidently present with similar percentages, the steatosis was defined as a 'mixed type'. The mean of steatosis quantifications for each tissue specimen determined by the three pathologists was used for comparison with the DRS analysis. Each tissue specimen was then divided into one of four preselected steatosis groups; 'none' 0% to 5% steatosis, 'mild' 5% to 33% steatosis, 'moderate' 33% to 66% steatosis and severe >66% steatosis. Finally, the liver tissue was also categorized by macrovesicular, microvesicular or mixed steatosis type.

Figure 1. Overview of the optical spectroscopy system and optical measurements performed. (A) Optical needle with close-up of the tip; (B) Schematic display of an *In vivo* measurement performed *before* liver resection; L - benign liver tissue; RM - planned resection margin; T - tumor; GB - gallbladder; ON - optical needle; (C) *In vivo* and (D) *Ex vivo* measurement in "normal" liver tissue.



Spectral data analysis

The light delivered to the tissue by the illumination fiber is subject to optical absorption and scattering before being collected by the detection fiber of the optical probe. Optical absorption is determined by the concentration of chromophores in the probed tissue. Each chromophore has its own intrinsic optical absorption characteristic, which is a function of wavelength. Fat and water are the dominant chromophores in the wavelength range between 1100 and 1600 nm³⁸. Oxygenated and deoxygenated hemoglobin and bile are the dominant chromophores in the wavelength range between 500-900 nm⁹⁵. The total absorption of the tissue as a function of wavelength can be written as the summation of the absorption of each chromophore multiplied by their concentrations in the tissue.

Optical scattering in tissue is dependent on the cellular structure of the target tissue and is sensitive to size and density of cellular and subcellular structures. Optical scattering can be described by the reduced scattering coefficient at a certain wavelength. To interpret the acquired DRS spectra, a widely accepted analytic model, introduced by Farrell *et al*³⁶, was used to estimate the various DRS absorption and scattering coefficients. The acquired spectra were fitted and analyzed over the wavelength range from 500 to 1600 nm. Spectral characteristics analysis was performed with a Matlab software package (MathWorks Inc., Natick, MA). Median values for fat, water, oxygenated and deoxygenated hemoglobin, bile and the scattering parameters were calculated from the obtained spectra of each optical measurement.

Statistical analysis

The lipid fraction scored by the pathologist was considered to be a two dimensional analysis of the same three dimensional volume of liver tissue analyzed with DRS. To be able to compare the pathological analysis to the DRS analysis, the pathological lipid fractions were recalculated using the principle postulated by Weibel *et al*²³⁵ and the following formula $L_{volume} = \frac{4}{3\sqrt{\pi}}(L_{area})^{3/2}$. L_{area} is the lipid fraction from the histological slide of the liver tissue scored by the pathologist and L_{volume} is the histological volume lipid fraction assuming a homogeneous volume distribution of lipid spheres.

Inter-observer variability between pathologists was determined using a one-way single score intraclass correlation (ICC). We used a Spearman's rank correlation test for the correlation between both the DRS *ex vivo* measurements and the pathologists' quantification of steatosis as well as for the correlation between *in vivo* and *ex vivo* measurements within the same 17 patients. Analyses were performed using SPSS (Statistical Package for the Social Sciences, version 16.0).

RESULTS

A total of 41 patients (24 male and 17 female) were included in this study. The average age of all patients was 64 years (range 38 to 83 years). Patient characteristics as well as the histological characterization of the liver tissue are displayed in table 1.

Histological characteristics

To be able to assign specific DRS patterns to differences in liver tissue composition, detailed histopathological examinations were performed for the tissue areas measured. Examples of the steatosis patterns encountered are displayed in figure 2. The generally observed pattern of steatosis was a diffuse and relatively homogeneously spread of clusters of lipid droplets as depicted in figure 2A+B. Within a liver lobule the lipid droplets particularly accumulate near the central vein (Figure 2C). Histological analysis determined 22 patients in the group with less than 5% steatosis (represented as the group 'none'). Twelve of these 22 patients had between 1% and 5% steatosis, the other 10 patients had 0% steatosis. Fifteen patients had 'mild' steatosis (5% to 33%), four had 'moderate' steatosis (33% to 66%), and no patients were diagnosed with 'severe' steatosis (>66%). Differentiation of the steatosis type was performed on the 19 patients diagnosed with $\geq 5\%$ steatosis. Most of these patients (N = 12) displayed a mixed pattern of both microvesicular and macrovesicular steatosis (figure 2D). Macrovesicular steatosis, with lipid droplets up to 80 μm , was observed in 6 of these 19 cases, while microvesicular steatosis was only observed in 1 patient. High magnification illustrations of both steatosis subtypes are respectively displayed in figures 2E and 2F. Three independent pathologists determined the quantification of steatosis for each individual patient. The calculated intraclass correlation (ICC) between the pathologists was 0.949, indicating good agreement with each other.

DRS steatosis analysis

On average, 15 DRS measurements were performed within each liver specimen. Examples of the optical spectra from one patient of each defined group and their corresponding histopathological slides are displayed in figure 3. The spectrum in the vicinity of 1200 nm is dominated by the absorption of light by lipid cells. A more prominent inverse sharp peak in the light spectrum at this wavelength corresponds to a higher fat concentration in the tissue and consequently a higher steatosis score was observed.

Figure 4 shows boxplots of the calculated concentrations of fat, water and bile as well as the scattering coefficient from all tissue measurements for each defined steatosis group. The amount of fat, as determined by DRS, clearly increases with a higher grade of steatosis on histopathology. In addition, with an increasing steatosis score a significant

decrease in water and bile concentration is observed together with an increase in scattering at 800nm.

The results of the average concentration of steatosis determined by both DRS and histology for each measured liver tissue specimen are displayed in figure 5. A high level of agreement is presented with a correlation of 0.854 when comparing the results of both quantification methods for each measured tissue specimen.

The comparison of the DRS analysis for each of the 17 patients for which steatosis was determined both *in vivo* and *ex vivo* is depicted in figure 6. The correlation of 0.925 indicates little difference in the quantification of liver steatosis by the optical needle before and after resection.

Table 1. Patient and histological characteristics. *Chemotherapy regime for colorectal metastases consisted of a combination of Capecitabine and Oxalipatin. 7 patients also were treated with Bevacizumab. Mesothelioma was pretreated with Cisplatin and Pemetrexel and mamma carcinoma metastases were pretreated with Capecitabine and Lapatinib

		N (percentage)
Included patients	Total	41
	Male	24 (58.5%)
	Female	17 (41.5%)
Indications for resection	Colorectal metastases	38 (92.8%)
	Mesothelioma	1 (2.4%)
	Mamma carcinoma metastases	1 (2.4%)
	Hepatocellular carcinoma	1 (2.4%)
Neoadjuvant chemotherapy	Yes	22 (53.7%)*
	No	19 (46.3%)
Histological steatosis quantification	None (0% - 5%)	22 (53.7%)
	Mild (6 - 33%)	15 (36.6%)
	Moderate (34 - 66%)	4 (9.7%)
	Severe (> 67%)	0
Histological steatosis characterization	No steatosis	10 (24.4%)
	Microsteatosis	2 (4.9%)
	Macrosteatosis	14 (34.1%)
	Mixed steatosis	15 (36.6%)

Figure 2. Examples of steatosis after standard hematoxylin and eosin (H&E) staining. (A, B) Typical example of the diffuse pattern of steatosis in liver tissue in one patient specimen; (C) Lipid droplets generally accumulate in the zone around the central veins in each liver lobule (D) Normal liver with mixed pattern of both macro- and microsteatosis; High magnification of (E) Microsteatosis; and (F) Macrosteatosis. Magnifications are added in the bottom right corner of each photo.

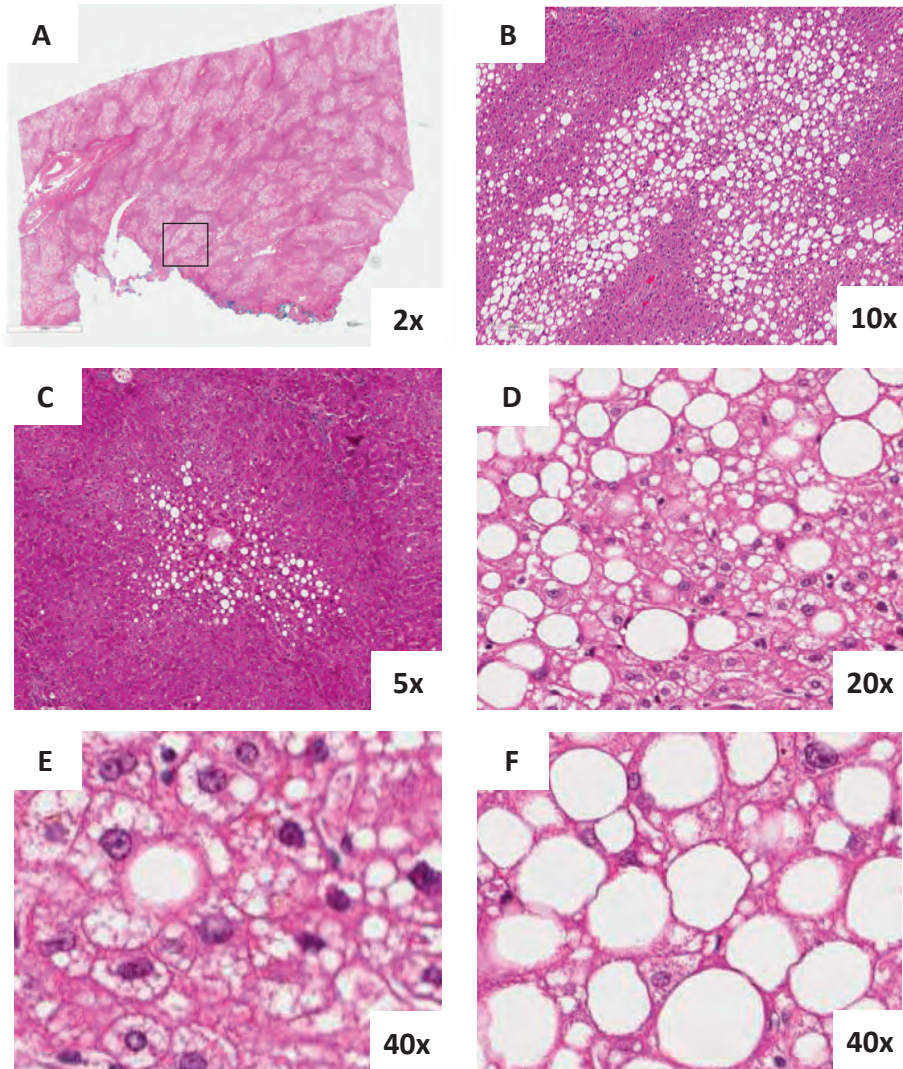
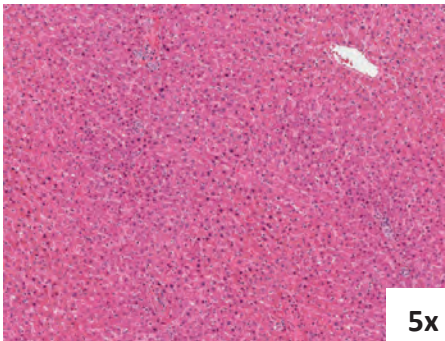


Figure 3. Examples of steatosis of the liver of increasing severity and the corresponding light spectra of the tissue generated with DRS. The estimated steatosis percentages for each tissue sample by three specialized pathologists and the corresponding DRS spectra are displayed. Specific wavelengths from which the fat volume concentration was calculated are indicated between the *dashed lines*. Magnifications are added in the bottom right corner of each photo.

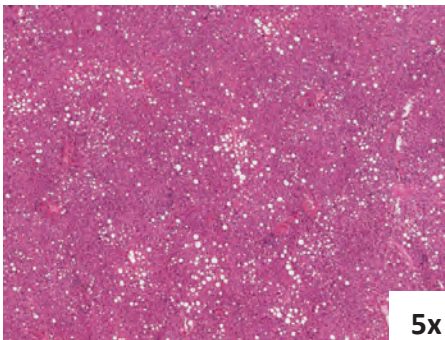
No Steatosis

Steatosis Pathology: 0%



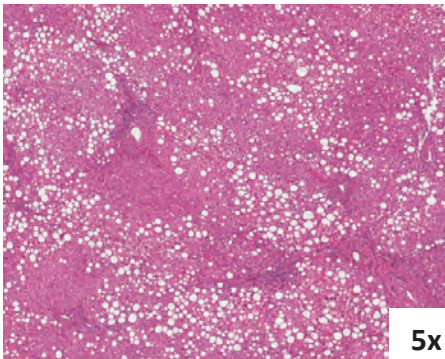
Mild Steatosis

Steatosis Pathology: 27%

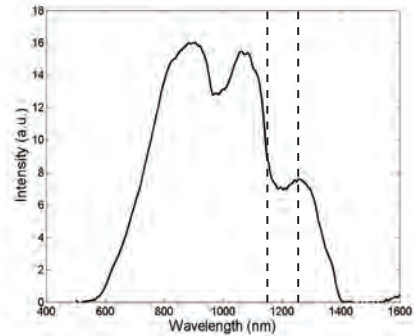


Moderate Steatosis

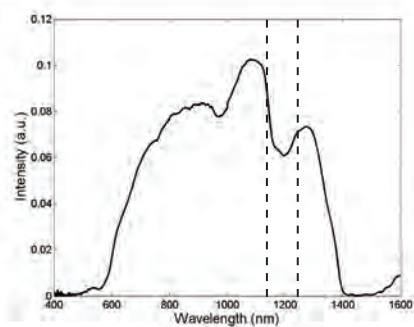
Steatosis Pathology: 47%



Steatosis DRS: 0%



Steatosis DRS: 30%



Steatosis DRS: 57%

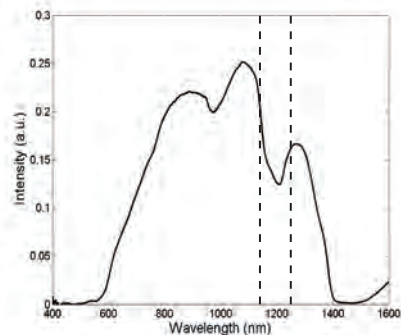


Figure 4. Boxplots of the concentrations of (A) Fat ; (B) Water ; (C) Bile and (D) the Scattering at 800nm of all included patients by steatosis group as defined by histology.

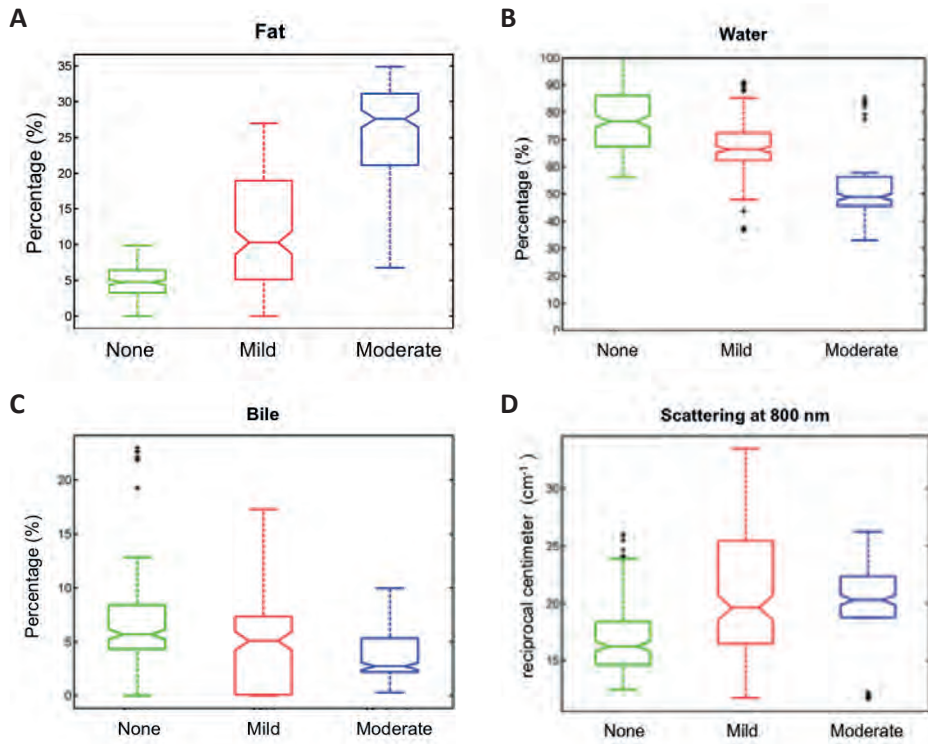


Figure 5. Comparison of the steatosis analysis by DRS versus Pathology in 41 patients. Spearman rank correlation = 0.854

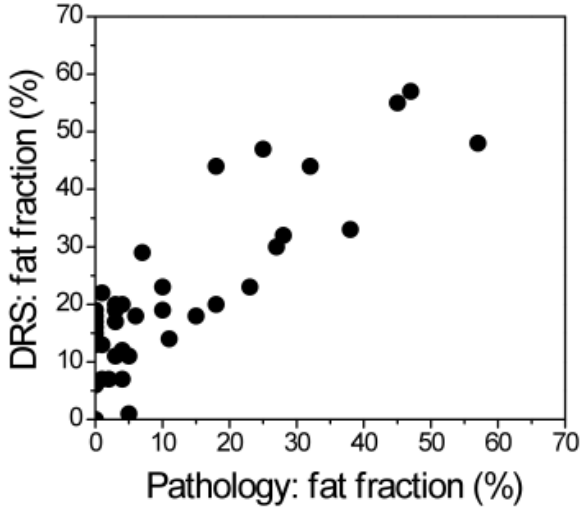
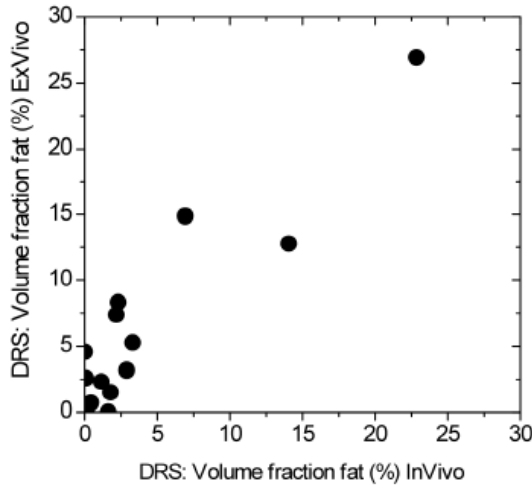


Figure 6. Comparison of steatosis analysis by DRS per patient for 17 patients *in vivo* versus *ex vivo*. Spearman rank correlation: 0.925



DISCUSSION

Liver steatosis may significantly affect the function and survival rate of donor livers after transplantation. This renders identification of moderate and severe steatosis of significant clinical relevance. Invasive histological evaluation remains the gold standard for the assessment of steatosis in liver tissue²³². However, limitations in the histological assessment have necessitated the search for novel tools capable of accurate quantification of fat in liver tissue²³³. DRS has the ability to determine the lipid fraction within a tissue specimen with high accuracy^{23,33,163,236}. Our group recently compared the accuracy of DRS quantification of liver steatosis in murine livers with analysis by magnetic resonance spectroscopy, magic angle spinning - nuclear magnetic resonance, high-performance thin-layer chromatography and histopathology. A good agreement of the estimated lipid fractions was demonstrated between DRS, the various imaging techniques and histopathologic analysis²³⁴. The next step towards the introduction of DRS into daily clinical practice of liver surgery, such as liver transplantation, is to first explore the accuracy quantifying liver steatosis in human liver tissue *in vivo*.

In this present study we have analyzed liver tissue in comparable conditions to those during liver transplantation: in a controlled situation in the operating theater during abdominal surgery directly before and after liver tissue resection. Our results confirmed that diffuse reflectance spectroscopy shows good agreement (correlation of 0.854) in fat quantification of liver tissue in comparison with the mean histological quantification of three independent expert pathologists. We subsequently demonstrated that DRS could quantify liver steatosis *in vivo* and *ex vivo* with comparable accuracy. The results of this preliminary study demonstrate that DRS could have the potential to improve real time quantification of steatosis during liver surgery.

The main advantages of DRS compared to other available imaging techniques as well as to histopathology are that the quantification of steatosis can be performed in the operating theatre during surgery and it can be performed real time with feedback of the estimated lipid fraction within seconds. In contrast, histological analysis requires specific staining at the pathology department and will generally take at least 30 minutes before reliable conclusions can be drawn. This is an important feature considering that the time factor is critical in all transplantation surgery.

In addition, incorporation of DRS into a needle as shown in this study allows a single point measurement of several mm³ at the tip of the optical needle. This could arguably be assumed a disadvantage considering the aim to determine the steatosis level in the whole liver. Yet, performing continuous measurements with direct feedback of the tissue parameters during the insertion of the optical needle into the target tissue allows direct characterization of tissue all along the whole needle path. When we take the most

common diffusely clustered pattern of liver steatosis (Figure 2A) into account, multiple DRS measurements along the needle tract could arguably provide a good representation of the average steatosis fraction throughout a larger area of the liver specimen compared to standard histological analysis of a single core biopsy. A notable observation in the liver specimens of the patients included in this study was that there was little variation of the steatosis concentration determined with DRS between different locations within each individual patient. The individual standard variation of the fat fraction varied from 1.0% and 13.0% steatosis.

The main disadvantage regarding DRS in this particular study is that it concerns an invasive technique. During the invasive measurements *in vivo* we did not observe any bleeding complications of the examined liver tissue. Microscopic analysis of the examined tissue specimen did not reveal obvious tissue damage or local bleeding caused by the optical needle. Moreover, an improved version of our optical needle has recently been developed for clinical study, now 20G (= 0.8 mm) instead of 15G ²³⁷. These arguments render our DRS a less invasive technique when comparing it to the generally performed core biopsy for histopathology analysis, the current gold standard.

Our results displayed in figure 5 show that liver specimens with histologically small percentages of steatosis appear to have higher percentages of steatosis detected with the DRS system. Percent differences up to 20% were observed between the analysis methods. The staining method we used was a standard H&E staining. Levene *et al* ²³⁸ demonstrated that this staining method could cause an underestimation of the quantification of steatosis by expert pathologists when the lipid droplets are mainly microvesicular, as shown by an alternative staining method with Oil Red-O on frozen liver samples. However, this method is not routinely used in clinical practice. The discrepancies in steatosis concentrations in our study could be caused by an underestimation of the hepatic steatosis by the pathologists due to the standard staining method used. The clinical consequences of this discrepancy, however, are limited as it is well known that minimal degree of steatosis has no impact on outcome after liver transplantation ²²⁵⁻²²⁸. The good ICC between the three pathologists is notable when compared to previous studies. We believe that this high correlation is due to the fact that more than half (N = 22) of the included patients were assigned to the 'no' steatosis group. Thus resulting in a relatively low variation in steatosis concentration over the entire cohort.

Within the steatosis groups as defined by histology, important differences were displayed in concentrations of water and bile (Figure 4). Both tissue parameters significantly decreased with an increase of lipid deposit in the hepatic tissue. The decrease in water concentration with increased steatosis is in line with observations made by Marsman *et al* ²³⁹ in murine studies. In a subsequent study, the same group confirmed these results, hypothesizing the decrease of water concentration to be a result of

exudation from the liver tissue ²⁴⁰. The decrease of bile within the liver tissue could be caused by decreased hepatic uptake of serum bilirubin due the lipid deposits within the hepatocytes. This hypothesis is supported by several groups who have reported increased serum bilirubin levels in patients with moderate and severe hepatic steatosis ^{159,241}.

The predominance of macrovesicular and mixed steatosis in our patient cohort is comparable to previously published papers ^{128,160,242}. Poor graft outcome which is commonly associated with macrovesicular steatosis has proven the clinical relevance to determine steatosis subtype ²²⁵⁻²²⁸. Because of the minimal number of patients with microvesicular steatosis an analysis to distinguish both steatosis subtypes by DRS within our patient cohort was not possible. Due to this limitation in our study we could not draw any conclusions towards a possible applicability of DRS distinguishing micro- and macrovesicular steatosis.

In future studies with more tissue specimens, we aim to determine if DRS can qualify both steatosis subtypes based on the described scattering properties of DRS. We hypothesize that discrimination of microvesicular from macrovesicular steatosis could be made using DRS based on differences in the scattering of light. Optical scattering depends on the size and distribution of cellular particles compared to the wavelength of light [36]. Notable differences in the scattering of light at 800nm between the defined steatosis groups were apparent as displayed in figure 4. Graaff *et al* ²⁴³ demonstrated that the wavelength dependence of the scattering parameters depends on the size of the scattering particles. Since microvesicular and macrovesicular steatosis droplets significantly differ in size, careful analysis of the wavelength dependence of the scattering parameters might allow discrimination between the two types of steatosis.

Conclusion

In a preliminary study, we have demonstrated that DRS can quantify steatosis in liver tissue both *in vivo* and *ex vivo* with good agreement when compared to histopathology analysis, the current gold standard. DRS analyses of liver steatosis can be performed within seconds and could therefore be used for a rapid clinical assessment of the liver tissue during liver donation and prior to transplantation. Future studies will focus on the question of whether DRS can also distinguish between microvesicular and macrovesicular steatosis in real-time and to explore effects on transplantation of a liver organ.

Part 4



Chapter **11¹**

General discussion and future prospective

Many years of basic research with optical spectroscopy have demonstrated its potential to be translated into every-day medical practice and to enhance to clinical decision-making. The preceding chapters demonstrate our scientific achievements towards the applicability of diffuse reflectance and fluorescence spectroscopy for tissue differentiation during medical interventions.

In the preclinical phase, we developed and validated an optical spectroscopy system based on the knowledge of previous publications in the optical spectroscopy field. Innovative features compared to preceding work by other groups were incorporated into our spectroscopy system. The spectroscopic analysis range was extended into the near-infrared light spectrum up to 1600nm. We could now quantify ‘new’ tissue chromophores water, lipid and collagen and include this information into the spectral analysis algorithm. We enlarged the distance between the optical needle fibers. This rendered our optical system more sensitive to subtle changes in chromophore concentration. Finally, intensive research was put into the development and optimization of the analysis software and miniaturized optical needles^{23,26,33,38,95,234}. With these new features, we aimed to take a significant step towards introducing optical spectroscopy into daily clinical practice via feasibility studies first *ex vivo* and later *in vivo* human.

EX VIVO SPECTROSCOPY ANALYSES (CHAPTERS 4-7)

The primary focus for our research was on malignancies of lung, liver and breast tissue. In an *ex vivo* analysis of these tissues, we first explored the discriminating accuracy of DRS between normal and malignant tissue. The performance of a combination of DRS and FS was then compared to DRS alone in human lung tissue. Secondary focus was on advanced development and refinement of our data analysis algorithm, measurement procedure and equipment design towards actual clinical deployment.

We can draw several general conclusions from the results of the four *ex vivo* studies. The two most important observations were: (1) the high overall accuracy of DRS discriminating tumor from normal tissue we derived and (2) the rapid spectral feedback obtained from each measurement that was within seconds rendering real-time analysis possible. The overall accuracy varied from 81% in the primary lung tissue analysis to 94% in liver tissue analysis. The sensitivities and specificities for the *ex vivo* studies are displayed in table 1. These figures can be considered high when compared to previous studies involving DRS on human tissue (see chapter 3). Although it is difficult to put these results into perspective due to dissimilarities in both study design and data analysis, our results were considered very encouraging and reason for us to continue towards clinical applications via *in vivo* human studies.

Tabel 1. Sensitivity (Sens) and Specificity (Spec) for DRS and FS in our four *ex vivo* studies.

	DRS		FS	
	Sens	Spec	Sens	Spec
Lung DRS Chapter 4	89% & 78%	79% & 86%	*	*
Liver Chapter 5	94%	94%	*	*
Mamma Chapter 6	90%	88%	*	*
Lung DRS+FS Chapter 7	98%	86%	90%	75%

Two analysis methods were used to examine the derived data. In the first lung study (Chapter 4) we performed an empiric and a model-based approach. The results of the model-based approach were slightly superior to the empiric analysis. These results concurred with the conclusions drawn by our group in a preceding paper on breast tissue examination with DRS³⁸. An additional advantage of the model-based approach is that it yields information of chromophore concentration, which can be also compared to histology analysis. These results induced the decision to solely use and further optimize our model-based algorithm in subsequent studies.

We achieved notable DRS improvements of the overall accuracy of the second lung tissue study (Chapter 7). The improved algorithm is believed to be one of the explanations. The other is arguably the more standardized approach performing optical measurements in normal lung parenchyma. In the first *ex vivo* lung study normal lung tissue was randomly chosen and included. The spectroscopic results of this tissue showed significant variation that corresponded to large differences in tissue histology. The DRS spectrum in macroscopic pink lung tissue that corresponded with non-collapsed alveoli still being filled with air was significantly different from the DRS spectrum in macroscopic dark purple colored lung tissue that corresponded with collapsed alveoli. Additionally, air-filled lung parenchyma is arguably more comparable to the *in vivo* situation. We therefore only performed measurements in normal lung parenchyma with a pink appearance in the second *ex vivo* lung study.

Applying fluorescence spectroscopy for lung tumor detection did not significantly enhance the discrimination capacity compared to DRS spectroscopy alone. The fluorescence spectroscopy measurements were performed in the visual light spectrum between 400 and 750 nm. Hemoglobin absorbs light wavelengths mainly between 500 and 650 nm. Blood residue in the alveoli in front of the optical needle tip can absorb part of the fluorescent light signal restricting the collection of data for the fluorescent spectral

analysis. This is the main reason for the limited added value to the overall discriminative accuracy of DRS and FS combined.

The main similarity of all previous published data on spectroscopy analyses in human tissue is the analysis process on cohort data from all included patients. Significant variation of tissue between different individuals when studied at cellular level is notable. This becomes more prominent when studying inhomogeneous human tissues such as breast tissue as we displayed in chapter 6. Intratumoral heterogeneity has also been shown in recent studies^{244,245,246}. We believe that inter-patient variation will reflect on an increased variance of the concentrations of measurable optical chromophores in the tissues. As a result, the accuracy of discrimination between different tissue types can be impeded when optical spectroscopy analysis is performed on a cohort data basis. One solution to counter this phenomenon would be to create a database of the normal values of each tissue chromophore within an enormous cohort of people. However, at this stage this is a very time-consuming effort for a technology that still has to prove its possible role in modern medicine. We therefore opted for a different approach by studying and developing an analysis approach on derived data within individual patients. We revealed substantial limited variation in chromophore concentration within patients compared to cohort data analysis. We therefore focused on a method of gathering and using spectral information of normal tissue to subsequently detect and identify the spectral changes in malignant tissue. These results reflected in the superior discrimination accuracy of our individual data analysis approach compared to the cohort analysis method as displayed in chapters 5-7 for liver, breast and lung malignancies, respectively.

The general observations of differences in chromophore concentration and scattering coefficient determined in tumor tissue compared to normal tissue of the lung, liver and breast are displayed in table 2. No comparisons of our results could be made with previous publications on liver and lung in the spectroscopy field, due to a lack of comparable studies. Our conclusions in breast tissue are similar to those in previous studies. Brown *et al*⁶⁰ and Volynskaya *et al*⁶⁹ demonstrated increased total hemoglobin concentrations in breast cancer. Zhu *et al*⁷¹ and Keller *et al*⁷² both found higher collagen levels in breast malignancies. Zhu *et al*⁵⁹ also observed an increased scattering coefficient in breast cancers compared to normal breast tissue. In a recent overview, Bydlon *et al*²⁴⁷ displayed the current knowledge on all tissue chromophores.

Tissue saturation was also determined in all *ex vivo* studies. We disregarded the results from the *ex vivo* analysis because it is unclear what the value of this parameter was in non-perfused human tissue. Tissue hypoxia has been demonstrated to be an important tissue factor in tumor tissue biology^{102,166,248}. Hence, we do believe that this tissue parameter can be of importance in future *in vivo* studies of the optical spectroscopy in the oncological field.

A final observation of the histology of the measured tissue specimen in all *ex vivo* studies is that there was no obvious tissue damage caused by the optical needle. This was considered an important conclusion for the advancement towards *in vivo* spectroscopy analyses.

In conclusion, from our results of the four *ex vivo* studies, we argued that our optical spectroscopy system could detect the difference between normal tissue and malignant tissue within an individual patient in an *ex vivo* analysis with high accuracy. The next step towards clinical applications of these optical spectroscopy techniques was to explore their consistency in *in vivo* analyses.

Table 2. General differences in chromophore concentration and scattering coefficient in tumor compared to normal tissue. The arrows indicate a decrease (↓) or an increase (↑) of the measured chromophore in malignant tissue compared to the levels in normal tissue.

	Lung DRS Chapter 4	Liver Chapter 5	Mamma Chapter 6	Lung DRS+FS Chapter 7
Total hemoglobin	↓	↓	↑	↓
Fat		↓	↓	
Collagen			↑	↑
Scattering	↓	↓	↑	↓
Water	↑			↑
Bile		↓		

IN VIVO SPECTROSCOPY ANALYSES (CHAPTERS 8-10)

We first developed a custom-made optical console for *in vivo* human studies. A CE marked 15G optical needle was then developed by Invivo (Schwerin, Germany). For the murine studies, we developed a 21G fiber-optic needle.

The main objective of the *in vivo* human studies was to explore the accuracy of DRS and FS between normal and malignant tissue in viable liver tissue (Chapter 8). Other objectives towards specific clinical applications focused on the ability to monitor chemotherapy response (Chapter 9) and the ability to quantify liver steatosis (Chapter 10)

Human liver *in vivo* analysis (chapter 8)

We displayed a comparable accuracy for the discrimination of colorectal liver metastases from normal liver parenchyma *in vivo* when compared to our previous *ex vivo* DRS results. The *in vivo* sensitivity and specificity were 95% and 92%, respectively (both

94% in *ex vivo* analysis, Chapter 5). The main discriminative liver tissue chromophores were total hemoglobin content, methemoglobin and bile. In FS, the only significant tissue parameter was the Optical redox ratio. The addition of FS to the optical system did not enhance the discriminative accuracy. In addition, we visualized specific protoporphyrin-like peaks in the fluorescence spectra within the examined tissues. Increased intensity of these peaks was shown in colorectal metastases compared to normal liver parenchyma suggesting higher concentrations of these fluorescent molecules in malignant tissue. Finally, we showed that preoperative treatment with chemotherapy did not influence the discriminative accuracy of our spectroscopy system. This remained above the 90% for all patients, with or without systemic pretreatment.

If DRS and FS could be incorporated into a biopsy needle, these techniques could in theory aid the physician to perform a targeted biopsy. In a time of personalized medicine, this could reduce the need for repeated biopsy for tumor diagnosis and genetic profiling due to indeterminate histology analysis. The optical screening area of our spectroscopy needle is only several mm³. However, in theory the direct feedback during introduction of an optical needle provides an optical tissue profile of a relatively large tissue volume along the needle track. This could be an interesting feature for real-time tissue characterization at the tip of a needle during percutaneous interventions with needle guidance by an imaging modality like ultrasound, X-ray or MRI.

It must be noted that our *in vivo* liver tissue analysis was only performed on liver metastases, no primary liver tumor. We demonstrated that bile is an important tissue parameter for metastases differentiation from normal liver tissue. Discrimination of primary liver disease (e.g. hepatocellular carcinoma) can in theory be more difficult using DRS due to the expected diminished differences of bile concentration and the less abrupt marginal differences compared to colorectal liver metastases. Future studies will be needed to focus on this hypothesis.

Murine chemotherapy response monitoring (Chapter 9)

Palmer *et al* previously demonstrated the ability of DRS and FS to monitor tumor metabolism in an *in vivo* mouse model¹⁸. We explored the possibility of DRS and FS to monitor chemotherapy response in a comparable model using systemic Cisplatin. Our results demonstrated that the quantitative functional information provided by DRS and FS corresponded well to the degree of measurable pathologic response based on the levels of vital tumor and tissue fibrosis. Histology is still considered the gold standard for therapy response. Several tissue parameters were significant different in treated and non-treated tumors; Mie scattering slope, Mie-to-total scattering fraction, Tissue oxygenation, Fat volume fraction and Fluorescence residual. Cisplatin treatment resulted in an increased tissue oxygenation in the treated tumors, whereas the untreated tumors remained more

hypoxic. This is consistent with results of tumor metabolism in previous studies with or without systemic chemotherapy treatment^{19,41,111,166}. We found increased intracellular levels of fluorescence emission in the cisplatin treated mammary tumors between 600 and 700nm. We suggest that increased levels of porphyrins-like molecules in the tumor cells could cause these spectral changes^{147,249}. Yet, we did not detect increased levels of tumor necrosis within the cisplatin treated tumors in accordance with our other studies. The exact metabolic cause of these fluorescence peaks remains to be explored.

Current response monitoring is mainly performed using functional, non-invasive techniques such as fMRI, PET-CT and SPECT⁵. These imaging techniques still lack the sensitivity to detect therapy response in the first weeks after commencing systemic treatment.

The results of this murine study suggest that DRS and FS can display tissue alterations due to chemotherapy as soon as the histological response can be noted. These results arguably enhance the hypothesis that spectroscopy could be a valid tool for monitoring and prediction of cancer therapy efficacy in the near future. Our next step towards this goal would be to investigate the optical profile of chemotherapy resistant tumor models as well as the effects of various chemotherapeutic drugs on the results of optical sensing with DRS and FS.

Liver steatosis analysis (Chapter 10)

In chapter 5, we demonstrated the ability of the DRS system to calculate liver fat concentration or steatosis with high accuracy *ex vivo*. Liver steatosis is becoming more common in modern age with the increasing prevalence of diabetes mellitus²³². Some chemotherapy regimens have also shown increased levels of liver fibrosis and steatosis^{126,250}. Histology is still considered the gold standard for steatosis quantification²³⁸. From all conventional imaging techniques, MRI is the best technique for steatosis analysis but has its limitations. Most importantly, it cannot be used in the operating theater²⁵¹. Steatosis can have serious detrimental effects on patients after major liver surgery, such as liver resection and orthotopic liver transplantation^{252,253}. We therefore explored a possible clinical role of DRS for liver steatosis analysis *in vivo* during operations.

We displayed a high accuracy quantifying liver steatosis *in vivo*. The quantification results could also be displayed in real-time and in different parts of the liver along the needle path, which makes this technique interesting for clinical applications such as the selection of donor livers for transplantation. The main objective for future analyses will focus on the differentiation of the two main types of liver steatosis; macro- and microsteatosis.

In conclusion, we argue that the results of our pre-clinical and clinical feasibility evaluation of tissue discrimination with optical spectroscopy can be considered very

promising. We have shown that the spectroscopy console with optical needles and analysis software we developed can differentiate normal from tumorous tissue with high accuracies, can calculate liver steatosis with comparable accuracy to a pathologist and can detect tissue alterations soon after chemotherapy treatment.

Future focus and investigation

The next step towards clinical application of DRS and FS into daily medical practice is to explore the benefits of their incorporation into existing medical devices and the clinical workflow. We believe that an individualized approach to tissue sensing with optical spectroscopy is the key step towards clinical application of this technology. We also believe that optical spectroscopy is a technology that will aid the physician in daily practice, not by replacing but by enhancing existing technical modalities. Take for example the increasing use of hybrid operating theaters in which standard use of imaging technologies such as CT and ultrasound will be available. These techniques assist the physician in pinpointing the target tissue macroscopically. Based on the results revealed in this dissertation, we believe optical spectroscopy could subsequently be used for further microscopic analysis of the target tissue such as margin analysis and tissue characterization at the tip of the interventional device.

Applications in several medical fields are currently being considered. In Surgery, optical spectroscopy could contribute as an additional tissue-sensing tool in laparoscopy where tactile information of target tissue is not possible. The local tissue characterization options of this technique, such as liver steatosis quantification, could aid surgeons in peroperative decisions regarding extent of organ resection and possibility of organ selection for transplantation. DRS can accurately detect malignant tissue in several human organs; accurate tissue margin analysis after malignant resection for possible residual disease would be of high clinical relevance. A focus should be put towards development of a multi-channel optical spectral device to allow rapid analysis of larger tissue surface areas.

In Interventional Radiology, important steps are currently being made towards the development of an optical biopsy device. This could improve the first attempt accuracy of tissue biopsy procedures by rendering tissue-sensing options at the tip of the biopsy needle. Minimal invasive therapeutic interventions such as radio-frequency ablation could also benefit from the inter-procedural presence of DRS and FS. Current options for direct ablation monitoring are lacking. This inferior monitoring may contribute to local disease recurrence after radiofrequency ablation. FS has been shown to be able to predict the margin of the ablation zone^{94,96}. Our group is currently exploring this clinical question.

In Anesthesiology, the use of optical spectroscopy is being explored for enhanced nerve detection in minimal invasive nerve blocking procedures. The first results of these studies were recently published^{254,255}.

Finally, an increased interest by several groups is notable towards the use of optical spectroscopy for monitoring of systemic therapy response in the Medical Oncology field. The possibility of targeted biopsies for tumor profiling enhances the possible role spectroscopy could have in this medical field.



Chapter **11²**

References

1. Evers D, Hendriks B, Lucassen G, Ruers T. Optical Spectroscopy; current advances and future applications in cancer diagnostics and therapy. *Future Oncology* 2012; **8**(3): 1-14.
2. Dougherty L, Isaac G, Rosen M, *et al* High frame-rate simultaneous bilateral breast DCE-MRI. *Magn Reson Med* 2007; **57** (1): 220-5.
3. Chou C, Wu M, Chang H, *et al* Monitoring breast cancer response to neoadjuvant systemic chemotherapy using parametric contrast-enhanced MRI: a pilot study. *Acad Radiol* 2007; **14** (5): 561-73.
4. Kapse N, V G. Functional imaging of colorectal cancer: positron emission tomography, magnetic resonance imaging, and computed tomography. *Clin Colorectal Cancer* 2009; **8** (2): 77-87.
5. Harry V, Semple S, Parkin D, Gilbert F. Use of new imaging techniques to predict tumour response to therapy. *Lancet Oncol* 2010; **11** (1): 92-102.
6. Fujimoto J, Pitris C, Boppart S, Brezinski M. Optical coherence tomography: an emerging technology for biomedical imaging and optical biopsy. *Neoplasia* 2000; **2**: 9-25.
7. Podoleanu A. Optical coherence tomography. *J Microsc* 2012; **247**(3): 209-19.
8. Adhi M, Duker J. Optical coherence tomography--current and future applications. *Curr Opin Ophthalmol* 2013; **24**(3): 213-21.
9. Xu M, Wang L. Photoacoustic imaging in biomedicine. *Review of Scientific Instruments* 2004; **77**: 041101.
10. Li C, Wang L. Photoacoustic tomography and sensing in biomedicine. *Phys Med Biol* 2009; **54**(19): R59-R97.
11. Yao J, Wang L. Photoacoustic tomography: fundamentals, advances and prospects. *Contrast Media Mol Imaging* 2011; **6**(5): 332-45.
12. Hielscher A, Bluestone A, Abdoulaev G, *et al* Near-infrared diffuse optical tomography. *Disease Markers* 2002; **18**: 313-37.
13. Flexman M, Kim H, Gunther J, *et al* Optical biomarkers for breast cancer derived from dynamic diffuse optical tomography. *J Biomed Opt* 2013; **18**(9): 096012.
14. Fantini S, Sassaroli A. Near-Infrared Optical Mammography for Breast Cancer Detection with Intrinsic Contrast. *Ann Biomed Eng* 2012; **40**(2): 398-407.
15. Frangioni J. New technologies for human cancer imaging. *J Clin Oncol* 2008; **26** (24): 4012-21.
16. Kondepoti V, Heise H, Backhaus J. Recent applications of near-infrared spectroscopy in cancer diagnosis and therapy. *Anal Bioanal Chem* 2008; **390** (1): 125-39.

17. Brown J, Vishwanath K, Palmer G, Ramanujam N. Advances in quantitative UV-visible spectroscopy for clinical and pre-clinical application in cancer. *Curr Opin Biotechnol* 2009; **20** (1): 119-31.
18. Palmer G, Viola R, Schroeder T, Yarmolenko P, Dewhirst M, Ramanujam N. Quantitative diffuse reflectance and fluorescence spectroscopy: tool to monitor tumor physiology *in vivo*. *J Biomed Opt* 2009; **14**(2): 024010.
19. Cerussi A, Hsiang D, Shah N, *et al* Predicting response to breast cancer neoadjuvant chemotherapy using diffuse optical spectroscopy. *PNAS* 2007; **104** (10): 4014-9.
20. Zhou C, Choe R, Shah N, *et al* Diffuse optical monitoring of blood flow and oxygenation in human breast cancer during early stages of neoadjuvant chemotherapy. *J Biomed Opt* 2007; **12**(5): 051903.
21. Wagnières G, Star W, Wilson B. *In vivo* fluorescence spectroscopy and imaging for oncological applications. *Photochem Photobiol* 1998; **68**(5): 603-32.
22. Richards-Kortum R, Sevick-Muraca E. Quantitative optical spectroscopy for tissue diagnosis. *Annu Rev Phys Chem* 1996; **47**: 555-606.
23. Nachabé R, Hendriks B, Desjardins A, van der Voort M, van der Mark M, Sterenborg H. Estimation of lipid and water concentrations in scattering media with diffuse optical spectroscopy from 900 to 1,600 nm. *J Biomed Opt* 2010; **15** (3): 037015.
24. He S, Dunn K, Espino P, *et al* Chromatin organization and nuclear microenvironments in cancer cells. *J Cell Biochem* 2008; **104** (6): 2004-15.
25. Saidi I, Jacques S, Tittel F. Mie and Rayleigh modeling of visible-light scattering in neonatal skin. *Appl Opt* 1995; **34**(31): 7410-8.
26. Müller M, Hendriks B. Recovering intrinsic fluorescence by Monte Carlo modeling. *J Biom Optics* 2013; **18**(2): 027009.
27. Ramanujam N. Fluorescence spectroscopy of neoplastic and non-neoplastic tissues. *Neoplasia* 2000; **2** (1-2): 89-117.
28. Berg J, Tymoczko J, Stryer L. *Biochemistry*, 5th edition. 5th ed. New York: W.H. Freeman and Company; 2002.
29. Croce A, Santamaria G, De Simone U, Lucchini F, Freitas I, Bottiroli G. Naturally-occurring porphyrins in a spontaneous-tumour bearing mouse model. *Photochem Photobiol Sci* 2011; **10**(7): 1189-95.
30. Moesta K, Ebert B, Handke T, *et al* Protoporphyrin IX occurs naturally in colorectal cancers and their metastases. *Cancer Res* 2001; **61**(3): 991-9.

31. Troyan S, Kianzad V, Gibbs-Strauss S, *et al* The FLARE intraoperative near-infrared fluorescence imaging system: a first-in-human clinical trial in breast cancer sentinel lymph node mapping. *Ann Surg Oncol* 2009; **16** (10): 2943-52.
32. Tanaka E, Choi H, Fujii H, Bawendi M, Frangioni J. Image-guided oncologic surgery using invisible light: completed pre-clinical development for sentinel lymph node mapping. *Ann Surg Oncol* 2006; **13** (12): 1671-81.
33. Nachabé R, Hendriks B, van der Voort M, Desjardins A, Sterenborg H. Estimation of biological chromophores using diffuse optical spectroscopy - benefit of extending the UV-VIS wavelength range to include 1000 to 1600nm. *Biomed Optics Express* 2010; **18**(24): 1432-42.
34. Barker M, Rayens W. Partial least squares of discrimination. *J Chemometrics* 2003; **17**(3): 166-73.
35. Nachabé R. Diagnosis with near infrared spectroscopy during minimally invasive procedures. Rotterdam: Erasmus University; 2012.
36. Farrell T, Patterson M, Wilson B. A diffusion theory model of spatially resolved, steady-state diffuse reflectance for the noninvasive determination of tissue optical properties *in vivo*. *Med Phys* 1992; **19**(4): 879-88.
37. Breiman L, Friedman J, Olshen R, Stone C. Classification and Regression Trees. Belmont, CA. : Wadsworth Publishing Company; 1984.
38. Nachabé R, Evers D, Hendriks B, *et al* Diagnosis of breast cancer using diffuse optical spectroscopy from 500 to 1600 nm: a comparison of classification methods. *J Biomed Opt* 2011; **16**(8): 087010.
39. Müller M, Georgakoudi I, Zhang Q, Wu J, Feld M. Intrinsic fluorescence spectroscopy in turbid media: disentangling effects of scattering and absorption. *Appl Opt* 2001; **40**(25): 4633-46.
40. Zhang Q, Müller M, Wu J, Feld M. Turbidity-free fluorescence spectroscopy of biological tissue. *Opt Lett* 2000 Oct 1; **25**(19):1451-3 2000; **25**(19): 1451-3.
41. Vishwanath K, Yuan H, Barry W, Dewhirst M, Ramanujam N. Using optical spectroscopy to longitudinally monitor physiological changes within solid tumors. *Neoplasia* 2009; **11** (9): 889-900.
42. Hanlon E, Manoharan R, Koo T, *et al* Prospects for *in vivo* Raman spectroscopy. *Phys Med Biol* 2000; **45** (2): R1-59.
43. Krafft C, Steiner G, Beleites C, Salzer R. Disease recognition by infrared and Raman spectroscopy. *J Biophotonics* 2009; **2** (1-2): 13-28.

44. Brancalion L, Durkin A, Tu J, Menaker G, Fallon J, Kollias N. *In vivo* fluorescence spectroscopy of nonmelanoma skin cancer. *Photochem Photobiol* 2001; **73** (2): 178-83.
45. Rajaram N, Aramil T, Lee K, Reichenberg J, Nguyen T, Tunnell J. Design and validation of a clinical instrument for spectral diagnosis of cutaneous malignancy. *Appl Opt* 2010; **49** (2): 142-52.
46. Gniadecka M, Philipsen P, Sigurdsson S, *et al* Melanoma diagnosis by Raman spectroscopy and neural networks: structure alterations in proteins and lipids in intact cancer tissue. *J Invest Dermatol* 2004; **122** (2): 443-39.
47. Choi J, Choo J, Chung H, *et al* Direct observation of spectral differences between normal and basal cell carcinoma (BCC) tissues using confocal Raman microscopy. *Biopolymers* 2005; **77** (5): 264-72.
48. Nijssen A, Maquelin K, Santos L, *et al* Discriminating basal cell carcinoma from perilesional skin using high wave-number Raman spectroscopy. *J Biomed Opt* 2007; **12** (3): 034004.
49. Lieber C, Majumder S, Ellis D, Billheimer D, Mahadevan-Jansen A. *In vivo* nonmelanoma skin cancer diagnosis using Raman microspectroscopy. *Lasers Surg Med* 2008; **40** (7): 461-7.
50. Amelink A, Kaspers O, Sterenborg H, van der Wal J, Roodenburg J, Witjes M. Non-invasive measurement of the morphology and physiology of oral mucosa by use of optical spectroscopy. *Oral Oncol* 2008; **44** (1): 65-71.
51. Mallia R, Narayanan S, Madhavan J, *et al* Diffuse reflection spectroscopy: an alternative to autofluorescence spectroscopy in tongue cancer detection. *Appl Spectrosc* 2010; **64** (4): 409-18.
52. Mallia R, Thomas S, Mathews A, *et al* Oxygenated hemoglobin diffuse reflectance ratio for *in vivo* detection of oral cancer. *J Biomed Opt* 2008; **13** (4): 041306.
53. de Veld D, Skurichina M, Witjes M, Duin R, Sterenborg H, Roodenburg J. Autofluorescence and diffuse reflectance spectroscopy for oral oncology. *Lasers Surg Med* 2005; **36** (5): 356-64.
54. Schwarz R, Gao W, Redden Weber C, *et al* Noninvasive evaluation of oral lesions using depth-sensitive optical spectroscopy. *Cancer* 2009; **115** (8): 1669-79.
55. McGee S, Mardirossian V, Elackattu A, *et al* Anatomy-based algorithms for detecting oral cancer using reflectance and fluorescence spectroscopy. *Ann Otol Rhinol Laryngol* 2009; **118** (11): 817-26.

56. Cerussi A, Shah N, Hsiang D, Durkin A, Butler J, Tromberg B. *In vivo* absorption, scattering, and physiologic properties of 58 malignant breast tumors determined by broadband diffuse optical spectroscopy. *J Biomed Opt* 2006; **11** (4): 044005.
57. Kukreti S, Cerussi A, Tanamai W, Hsiang D, Tromberg B, Gratton E. Characterization of metabolic differences between benign and malignant tumors: high-spectral-resolution diffuse optical spectroscopy. *Radiology* 2010; **254** (1): 277-84.
58. Bigio I, Bown S, Briggs G, *et al* Diagnosis of breast cancer using elastic-scattering spectroscopy: preliminary clinical results. *J Biomed Opt* 2000; **5** (2): 221-8.
59. Zhu C, Palmer G, Breslin T, Harter J, Ramanujam N. Diagnosis of breast cancer using diffuse reflectance spectroscopy: Comparison of a Monte Carlo versus partial least squares analysis based feature extraction technique. *Lasers Surg Med* 2006; **38** (7): 714-24.
60. Brown J, Wilke L, Geradts J, Kennedy S, Palmer G, Ramanujam N. Quantitative optical spectroscopy: a robust tool for direct measurement of breast cancer vascular oxygenation and total hemoglobin content *in vivo*. *Cancer Res* 2009; **69** (7): 2919-26.
61. van Veen R, Amelink A, Menke-Pluymers M, van der Pol C, Sterenborg H. Optical biopsy of breast tissue using differential path-length spectroscopy. *Phys Med Biol* 2005; **50** (11): 2573-81.
62. Gupta P, Majumder S, Uppal A. Breast cancer diagnosis using N2 laser excited autofluorescence spectroscopy. *Lasers Surg Med* 1997; **21** (5): 417-22.
63. Palmer G, Keely P, Breslin T, Ramanujam N. Autofluorescence spectroscopy of normal and malignant human breast cell lines. *Photochem Photobiol* 2003; **78** (5): 462-9.
64. Chowdary M, Mahato K, Kumar K, *et al* Autofluorescence of breast tissues: evaluation of discriminating algorithms for diagnosis of normal, benign, and malignant conditions. *Photomedicine and laser surgery* 2009; **27** (2): 241-52.
65. Haka A, Volynskaya Z, Gardecki J, *et al* *In vivo* margin assessment during partial mastectomy breast surgery using raman spectroscopy. *Cancer Res* 2006; **66** (6): 3317-22.
66. Haka A, Volynskaya Z, Gardecki J, *et al* Diagnosing breast cancer using Raman spectroscopy: prospective analysis. *J Biomed Opt* 2009; **14** (5): 054023.
67. Haka A, Shafer-Peltier K, Fitzmaurice M, Crowe J, Dasari R, Feld M. Diagnosing breast cancer by using Raman spectroscopy. *PNAS* 2005; **102** (35): 12371-6.
68. Breslin T, Xu F, Palmer G, Zhu C, Gilchrist K, Ramanujam N. Autofluorescence and diffuse reflectance properties of malignant and benign breast tissues. *Ann Surg Oncol* 2004; **11** (1): 65-70.

69. Volynskaya Z, Haka A, Bechtel K, *et al* Diagnosing breast cancer using diffuse reflectance spectroscopy and intrinsic fluorescence spectroscopy. *J Biomed Opt* 2008; **13** (2): 024012.
70. Zhu C, Breslin T, Harter J, Ramanujam N. Model based and empirical spectral analysis for the diagnosis of breast cancer. *Biomed Opt Express* 2008; **16**(19): 14961-78.
71. Zhu C, Palmer G, Breslin T, Harter J, Ramanujam N. Diagnosis of breast cancer using fluorescence and diffuse reflectance spectroscopy: a Monte-Carlo-model-based approach. *J Biomed Opt* 2008; **13**(3): 034015.
72. Keller M, Majumder S, Kelley M, *et al* Autofluorescence and diffuse reflectance spectroscopy and spectral imaging for breast surgical margin analysis. *Lasers Surg Med* 2010; **42** (1): 15-23.
73. Majumder S, Keller M, Boulos F, Kelley M, Mahadevan-Jansen A. Comparison of autofluorescence, diffuse reflectance, and Raman spectroscopy for breast tissue discrimination. *J Biomed Opt* 2008; **13** (5): 054009.
74. Cardenas-Turanzas M, Freeberg J, Benedet J, *et al* The clinical effectiveness of optical spectroscopy for the *in vivo* diagnosis of cervical intraepithelial neoplasia: where are we? *Gynecol Oncol* 2007; **107** (1 Suppl 1): S138-46.
75. Murali Krishna C, Sockalingum GD, Vidyasagar MS, *et al* An overview on applications of optical spectroscopy in cervical cancers. *Journal of cancer research and therapeutics* 2008; **4**(1): 26-36.
76. Mourant J, Bocklage T, Powers T, *et al* *In vivo* light scattering measurements for detection of precancerous conditions of the cervix. *Gynecol Oncol* 2007; **105** (2): 439-45.
77. Chang V, Cartwright P, Bean S, Palmer G, Bentley R, Ramanujam N. Quantitative physiology of the precancerous cervix *in vivo* through optical spectroscopy. *Neoplasia* 2009; **11** (4): 325-32.
78. Keller M, Kanter E, Lieber C, *et al* Detecting temporal and spatial effects of epithelial cancers with Raman spectroscopy. *Dis Markers* 2008; **25** (6): 323-37.
79. Bard M, Amelink A, Hegt V, *et al* Measurement of hypoxia-related parameters in bronchial mucosa by use of optical spectroscopy. *Am J Respir Crit Care Med* 2005; **171** (10): 1178-84.
80. Bard M, Amelink A, Skurichina M, *et al* Optical spectroscopy for the classification of malignant lesions of the bronchial tree. *Chest* 2006; **129** (4): 995-1001.

81. Fawzy Y, Petek M, Tercelj M, Zeng H. *In vivo* assessment and evaluation of lung tissue morphologic and physiological changes from non-contact endoscopic reflectance spectroscopy for improving lung cancer detection. *J Biomed Opt* 2006; **11** (4): 044003.
82. Fawzy Y, Zeng H. Intrinsic fluorescence spectroscopy for endoscopic detection and localization of the endobronchial cancerous lesions. *J Biomed Opt* 2008; **13** (6): 064022.
83. Yamazaki H, Kaminaka S, Kohda E, Mukai M, Hamaguchi H. The diagnosis of lung cancer using 1064-nm excited near-infrared multichannel Raman spectroscopy. *Radiat Med* 2003; **21** (1): 1-6.
84. Georgakoudi I, Jacobson B, Van Dam J, *et al* Fluorescence, reflectance, and light-scattering spectroscopy for evaluating dysplasia in patients with Barrett's esophagus. *Gastroenterology* 2001; **120** (7): 1620-9.
85. Lovat L, Johnson K, Mackenzie G, *et al* Elastic scattering spectroscopy accurately detects high grade dysplasia and cancer in Barrett's oesophagus. *Gut* 2006; **55** (8): 1078-83.
86. Teh S, Zheng W, Ho K, Teh M, Yeoh K, Huang Z. Diagnostic potential of near-infrared Raman spectroscopy in the stomach: differentiating dysplasia from normal tissue. *Br J Cancer* 2008; **98** (2): 457-65.
87. Teh S, Zheng W, Ho K, Teh M, Yeoh K, Huang Z. Near-infrared Raman spectroscopy for early diagnosis and typing of adenocarcinoma in the stomach. *Br J Surg* 2010; **97** (4): 550-7.
88. Dhar A, Johnson K, Novelli M, *et al* Elastic scattering spectroscopy for the diagnosis of colonic lesions: initial results of a novel optical biopsy technique. *Gastrointest Endosc* 2006; **63** (2): 257-61.
89. Wang H, Jiang J, Lin C, Lin J, Huang G, Yu J. Diffuse reflectance spectroscopy detects increased hemoglobin concentration and decreased oxygenation during colon carcinogenesis from normal to malignant tumors. *Biomed Opt Express* 2009; **17** (4): 2805-17.
90. Chowdary M, Kumar K, Thakur K, *et al* Discrimination of normal and malignant mucosal tissues of the colon by Raman spectroscopy. *Photomedicine and laser surgery* 2007; **25** (4): 269-74.
91. Buttemere C, Chari R, Anderson C, Washington M, Mahadevan-Jansen A, Lin W. *In vivo* assessment of thermal damage in the liver using optical spectroscopy. *J Biomed Opt* 2004; **9** (5): 1018-27.

92. Anderson C, Lin W, Buttemere C, *et al* Real-time spectroscopic assessment of thermal damage: implications for radiofrequency ablation. *J Gastrointest Surg* 2004; **8** (6): 660-9.
93. Anderson C, Lin W, Beckham J, *et al* Fluorescence spectroscopy accurately detects irreversible cell damage during hepatic radiofrequency ablation. *Surgery* 2004; **136** (3): 524-31.
94. Hsu C, Razavi M, So S, Parachikov I, Benaron D. Liver tumor gross margin identification and ablation monitoring during liver radiofrequency treatment. *J Vasc Interv Radiol* 2005; **16** (11): 1473-8.
95. Nachabé R, Evers D, Hendriks B, *et al* Effect of bile absorption coefficients on the estimation of liver tissue optical properties and related complications in discriminating healthy and tumorous samples. *Biomed Optics Express* 2011; **2**(3): 600-14.
96. Parekh D, Lin W, Herrell S. Optical spectroscopy characteristics can differentiate benign and malignant renal tissues: a potentially useful modality. *J Urol* 2005; **174** (5): 1754-8.
97. Bensalah K, Peswani D, Tuncel A, *et al* Optical reflectance spectroscopy to differentiate benign from malignant renal tumors at surgery. *Urology* 2009; **73** (1): 178-81.
98. Bensalah K, Fleureau J, Rolland D, *et al* Raman spectroscopy: a novel experimental approach to evaluating renal tumours. *Eur Urol* 2010; **58** (4): 602-8.
99. Wills H, Kast R, Stewart C, *et al* Diagnosis of Wilms' tumor using near-infrared Raman spectroscopy. *J Pediatr Surg* 2009; **44**(6): 1152-8.
100. Lieber C, Kabeer M. Characterization of pediatric Wilms' tumor using Raman and fluorescence spectroscopies. *J Pediatr Surg* 2010; **45**(3): 549-54.
101. Osinsky S, Zavelevich M, Vaupel P. Tumor hypoxia and malignant progression. *Exp Oncol* 2009; **31** (2): 80-6.
102. Vaupel P, Mayer A, Briest S, Höckel M. Hypoxia in breast cancer: role of blood flow, oxygen diffusion distances, and anemia in the development of oxygen depletion. *Adv Exp Med Biol* 2005; **566** 333-42.
103. Walker R. The complexities of breast cancer desmoplasia. *Breast Cancer Res* 2001; **3** (3): 143-5.
104. Georgakoudi I, Jacobson B, Müller M, *et al* NAD(P)H and collagen as *in vivo* quantitative fluorescent biomarkers of epithelial precancerous changes. *Cancer Res* 2002; **62** (3): 682-7.

105. Zhu C, Burnside E, Sisney G, *et al* Fluorescence spectroscopy: an adjunct diagnostic tool to image-guided core needle biopsy of the breast. *IEEE Trans Biomed Eng* 2009; **56** (10): 2518-28.
106. Wilke L, Brown J, Bydlon T, *et al* Rapid noninvasive optical imaging of tissue composition in breast tumor margins. *Am J Surg* 2009; **198** (4): 566-74.
107. Alchab L, Dupuis G, Balleyguier C, Mathieu M, Fontaine-Aupart M, Farcy R. Towards an optical biopsy for the diagnosis of breast cancer *in vivo* by endogenous fluorescence spectroscopy. *J Biophotonics* 2010; **3** (5-6): 373-84.
108. Ostrander J, McMahon C, Lem S, *et al* Optical redox ratio differentiates breast cancer cell lines based on estrogen receptor status. *Cancer Res* 2010; **70** (11): 4759-66.
109. Cerussi A, Tanamai V, Mehta R, Hsiang D, Butler J, Tromberg B. Frequent optical imaging during breast cancer neoadjuvant chemotherapy reveals dynamic tumor physiology in an individual patient. *Acad Radiol* 2010; **17**(8): 1031-9.
110. Tromberg BJ, Cerussi AE. Imaging breast cancer chemotherapy response with light. Commentary on Soliman *et al*, p. 2605. *Clin Cancer Res* 2010; **16**(9): 2486-8.
111. Soliman H, Gunasekara A, Rycroft M, *et al* Functional imaging using diffuse optical spectroscopy of neoadjuvant chemotherapy response in women with locally advanced breast cancer. *Clin Cancer Res* 2010; **16** (9): 2605-14.
112. Gong Y, Sneige N, Guo M, Hicks M, Moran C. Transthoracic fine-needle aspiration vs concurrent core needle biopsy in diagnosis of intrathoracic lesions: a retrospective comparison of diagnostic accuracy. *Am J Clin Pathol* 2006; **125**: 438-44.
113. Rivera M, Detterbeck F, Mehta A. Diagnosis of lung cancer: the guidelines. *Chest* 2003; **123**(1 Suppl): 129S-36S.
114. Priola A, Priola S, Cataldi A, *et al* Diagnostic accuracy and complication rate of CT-guided fine needle aspiration biopsy of lung lesions: a study based on the experience of the cytopathologist. *Acta Radiol* 2010; **51**(5): 527-33.
115. Kothary N, Lock L, Sze D, Hofmann L. Computed tomography-guided percutaneous needle biopsy of pulmonary nodules: impact of nodule size on diagnostic accuracy. *Clin Lung Cancer* 2009; **10**(5): 360-3.
116. Aviram G, Greif J, Man A, *et al* Diagnosis of intrathoracic lesions: are sequential fine-needle aspiration (FNA) and core needle biopsy (CNB) combined better than either investigation alone? *Clin Radiol* 2007; **62**(3): 221-6.
117. Sćepanović O, Volynskaya Z, Kong C, Galindo L, Dasari R, Feld M. A multimodal spectroscopy system for real-time disease diagnosis. *Rev Sci Instrum* 2009; **80**(4): 043103.

118. Hirsch F, Prindiville S, Miller Y, *et al* Fluorescence versus white-light bronchoscopy for detection of preneoplastic lesions: a randomized study. *J Natl Cancer Inst* 2001; **93**(18): 1385-91.
119. Kruskal W, Wallis W. Use of Ranks in One-Criterion Variance Analysis. *Journal of the American Statistical Association* 1952; **47**(260): 583-621.
120. Kennedy S, Geradts J, Bydlon T, *et al* Optical breast cancer margin assessment: an observational study of the effects of tissue heterogeneity on optical contrast. *Breast Cancer Res Treat* 2010; **12**(6): R91.
121. Wong S, Mangu P, Choti M, *et al* American Society of Clinical Oncology 2009 clinical evidence review on radiofrequency ablation of hepatic metastases from colorectal cancer. *J Clin Oncol* 2010; **28**(3.): 493-508.
122. Pawlik TM, Scoggins CR, Zorzi D, *et al* Effect of surgical margin status on survival and site of recurrence after hepatic resection for colorectal metastases. *Ann Surg* 2005; **241**(5): 715-22, discussion 22-4.
123. Nordlinger B, Sorbye H, Glimelius B, *et al* Perioperative chemotherapy with FOLFOX4 and surgery versus surgery alone for resectable liver metastases from colorectal cancer (EORTC Intergroup trial 40983): a randomised controlled trial. *Lancet* 2008; **371**(9617): 1007-16.
124. Muratore A, Ribero D, Zimmitti G, Mellano A, Langella S, Capussotti L. Resection margin and recurrence-free survival after liver resection of colorectal metastases. *Ann Surg Oncol* 2009; **17**(5): 1324-9.
125. Doornbos R, Lang R, Aalders M, Cross F, Sterenborg H. The determination of *in vivo* human tissue optical properties and absolute chromophore concentrations using spatially resolved steady-state diffuse reflectance spectroscopy. *Phys Med Biol* 1999; **44**(4): 967-81.
126. Pessaux P, Chenard M, Bachellier P, Jaeck D. Consequences of chemotherapy on resection of colorectal liver metastases. *J Visc Surg* 2010; **147**(4): 193-201.
127. Morris-Stiff G, Tan Y, Vauthey J. Hepatic complications following preoperative chemotherapy with oxaliplatin or irinotecan for hepatic colorectal metastases. *Eur J Surg Oncol* 2008; **34**(6): 609-14.
128. McCormack L, Petrowsky H, Jochum W, Furrer K, Clavien P. Hepatic steatosis is a risk factor for postoperative complications after major hepatectomy: a matched case-control study. *Ann Surg* 2007; **245**(6): 923-30.
129. de Meijer V, Kalish B, Puder M, Ijzermans J. Systematic review and meta-analysis of steatosis as a risk factor in major hepatic resection. *Br J Surg* 2010; **97**(9): 1331-9.

130. Gioux S, Choi H, Frangioni J. Image-guided surgery using invisible near-infrared light: fundamentals of clinical translation. *Mol Imaging* 2010; **9**(5): 237-55.
131. Keereweer S, Kerrebijn J, van Driel P, *et al* Optical image-guided surgery--where do we stand? *Mol Imaging Biol* 2011; **13**(2): 199-207.
132. Ariga R, Bloom K, Reddy V, *et al* Fine-needle aspiration of clinically suspicious palpable breast masses with histopathologic correlation. *Am J Surg* 2002; **184** (5): 410-3.
133. Burns R, Brown J, Roe S, Sprouse L, Yancey A, Witherspoon L. Stereotactic core-needle breast biopsy by surgeons: minimum 2-year follow-up of benign lesions. *Ann Surg* 2000; **232** (4): 542-8.
134. Chaiwun B, Settakorn J, Ya-In C, Wisedmongkol W, Rangdaeng S, Thorner P. Effectiveness of fine-needle aspiration cytology of breast: analysis of 2,375 cases from northern Thailand. *Diagn Cytopathol* 2002; **26** (3): 201-5.
135. Youk J, Kim E, Kim M, Lee J, Oh K. Missed breast cancers at US-guided core needle biopsy: how to reduce them. *Radiographics* 2007; **27**(1): 79-94.
136. Zonios G, Perelman L, Backman V, *et al* Diffuse reflectance spectroscopy of human adenomatous colon polyps *in vivo*. *Appl Opt* 1999; **38**(31): 6628-37.
137. Laughney A, Krishnaswamy V, Garcia-Allende P, *et al* Automated classification of breast pathology using local measures of broadband reflectance. *J Biomed Opt* 2010; **15**(6): 066019.
138. Taroni P, Bassi A, Comelli D, Farina A, Cubeddu R, Pifferi A. Diffuse optical spectroscopy of breast tissue extended to 1100 nm. *J Biomed Opt* 2009; **14**(5): 054030.
139. Taroni P, Comelli D, Pifferi A, Torricelli A, Cubeddu R. Absorption of collagen: effects on the estimate of breast composition and related diagnostic implications. *J Biomed Opt* 2007; **12**(1): 014021.
140. Taroni P, Pifferi A, Quarto G, *et al* Noninvasive assessment of breast cancer risk using time-resolved diffuse optical spectroscopy. *J Biomed Opt* 2010; **15**(6): 060501.
141. Georgakoudi I, Sheets EE, Müller MG, *et al* Trimodal spectroscopy for the detection and characterization of cervical precancers *in vivo*. *American Journal of Obstetrics and Gynecology* 2002; **186**(3): 374-82.
142. Mirabal YN, Chang SK, Atkinson EN, Malpica A, Follen M, Richards-Kortum R. Reflectance spectroscopy for *in vivo* detection of cervical precancer. *J Biomed Opt* 2002; **7**(4): 587-94.

143. Müller MG, Valdez TA, Georgakoudi I, *et al* Spectroscopic detection and evaluation of morphologic and biochemical changes in early human oral carcinoma. *Cancer* 2003; **97**(7): 1681-92.
144. Nordstrom RJ, Burke L, Niloff JM, Myrtle JF. Identification of cervical intraepithelial neoplasia (CIN) using UV-excited fluorescence and diffuse-reflectance tissue spectroscopy. *Lasers in Surgery and Medicine* 2001; **29**(2): 118-27.
145. Utzinger U, Brewer M, Silva E, *et al* Reflectance spectroscopy for *in vivo* characterization of ovarian tissue. *Lasers in Surgery and Medicine* 2001; **28**(1): 56-66.
146. Wallace MB, Perelman LT, Backman V, *et al* Endoscopic detection of dysplasia in patients with Barrett's esophagus using light-scattering spectroscopy. *Gastroenterology* 2000; **119**(3): 677-82.
147. Moesta KT, Ebert B, Handke T, *et al* Protoporphyrin IX occurs naturally in colorectal cancers and their metastases. *Cancer Research* 2001; **61**(3): 991-.
148. Evers D, Nachabé R, Klomp H, *et al* Diffuse reflectance spectroscopy; a new guidance tool for improvement of biopsy procedures in lung malignancies. *Clinical Lung Cancer* 2012; **13**(6): 424-31.
149. Zhang Q, Müller MG, Wu J, Feld MS. Turbidity-free fluorescence spectroscopy of biological tissue. *Optics Letters* 2000; **25**(19): 1451-3.
150. Skala MC, Riching KM, Gendron-Fitzpatrick A, *et al* *In vivo* multiphoton microscopy of NADH and FAD redox states, fluorescence lifetimes, and cellular morphology in precancerous epithelia. *Proc Natl Acad Sci USA* 2007; **104**(49): 19494-9.
151. Polo C, Frisardi A, Resnik E, Schoua A, Battle A. Factors influencing fluorescence spectra of free porphyrins. *Clin Chem* 1988; **34**: 757-60.
152. Davis A. Bronchogenic carcinoma in chronic obstructive pulmonary disease. *JAMA* 1976; **235**(6): 621.
153. Mason R, Buist A, Fisher E. Cigarette smoking and health. *Am J Respir Crit Care* 1985; **153**(2): 861-5.
154. Chance B, Schoener B, Oshino R, Itshak F, Nakase Y. Oxidation-reduction ratio studies of mitochondria in freeze-trapped samples. NADH and flavoprotein fluorescence signals. *J Biol Chem* 1979; **254**(11): 4764-71

155. Ausborn N, Le Q, Bradley J, *et al* Molecular profiling to optimize treatment in non-small cell lung cancer: a review of potential molecular targets for radiation therapy by the translational research program of the radiation therapy oncology group. *Int J Radiat Oncol Biol Phys* 2012; **83**(4): 453-64.
156. Moreira A, Thornton R. Personalized medicine for non-small-cell lung cancer: implications of recent advances in tissue acquisition for molecular and histologic testing. *Clin Lung Cancer* 2012; **13**: 334-9.
157. Harlaar N, Kelder W, Sarantopoulos A, *et al* Real-time near infrared fluorescence (NIRF) intra-operative imaging in ovarian cancer using an $\alpha(v)\beta(3)$ -integrin targeted agent. *Gynecol Oncol* 2013; **128**(3): 590-5.
158. Ntziachristos V, Yoo J, van Dam G. Current concepts and future perspectives on surgical optical imaging in cancer. *J Biomed Opt* 2010; **15**(6).
159. McCormack L, Petrowsky H, Jochum W, Mullhaupt B, Weber M, Clavien P. Use of severely steatotic grafts in liver transplantation: a matched case-control study. *Ann Surg* 2007; **246**(6): 940-6.
160. McCormack L, Dutkowski P, El-Badry A, Clavien P. Liver transplantation using fatty livers: always feasible? *J Hepatol* 2011; **54**(5): 1055-62.
161. Bydlon T, Nachabé R, Ramanujam N, Sterenborg H, Hendriks B. Chromophore based analyses of steady-state diffuse reflectance spectroscopy: current status and perspectives for clinical adoption. *J Biophotonics* 2014; **[Epub ahead of print]**.
162. Mehta S, Thomas E, Bell J, Johnston D, Taylor-Robinson S. Non-invasive means of measuring hepatic fat content. *World J Gastroenterol* 2008; **14**(22): 3476-83.
163. Evers D, Nachabé R, Hompes D, *et al* Optical sensing for tumor detection in the liver. *Eur J Surg Oncol* 2013; **39**(1): 68-75.
164. Zijlstra W, Buursma A, van Assendelft O. Visible and near infrared absorption spectra of human and animal haemoglobin: VSP BV; 2000.
165. Spliethoff J, Evers D, Klomp H, *et al* Improved identification of peripheral lung tumors by using diffuse reflectance and fluorescence spectroscopy. *Lung Cancer* 2013; **80**(2): 165-71.
166. Höckel M, Vaupel P. Tumor hypoxia: definitions and current clinical, biologic, and molecular aspects. *J Natl Cancer Inst* 2001; **93**(4): 266-76.
167. Turtoi A, Blomme A, Debois D, *et al* Organized proteomic heterogeneity in colorectal cancer liver metastases and implications for therapies. *Hepatology* 2014; **59**(3): 924-34.

168. Kleiner D, Brunt E, Van Natta M, *et al* Design and validation of a histological scoring system for nonalcoholic fatty liver disease. *Hepatology* 2005; **41**(6): 1313-21.
169. Ostrander JH, McMahon CM, Lem S, *et al* Optical redox ratio differentiates breast cancer cell lines based on estrogen receptor status. *Cancer Research* 2010; **70**(11): 4759-66.
170. Skala M, Ramanujam N. Multiphoton redox ratio imaging for metabolic monitoring *in vivo*. *Methods Mol Biol* 2010; **594**: 155-62.
171. Spliethoff J, Evers D, Jaspers J, Hendriks B, Rottenberg S, Ruers T. Monitoring of tumor response to Cisplatin using optical spectroscopy. *Transl Oncol* 2014; **7**(2): 230-9.
172. Weagle G, Paterson P, Kennedy J, Pottier R. The nature of the chromophore responsible for naturally occurring fluorescence in mouse skin. *J Photochem Photobiol B* 1988; **2**(3): 313-20.
173. Tranchart H, Chirica M, Faron M, *et al* Prognostic impact of positive surgical margins after resection of colorectal cancer liver metastases: reappraisal in the era of modern chemotherapy. *World J Surg* 2013; **37**(11): 2647-54.
174. Viganò L, Capussotti L, Lapointe R, *et al* Early recurrence after liver resection for colorectal metastases: risk factors, prognosis, and treatment. A LiverMetSurvey-based study of 6,025 patients. *Ann Surg Oncol* 2014; **21**(4): 1276-86.
175. Lordick F, Ruers T, Aust DE, *et al* European Organisation of Research and Treatment of Cancer (EORTC) Gastrointestinal Group: Workshop on the role of metabolic imaging in the neoadjuvant treatment of gastrointestinal cancer. *European Journal of Cancer* 2008; **44**(13): 1807-19.
176. Ollivier L, Balu-Maestro C, Leclère J. Imaging in evaluation of response to neoadjuvant breast cancer treatment. *Cancer imaging* 2005; **5**(1): 27-31.
177. Pons F, Duch J, Fuster D. Breast cancer therapy: the role of PET-CT in decision making. *Q J Nucl Med Mol Imaging* 2009; **53**(2): 210-23.
178. Lim JS, Yun MJ, Kim MJ, *et al* CT and PET in stomach cancer: preoperative staging and monitoring of response to therapy. *Radiographics* 2006; **26**(1): 143-56.
179. Eisenhauer EA, Therasse P, Bogaerts J, *et al* New response evaluation criteria in solid tumours: revised RECIST guideline (version 1.1). *Eur J Cancer* 2009; **45**(2): 228-47.
180. Wahl RL, Jacene H, Kasamon Y, Lodge MA. From RECIST to PERCIST : Evolving considerations for PET response criteria in solid tumors. *Response* 2009; **50**(5): 122-50.

181. Chung WS, Park MS, Shin SJ, *et al* Response evaluation in patients with colorectal liver metastases: RECIST version 1.1 versus modified CT criteria. *American Journal of Roentgenology* 2012; **199**(4): 809-15.
182. Byström P, Berglund A, Garske U, *et al* Early prediction of response to first-line chemotherapy by sequential [18F]-2-fluoro-2-deoxy-D-glucose positron emission tomography in patients with advanced colorectal cancer. *Annals of Oncology* 2009; **20**(6): 1057-61.
183. de Geus-Oei LF, van Laarhoven HW, Visser EP, *et al* Chemotherapy response evaluation with FDG-PET in patients with colorectal cancer. *Ann Oncol* 2008; **19**(2): 348-52.
184. Hendlisz A, Golfopoulos V, Garcia C, *et al* Serial FDG-PET/CT for early outcome prediction in patients with metastatic colorectal cancer undergoing chemotherapy. *Annals of Oncology* 2012; **23**(7): 1687-93.
185. Breslin TM, Xu F, Palmer GM, Zhu C, Gilchrist KW, Ramanujam N. Autofluorescence and diffuse reflectance properties of malignant and benign breast tissues. *Ann Surg Oncol* 2004; **11**(1): 65-70.
186. Keller MD, Majumder SK, Kelley MC, *et al* Autofluorescence and diffuse reflectance spectroscopy and spectral imaging for breast surgical margin analysis. *Lasers Surg Med* 2010; **42**(1): 15-23.
187. Volynskaya Z, Haka AS, Bechtel KL, *et al* Diagnosing breast cancer using diffuse reflectance spectroscopy and intrinsic fluorescence spectroscopy. *Journal of biomedical optics* 2008; **13**(2): 024012.
188. Bard MP, Amelink A, Skurichina M, *et al* Optical spectroscopy for the classification of malignant lesions of the bronchial tree. *Chest* 2006; **129**(4): 995-1001.
189. Spliethoff JW, Evers DJ, Klomp HM, *et al* Improved identification of peripheral lung tumors by using diffuse reflectance and fluorescence spectroscopy. *Lung cancer* 2013; **80**(2): 165-71.
190. O'Sullivan TD, Leproux A, Chen JH, *et al* Optical imaging correlates with magnetic resonance imaging breast density and reveals composition changes during neoadjuvant chemotherapy. *Breast Cancer Research* 2013; **15**(1): R14-R.
191. Ueda S, Roblyer D, Cerussi A, *et al* Baseline tumor oxygen saturation correlates with a pathologic complete response in breast cancer patients undergoing neoadjuvant chemotherapy. *Cancer Research* 2012; **72**(17): 4318-28.
192. Cerussi A, Hsiang D, Shah N, *et al* Predicting response to breast cancer neoadjuvant chemotherapy using diffuse optical spectroscopy. *Proc Natl Acad Sci U S A* 2007; **104**(10): 4014-9.

193. Cerussi AE, Tanamai VW, Mehta RS, Hsiang D, Butler J, Tromberg BJ. Frequent optical imaging during breast cancer neoadjuvant chemotherapy reveals dynamic tumor physiology in an individual patient. *Acad Radiol* 2010; **17**(8): 1031-9.
194. Falou O, Soliman H, Sadeghi-Naini A, *et al* Diffuse Optical Spectroscopy Evaluation of Treatment Response in Women with Locally Advanced Breast Cancer Receiving Neoadjuvant Chemotherapy. *Translational Oncology* 2012; **5**(4): 238-46.
195. Vishwanath K, Yuan H, Barry WT, Dewhirst MW, Ramanujam N. Using optical spectroscopy to longitudinally monitor physiological changes within solid tumors. *Neoplasia* 2009; **11**(9): 889-900.
196. Nachabé R, Evers DJ, Hendriks BH, *et al* Diagnosis of breast cancer using diffuse optical spectroscopy from 500 to 1600 nm: comparison of classification methods. *J Biomed Opt* 2011; **16**(8): 087010.
197. Evers DJ, Nachabé R, Hompes D, *et al* Optical sensing for tumor detection in the liver. *Eur J Surg Oncol* 2013; **39**(1): 68-75.
198. Hsu CP, Razavi MK, So SK, Parachikov IH, Benaron DA. Liver tumor gross margin identification and ablation monitoring during liver radiofrequency treatment. *J Vasc Interv Radiol* 2005; **16**(11): 1473-8.
199. Liu X, Holstege H, van der Gulden H, *et al* Somatic loss of BRCA1 and p53 in mice induces mammary tumors with features of human BRCA1-mutated basal-like breast cancer. *Proc Natl Acad Sci U S A* 2007; **104**(29): 12111-6.
200. Rottenberg S, Nygren AOH, Pajic M, *et al* Selective induction of chemotherapy resistance of mammary tumors in a conditional mouse model for hereditary breast cancer. *Proceedings of the National Academy of Sciences of the United States of America* 2007; **104**(29): 12117-22.
201. Inoue Y, Izawa K, Kiryu S, Tojo A, Ohtomo K. Diet and abdominal autofluorescence detected by *in vivo* fluorescence imaging of living mice. *Molecular Imaging* 2008; **7**(1): 21-7.
202. Nachabé R, Hendriks BH, Desjardins AE, van der Voort M, van der Mark MB, Sterenberg HJ. Estimation of lipid and water concentrations in scattering media with diffuse optical spectroscopy from 900 to 1,600 nm. *Journal of biomedical optics* 2010; **15**(3): 037015.
203. Farrell TJ, Patterson MS, Wilson B. A diffusion theory model of spatially resolved, steady-state diffuse reflectance for the noninvasive determination of tissue optical properties *in vivo*. *Med Phys* 1992; **19**(4): 879-88.

204. Zonios G, Dimou A. Light scattering spectroscopy of human skin *in vivo*. *Opt Express* 2009; **17**(3): 1256-67.
205. Nachabé R, Hendriks BH, van der Voort M, Desjardins AE, Sterenberg HJ. Estimation of biological chromophores using diffuse optical spectroscopy: benefit of extending the UV-VIS wavelength range to include 1000 to 1600 nm. *Biomed Opt Express* 2010; **1**(5): 1432-42.
206. Müller M, Hendriks BH. Recovering intrinsic fluorescence by Monte Carlo modeling. *Journal of biomedical optics* 2013; **18**(2): 27009.
207. Müller MG, Georgakoudi I, Zhang Q, Wu J, Feld MS. Intrinsic fluorescence spectroscopy in turbid media: disentangling effects of scattering and absorption. *Appl Opt* 2001; **40**(25): 4633-46.
208. Skala MC, Riching KM, Gendron-Fitzpatrick A, *et al* *In vivo* multiphoton microscopy of NADH and FAD redox states, fluorescence lifetimes, and cellular morphology in precancerous epithelia. *Proc Natl Acad Sci U S A* 2007; **104**(49): 19494-9.
209. Sorg BS, Moeller BJ, Donovan O, Cao Y, Dewhirst MW. Hyperspectral imaging of hemoglobin saturation in tumor microvasculature and tumor hypoxia development. *J Biomed Opt* 2005; **10**(4): 44004.
210. Teicher BA, Holden SA, Ara G, *et al* Influence of an anti-angiogenic treatment on 9L gliosarcoma: oxygenation and response to cytotoxic therapy. *Int J Cancer* 1995; **61**(5): 732-7.
211. Croce AC, Santamaria G, De Simone U, Lucchini F, Freitas I, Bottiroli G. Naturally-occurring porphyrins in a spontaneous-tumour bearing mouse model. *Photochem Photobiol Sci* 2011; **10**(7): 1189-95.
212. Brown JQ, Wilke LG, Geradts J, Kennedy SA, Palmer GM, Ramanujam N. Quantitative optical spectroscopy: a robust tool for direct measurement of breast cancer vascular oxygenation and total hemoglobin content *in vivo*. *Cancer Res* 2009; **69**(7): 2919-26.
213. Santos CR, Schulze A. Lipid metabolism in cancer. *FEBS Journal* 2012; **279**(15): 2610-23.
214. Boren J, Brindle KM. Apoptosis-induced mitochondrial dysfunction causes cytoplasmic lipid droplet formation. *Cell Death and Differentiation* 2012; **19**(9): 1561-70.
215. Partridge SC, Gibbs JE, Lu Y, *et al* MRI measurements of breast tumor volume predict response to neoadjuvant chemotherapy and recurrence-free survival. *Am J Roentgenol* 2005; **184**(6): 1774-81.

216. Gerlinger M, Rowan AJ, Horswell S, *et al* Intratumor Heterogeneity and Branched Evolution Revealed by Multiregion Sequencing. *N Engl J Med* 2012; **366**(10): 883-92.
217. Nachabé R. Diagnosis with near infrared spectroscopy during minimally invasive procedures [Ph.D. thesis]. Rotterdam, The Netherlands: Erasmus University Rotterdam; 2012.
218. Farrell G, Larter C. Nonalcoholic fatty liver disease: from steatosis to cirrhosis. *Hepatology* 2006; **43**(2 Suppl 1): S99-S112.
219. McCormack L, Clavien P. Understanding the meaning of fat in the liver. *Liver Transpl* 2005; **11**(2): 137-9.
220. Nocito A, El-Badry A, Clavien P. When is steatosis too much for transplantation? *J Hepatol* 2006; **45**(4): 494-9.
221. van Werven J, Marsman H, Nederveen A, *et al* Assessment of hepatic steatosis in patients undergoing liver resection: comparison of US, CT, T1-weighted dual-echo MR imaging, and point-resolved 1H MR spectroscopy. *Radiology* 2010; **256**(1): 159-68.
222. Sharkey F, Lytvak I, Prihoda T, Speeg K, Washburn W, Halff G. High-grade microsteatosis and delay in hepatic function after orthotopic liver transplantation. *Hum Pathol* 2011; **42**(9): 1337-42.
223. Salizzoni M, Franchello A, Zamboni F, *et al* Marginal grafts: finding the correct treatment for fatty livers. *Transpl Int* 2003; **16**(7): 486-93.
224. Fishbein T, Fiel M, Emre S, *et al* Use of livers with microvesicular fat safely expands the donor pool. *Transplantation* 1997; **64**(2): 248-51.
225. Verran D, Kusyik T, Painter D, *et al* Clinical experience gained from the use of 120 steatotic donor livers for orthotopic liver transplantation. *Liver Transpl* 2003; **9**(5): 500-5.
226. Noujaim H, de Ville de Goyet J, Montero E, *et al* Expanding postmortem donor pool using steatotic liver grafts: a new look. *Transplantation* 2009; **87**(6): 919-25.
227. Briceño J, Padillo J, Rufián S, Solórzano G, Pera C. Assignment of steatotic livers by the Mayo model for end-stage liver disease. *Transpl Int* 2005; **18**(5): 577-83.
228. Zamboni F, Franchello A, David E, *et al* Effect of macrovesicular steatosis and other donor and recipient characteristics on the outcome of liver transplantation. *Clin Transplant* 2001; **15**(1): 53-7.
229. Rey J, Wirges U, Dienes H, Fries J. Hepatic steatosis in organ donors: disparity between surgery and histology? *Transplant Proc* 2009; **41**(6): 2557-60.

230. Springer F, Machann J, Claussen C, Schick F, Schwenzler N. Liver fat content determined by magnetic resonance imaging and spectroscopy. *World J Gastroenterol* 2010; **16**(7): 1560-6.
231. Schwenzler N, Springer F, Schraml C, Stefan N, Machann J, Schick F. Non-invasive assessment and quantification of liver steatosis by ultrasound, computed tomography and magnetic resonance. *J Hepatol* 2009; **51**(3): 433-45.
232. Levene A, Goldin R. The epidemiology, pathogenesis and histopathology of fatty liver disease. *Histopathology* 2012; **61**(2): 141-52.
233. El-Badry A, Breitenstein S, Jochum W, *et al* Assessment of hepatic steatosis by expert pathologists: the end of a gold standard. *Ann Surg* 2009; **250**(5): 691-7.
234. Nachabé R, van der Hoorn J, van de Molengraaf R, *et al* Validation of interventional fiber optic spectroscopy with MR spectroscopy, MAS-NMR spectroscopy, high-performance thin-layer chromatography, and histopathology for accurate hepatic fat quantification. *Invest Radiol* 2012; **47**(4): 209-16.
235. Weibel E, Gomez D. A principle for counting tissue structures on random sections. *J Appl Physiol* 1962; **17**: 343-8.
236. Randeberg L, Haugen O, LO S. Optical diagnostics of liver pathology. In: Wagnieres G, editor. SPIE-OSA; 2003; p. 187-95.
237. Desjardins A, van der Voort M, Roggeveen S, *et al* Needle stylet with integrated optical fibers for spectroscopic contrast during peripheral nerve blocks. *J Biomed Opt* 2011; **16**(7): 077004.
238. Levene A, Kudo H, Armstrong M, *et al* Quantifying hepatic steatosis - more than meets the eye. *Histopathology* 2012; **60**(6): 971-81.
239. Marsman H, van Werven J, Nederveen A, *et al* Noninvasive quantification of hepatic steatosis in rats using 3.0 T 1H-magnetic resonance spectroscopy. *J Magn Reson Imaging* 2010; **32**(1): 148-54.
240. Heger M, Marsman H, Bezemer R, Cloos M, van Golen R, van Gulik T. Non-invasive quantification of triglyceride content in steatotic rat livers by (1)H-MRS: when water meets (too much) fat. *Acad Radiol* 2011; **18**(12): 1582-92.
241. Marsman H, Heger M, Kloek J, *et al* Reversal of hepatic steatosis by omega-3 fatty acids measured non-invasively by (1) H-magnetic resonance spectroscopy in a rat model. *J Gastroenterol Hepatol* 2011; **26**(2): 356-63.
242. Halon A, Patrzalek D, Rabczynski J. Hepatic steatosis in liver transplant donors: rare phenomenon or common feature of donor population? *Transplant Proc* 2006; **38**(1): 193-5.

243. Graaff R, Aarnoudse J, Zijp J, *et al* Reduced light-scattering properties for mixtures of spherical particles: a simple approximation derived from Mie calculations. *Appl Opt* 1992; **31**(10): 1370-6.
244. Baldus S, Schaefer K, Engers R, Hartleb D, Stoecklein N, Gabbert H. Prevalence and heterogeneity of KRAS, BRAF, and PIK3CA mutations in primary colorectal adenocarcinomas and their corresponding metastases. *Clin Cancer Res* 2010; **16**(1): 790-9.
245. Seol H, Lee H, Choi Y, *et al* Intratumoral heterogeneity of HER2 gene amplification in breast cancer: it's clinicopathological significance. *Mod Pathol* 2012; **25**(7): 938-48.
246. Gerlinger M, Rowan A, Horswell S, *et al* Intratumor heterogeneity and branched evolution revealed by multiregion sequencing. *N Engl J Med* 2012; **366**(10): 883-92.
247. Bydlon T, Nachabé R, Ramanujam N, Sterenborg H, Hendriks B. Chromophore based analyses of steady-state diffuse reflectance spectroscopy: current status and perspectives for clinical adoption. *J Biophotonics* 2014; **Epub ahead of print**.
248. Fox SB, Generali DG, Harris AL. Breast tumour angiogenesis. *Breast Cancer Res* 2007; **9**(6): 216.
249. Croce AC, Santamaria G, De Simone U, Lucchini F, Freitas I, Bottiroli G. Naturally-occurring porphyrins in a spontaneous-tumour bearing mouse model. *Photochemical and Photobiological Sciences* 2011; **10**(7): 1189-95.
250. Ramadori G, Cameron S. Effects of systemic chemotherapy on the liver. *Annals of Hepatology* 2010; **9**(2): 133-43.
251. Marsman H, van der Pool A, Verheij J, *et al* Hepatic steatosis assessment with CT or MRI in patients with colorectal liver metastases after neoadjuvant chemotherapy. *J Surg Oncol* 2011; **104**(1): 10-6.
252. Veteläinen R, van Vliet A, Gouma D, van Gulik T. Steatosis as a risk factor in liver surgery. *Ann Surg* 2007; **245**(1): 20-30.
253. de Meijer VE, Kalish BT, Puder M, Ijzermans JN. Systematic review and meta-analysis of steatosis as a risk factor in major hepatic resection. *British Journal of Surgery* 2010; **97**: 1331-9.
254. Desjardins A, van der Voort M, Roggeveen S, *et al* Needle stylet with integrated optical fibers for spectroscopic contrast during peripheral nerve blocks. *J Biomed Opt* 2011; **16**(7): 077004.
255. Balthasar A, Desjardins A, van der Voort M, *et al* Optical detection of peripheral nerves: an *in vivo* human study. *Reg Anesth Pain Med* 2012; **37**(3): 277-82.



Chapter **11³**

PhD Portfolio

PhD student: Daniel James Evers
PhD period: October 2009 - October 2014
PhD supervisors: Prof. dr. T.J.M. Ruers
Dr. B.H.W. Hendriks

PUBLICATIONS

DJ Evers & E Tanis, JW Spliethoff, VV Pully, K Kuhlmann, F van Coevorden, BHW Hendriks, W Prevoo, M-LF van Velthuysen, TJM Ruers. *In vivo* tumour detection in the liver with diffuse reflectance and fluorescence spectroscopy. *Submitted*

JW Spliethoff, E Tanis, **DJ Evers**, BHW Hendriks, W Prevoo, TJM Ruers. Monitoring of tumor radiofrequency ablation using derivative spectroscopy. *Accepted J. Biom Optics 2014*

DJ Evers, AC Westerkamp, JW Spliethoff, V Pully, D Hompes, BHW Hendriks, W Prevoo, M-LF van Velthuysen, RJ Porte, TJM Ruers. Diffuse reflectance spectroscopy: A promising new tool for real time quantification of steatosis in donor livers prior to transplantation. *Submitted*

JW Spliethoff, **DJ Evers**, JE Jaspers, BHW Hendriks, S Rottenberg, TJM Ruers. Monitoring of tumor response to cisplatin using optical spectroscopy. *Transl Oncol. 2014 Apr;7(2):230-9*

JW Spliethoff, **DJ Evers**, HM Klomp, JW van Sandick, MW Wouters, R. Nachabé, GW Lucassen, BHW Hendriks, J Wesseling, TJM Ruers. Improved identification of peripheral lung tumors by using diffuse reflectance and fluorescence spectroscopy. *Lung Cancer 2013; 80(2): 165-171*

DJ Evers, R Nachabé, D Hompes, F van Coevorden, GW Lucassen, BHW Hendriks, M-LF van Velthuysen, J Wesseling, TJM Ruers. Optical sensing for tumor detection in the liver. *Eur J Surg Oncol 2013; 39(1): 68-75*

DJ Evers, R Nachabé, MJ Vrancken Peeters, JA van der Hage, HS Oldenburg, EJ Rutgers, GW Lucassen, BHW Hendriks, J Wesseling, TJM Ruers. Diffuse Reflectance spectroscopy; towards clinical application in breast cancer. *Breast Cancer Res Treat 2012; 137(1): 155-165*

DJ Evers, R Nachabé, HM Klomp, JW van Sandick, MW Wouters, GW Lucassen, BHW Hendriks, J Wesseling, TJM Ruers. Diffuse Reflectance spectroscopy: a new guidance tool for improvement of biopsy procedures in lung malignancies. *Clinical Lung Cancer 2012; 13(6): 424-431*

DJ Evers, BHW Hendriks, GW Lucassen, TJM Ruers. Optical Spectroscopy; current advances and future applications in cancer diagnostics and therapy. *Future Oncology* 2012; 8(3): 1-14

R Nachabé, **DJ Evers**, BHW Hendriks, GW Lucassen, M van der Voort, J Wesseling, EJ Rutgers, MJ Vrancken Peeters, JA van der Hage, HS Oldenburg, TJM Ruers. Diagnosis of breast cancer using diffuse optical spectroscopy from 500 to 1600 nm: a comparison of classification methods. *J Biom Optics* 2011; 16(8): 087010

R Nachabé, **DJ Evers**, BHW Hendriks, GW Lucassen, M van der Voort, J Wesseling, TJM Ruers. Effect of bile absorption coefficients on the estimation of liver tissue optical properties and related implications in discriminating healthy and tumorous samples. *Biomedical Optics Express* 2011; 2(3): 600-614

PRESENTATIONS

Innovative optical technology for tumor detection in the liver. *European Society of Surgical Oncology Congress, Valencia. September 2012*

Diffuse reflectance spectroscopy; towards clinical application in breast cancer. *European Society of Surgical Oncology Congress, Valencia. September 2012*

Optical spectroscopy: A new diagnostic tool in oncology. Annual scientific meeting NKI-AvL, Amsterdam. *September 2011*

Diffuse reflectance spectroscopy as an optical guidance tool for breast biopsies. *European Multidisciplinary Cancer Congress, Sweden. September 2011*

Diffuse Reflectance Spectroscopy; a new guidance tool for improvement of minimal invasive procedures in lung and liver cancer. *European Multidisciplinary Cancer Congress, Sweden. September 2011*

Diffuse reflectance spectroscopy; a future instrument for intra-operative analysis of surgical resection margins. *Dutch National Surgery Congress NVVH. May 2011*

COURSES

Clinical Statistics, *Amsterdam*

Animal Welfare Course, *Leiden*



Chapter **11**⁴

Curriculum Vitae

Daniel James Evers was born on the 18th of November 1978 in Christchurch, New Zealand. His previous surname was Fogarty. He moved to The Netherlands in 1988 at the age of nine where the first priority was learning the Dutch language.

He graduated from the Gymnasium of the Were-di College in Valkenswaard in 1998. In that same year he started the study Biomedical Sciences at the Leiden University. In 2000, he also commenced the study Medicine at the same university and performed the studies simultaneously. He successfully achieved his M.D. and MSc. for both academic degrees in 2007. Several study projects resulted in three international publications during his student period.

Pursuing a professional career in Surgery, he began working at the Surgery department of the Haga Hospital in The Hague. After 15 months, he relocated to Amsterdam and the Surgery department of The Netherlands Cancer Institute, Antoni van Leeuwenhoek Hospital (NKI-AvL). His interest in clinical research resulted in two published papers on peritoneal malignancy. He then gained a fulltime research position studying the possibilities of differentiation between normal and malignant tissue using two optical spectroscopy techniques. This research is ultimately aimed at incorporation of spectroscopy techniques into existing medical instruments for refined tissue sensing. This prestigious project is a result of an ongoing collaboration between Twente University, the NKI-AvL and Philips Research. The current results of this research project were presented in this dissertation.

In 2012, he acceded the Dutch surgical training curriculum. He is currently working in the Rijnland Hospital, Leiderdorp in his third year of surgical training under supervision of Dr. A. M. Zeillemaker. He will complete his last two years of training at the Leiden University Medical Center under supervision of Prof. dr. J.F. Hamming, starting in January 2016.



Chapter **11⁵**

Acknowledgements

Henry Ford once said: “Coming together is a beginning, keeping together is progress and working together is success.” This quote perfectly describes the unique collaboration formed between the MIRA institute of Twente University, Philips Healthcare and several departments in the Antoni van Leeuwenhoek Hospital (NKI-AvL). All achievements presented in this thesis are a direct result of this important foundation that was constructed in 2009. Many individuals played a significant role in the creation of this translational research ultimately resulting in the dissertation in front of you. To each and everyone, I would like to express my deepest gratitude for all their time, their effort, their patience, their expertise and above all their enthusiasm during our collaboration in this project.

